THE
PHYSICAL REVIEW
A Journal of Experimental and Theoretical Physics
VOL. 46, NO. 6 SEPTEMBER 15, 1934 SECOND SERIES

The Effect of Pressure on the Intensity of X-Rays Scattered from Nitrogen at Small Angles

G. G. HARVEY,* *Ryerson Physical Laboratory, University of Chicago*
(Received July 26, 1934)

It is found that at small angles the scattering from a "permanent" gas diminishes due to intermolecular interference. The scattering curves at various pressures closely resemble those of a liquid or solid. It is concluded that this is due to the closeness of the scattering centers rather than to any preferred orientation of molecular groups since it is unlikely that such groups would be present in a gas so far from the liquid state.

IF the molecules of a gas are assumed to scatter independently, so that the scattering from n molecules is n times that from a single molecule, then on the basis of the classical theory Raman[1] and Compton[1] have shown that the distribution of intensity of x-rays scattered by a monatomic gas should be given by

$$S=1+(Z-1)f^2/Z^2, \qquad (1)$$

where S is the scattering per electron in terms of the Thomson value and f the atomic structure factor of the atom. If account be taken of the fact that the various electrons in the atom have different probability distributions[2, 3] and also that part of the scattered radiation is reduced in intensity due to the Compton effect then, as has been pointed out by Woo,[4] Eq. (1) becomes

$$S=\frac{f^2}{Z}+\frac{1-\left(\sum_{j=1}^{Z}E_{jj}^2\right)/Z}{(1+\alpha \text{ vers } \phi)^2} \qquad (2)$$

where ϕ is the angle of scattering, $\alpha=h/mc\lambda$ and E_{jj} is the contribution to f due to the jth electron so that $f=\sum E_{jj}$. Eq. (2) is in agreement with that obtained by Wentzel[5] for the total scattering from an atom on the basis of wave mechanics. The more exact result of Waller and Hartree[6] in which account is taken of the Pauli exclusion principle differs from Eq. (2) by the addition of a small negative term in the numerator of the second half of this equation, which, for the range of angles to be considered in this paper, is completely negligible.[7] Eq. (2) may easily be ex-

* National Research Fellow.
[1] C. V. Raman, Ind. J. Phys. **3**, 357 (1928); A. H. Compton, Phys. Rev. **35**, 925 (1930).
[2] G. E. M. Jauncey, Phys. Rev. **37**, 1193 (1931).
[3] G. Herzog, Zeits. f. Physik **69**, 207 (1931).
[4] Y. H. Woo, Phys. Rev. **41**, 21 (1932).
[5] G. Wentzel, Zeits. f. Physik **43**, 1, 779 (1927).
[6] I. Waller, Phil. Mag. **4**, 1228 (1927); Nature **120**, 155 (1927); Naturwiss. **15**, 969 (1927); Zeits. f. Physik **41**, 213 (1928); I. Waller and D. R. Hartree, Proc. Roy. Soc. **A124**, 119 (1929).
[7] Cf. G. G. Harvey, P. S. Williams and G. E. M. Jauncey, Phys. Rev. **46**, 365 (1934).

tended to the case of a polyatomic gas[8] by using a result due to Debye[9] and gives

$$S=\left\{\sum_i\sum_j f_i f_j \frac{\sin ks_{ij}}{ks_{ij}}+\sum_i \frac{Z_i-(\sum E_{ij}^2)_i}{(1+\alpha \text{ vers } \phi)^2}\right\}\Big/\sum Z_i, \quad (3)$$

where s_{ij} is the distance between the ith and jth atoms in a molecule (assumed constant) and $k=4\pi(\sin\phi/2)/\lambda$. For the particular case of a diatomic gas consisting of two like atoms Eq. (3) gives

$$S=\left(1+\frac{\sin ks}{ks}\right)\frac{f^2}{Z}+\frac{1-(\sum E_{ij}^2)/Z}{(1+\alpha \text{ vers } \phi)^2}. \quad (4)$$

Eqs. (2) and (4) have been well verified[10] for angles of scattering of 10° and larger and for moderate pressures. It will be seen that for $\phi\to 0$ Eq. (3) predicts $S\to\sum Z_i$. As has been said, the above equations are all based on the assumption that the molecules of the gas scatter independently. But at small angles of scattering this can no longer be true. On the basis of a statistical-thermodynamical treatment Einstein and Smoluchowski[11] have shown that the scattering of ordinary light by a fluid can be accounted for by the accidental fluctuations of density in the fluid. This result rests essentially on the fact that for optical wave-lengths the fluid may be treated as continuous and the fluctuations of density within a cube of edge considerably smaller than $\lambda/(\sin\phi/2)$ may be treated as completely independent. This in general will not be true for x-ray wave-lengths. It will, however, be true even for x-rays provided that ϕ is taken small enough. If we take as a rough estimate for the minimum size of cube, for which the optical theory is valid, one, fifty molecules thick, then at a pressure of 100 atmospheres the optical theory for a gas should also hold for x-rays out to angles of about 6′ for Mo $K\alpha$ radiation and although the theory would not be strictly valid beyond this it should be at least qualitatively true out to about a degree or more. A more complete treatment, applicable to the x-ray case, has been given by Raman and Ramanathan[12] in which account is taken of the fact that a fluid cannot be treated as a continuum for x-ray scattering except at very small angles. This theory predicts a peak in the scattering curve at an angle ϕ_0 given by

$$\lambda=2\lambda_0\sin\phi_0/2 \quad (5)$$

where λ_0 is the "mean distance between molecules" in the fluid, and at smaller angles a rapid decrease in intensity approaching the value given by the ordinary optical theory. The intensity distribution given by Raman and Ramanathan is

$$I=\text{const. }\exp\left\{-\frac{N}{16RT\beta}\cdot\lambda_0^3\cdot\left(1-\frac{\lambda_1^3}{\lambda_0^3}\right)^2\right\}, \quad (6)$$

where R and N are, respectively, the gas constant and Avogadro constant for a gram molecule, β the isothermal compressibility and λ_1 is given by

$$\lambda=2\lambda_1\sin\phi/2. \quad (7)$$

As explicitly pointed out by Raman and Ramanathan Eq. (6) of course takes no account of the structure of the individual molecules but only an average structure of the fluid as a whole. Its principal accomplishment is to account for the main diffraction peak observed in liquids and amorphous solids and the very small scattering at angles less than the position of this peak. It should also be applicable to a gas of very high density. On the assumption of the closest packing of spheres[13] $\lambda_0=2^{1/6}(M/N\rho)^{1/3}=1.33\,(M/\rho)^{1/3}=37.5\,p^{-1/3}$ where M is the molecular weight, ρ the density, p the pressure in atmospheres, and λ_0 is measured in A. Thus at atmospheric pressure the peak should occur at $(\sin\phi/2)/\lambda=0.0133$ or, for Mo $K\alpha$ radiation, $\phi_0=1°\ 10'$ and at a pressure of 100 atmospheres $\phi_0=5°$. At high pressures the decrease in intensity due to intermolecular interference should thus be easily observable.

[8] Y. H. Woo, Proc. Nat. Acad. Sci. **17**, 467, 470 (1931); Phys. Rev. **39**, 555 (1932); also reference 4.

[9] P. Debye, Ann. d. Physik **46**, 809 (1915); Phys. Zeits. **41**, 419 (1930).

[10] e.g. E. O. Wollan, Phys. Rev. **37**, 862 (1931); Proc. Nat. Acad. Sci. **17**, 475 (1931); Rev. Mod. Phys. **4**, 205 (1932); G. Herzog, Zeits. f. Physik **69**, 207 (1931); **70**, 583 and 590 (1931); P. Debye, L. Bewilogua and F. Ehrhardt, Phys. Zeits. **30**, 84 (1930); L. Bewilogua, Phys. Zeits. **32**, 265 (1931); R. W. James, Phys. Zeits. **33**, 737 (1932); W. Van der Grinten, Phys. Zeits. **34**, 609 (1933).

[11] von Smoluchowski, Ann. d. Physik **25**, 205 (1908); A. Einstein, Ann. d. Physik **33**, 1275 (1910). Cf. Fowler, *Statistical Mechanics*, pp. 143 and 515.

[12] C. V. Raman and K. R. Ramanathan, Proc. Ind. Assoc. Cultiv. Sci. **8**, 127 (1923).

[13] Jeans, *Dynamical Theory of Gases*, 4th Edition, p. 330.

Debye[14] has treated the subject of intermolecular interference from a different point of view. His calculation is based on the assumption that the gas consists of rigid spherical molecules of radius a. Thus the closest distance of approach of two molecules is $2a$, the radius of the sphere of influence. Debye assumes that for distances greater than $2a$ the distribution of matter is of uniform density and calculates the scattering from such a distribution. The result for a monatomic gas, written in terms of S, is

$$S_{\text{coh.}} = [1 - (\Omega/V)\phi(2ka)]f^2/Z, \tag{8}$$

where $$\phi(u) = (3/u^3)(\sin u - u\cos u) \tag{9}$$

and $$\Omega/V = (4\pi N/3)(2a)^3, \tag{10}$$

where N is the number of molecules in the volume V. For a diatomic gas

$$S_{\text{coh.}} = \left[1 + \frac{\sin kl}{kl} - 2\frac{\Omega}{V}\left(\frac{\sin kl/2}{kl/2}\right)^2 \phi(2ka)\right]\frac{f^2}{Z}, \tag{11}$$

where l is the interatomic distance and a is again the effective radius of the *molecule*. These equations are only supposed to be valid for small values of Ω/V.

The method of Zernicke and Prins[15] which takes account of the actual distribution of density in the scattering substance has met with considerable success in explaining the scattering curves obtained with liquids.[16] Warren has extended this to the case of glasses[17] and found that here too the results are very satisfactory. Quite recently Gingrich and Warren[18] have applied the method to a study of the scattering from a fluid at various densities and have again found very good agreement.

The present investigation was undertaken to see just how large the effect of intermolecular interference is in the case of a gas and to study its dependence on pressure.

[14] P. Debye, J. Math. and Phys. **4**, 133 (1925); Phys. Zeits. **28**, 135 (1927).
[15] F. Zernicke and J. A. Prins, Zeits. f. Physik **41**, 184 (1927).
[16] B. E. Warren, Phys. Rev. **44**, 969 (1933).
[17] B. E. Warren, Phys. Rev. **45**, 657 (1934).
[18] N. S. Gingrich and B. E. Warren, Phys. Rev. **46**, 248 (1934). The writer is indebted to Dr. Gingrich and Professor Warren for a copy of this paper previous to its publication.

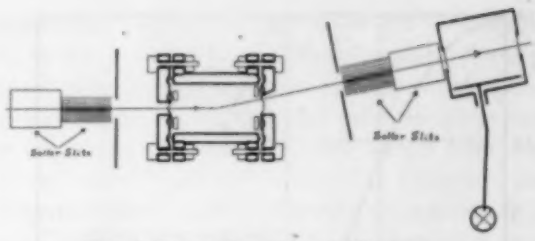

FIG. 1. Scattering cell and slit system.

EXPERIMENTAL

The first essential in such an investigation is a scattering cell which will withstand the pressures involved and yet transmit an appreciable portion of the radiation. A modification of the high pressure ionization chamber described by Williams[19] was used. A cross section of the cell is shown in Fig. 1; for details of construction reference may be made to the paper of Williams. The primary and scattered beams of x-rays were collimated by means of crossed Soller slits, giving a maximum angular divergence in any direction of less than one degree. An ordinary molybdenum target water-cooled tube was used together with a ZrO_2 filter. The ionization currents in a chamber filled with krypton were measured with a Compton electrometer operating at sensitivities of from 15,000 to 20,000 mm/volt. At best the currents were excessively weak, a ten centimeter deflection requiring from 7 to 15 minutes at various pressures. The procedure consisted in measuring the scattering with the cell filled with nitrogen at a given pressure and then again with the cell empty. In the latter case sufficient aluminum was placed in the primary beam so that the absorption of the gas-filled cell was the same as that of the cell plus aluminum. This background reading consists of scattering from the cell windows, scattering from the slits, and natural drift of the electrometer due to alpha-particles and radioactive contamination of the laboratory. The background was always a large portion of the total measured effect, sometimes as much as eighty percent. A run consisted of measurements every half degree throughout the available range of angles, taking one or two readings at each setting and going back and forth over this range until at least five or six values were obtained for each angle. This procedure was followed so as to eliminate any change in deflection with time, al-

[19] J. H. Williams, Rev. Sci. Inst. **3**, 586 (1932).

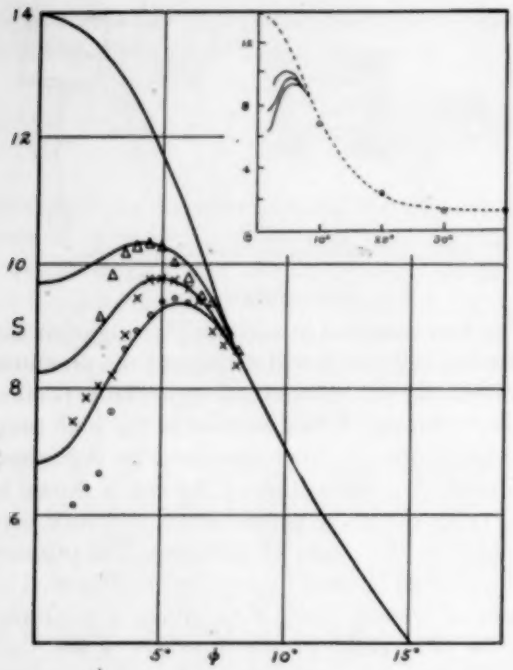

FIG. 2. Solid curves: Scattering according to Debye's theory for 0, 60, 80, and 100 atmospheres, respectively. Experimental points: triangles, 60 atmospheres; crosses, 80 atmospheres; circles, 100 atmospheres. Inset shows complete curve out to 40°. Dotted curve, scattering from free atom; solid curves, experimental results at 60, 80 and 100 atmospheres. Circles, Wollan's data (see reference 22).

though no readings were considered of any value unless the electrometer remained very steady throughout the entire run of from twenty to thirty hours. The input to the x-ray tube was always very constant. To keep the background intensity as low as possible the thickness of the windows (celluloid) of the scattering cell was so chosen at each pressure used as to be just great enough to withstand that pressure without breaking, an extra 100 pounds usually causing it to burst; the scattering from the cell windows always constituted the largest part of the background except at the smallest angles. Measurements were made at pressures corresponding to 60, 80 and 100 atmospheres at 0°C. The deviations from Boyle's law in this range are about one percent[20] so that the pressures may be taken as proportional to the densities of the gas. Fig. 2 shows the results obtained. Since absolute measurements could not be made the ordinates of the experimental curves were adjusted so as to give the best fit with the theoretical ones in the vicinity of the peak and this in general gave a good fit at larger angles where the effect of intermolecular interference rapidly diminishes in importance. The theoretical curves are calculated from Eq. (11) for 0, 60, 80 and 100 atmospheres with the addition of the small term $1-(\sum E_{ij}^2)/Z$ to take account of the incoherent scattering. The value of l was taken to be 1.09A.[21a] The value of $2a$ used, 3.56A, was taken from data on the equation of state for nitrogen.[21b] Although the absolute values of the theoretical curves depend on the value of a used the positions of the peaks are practically independent of this, at least for small variations. It is thus satisfactory to find that the peak positions as measured experimentally are practically identical with the theoretical positions. The inset in Fig. 2 perhaps gives a more comprehensive view of the results. The solid curves represent the experimental values while the dotted curve is the theoretical scattering from a free atom. The points at 10°, 20°, 30° and 40° are taken from the data of Wollan.[22]

It is of course true that the density distribution assumed by Debye is only a rough approximation and it would be more correct to apply the method of Zernicke and Prins, as has been done by Gingrich and Warren.[18] This has not been attempted for two reasons. First, the experimental data are not as reliable as might be desired, not only because of the weak intensity but also due to uncertainty in applying corrections to the measured values. For example, the calculation of the effective scattering volume depends on the assumption that the x-ray beam is of uniform intensity throughout. Although the scattering volume changes by a maximum amount of thirteen percent between 1° 10′ and 8° the effect of lack of uniformity of the beam would not be negligible. The second reason for not applying the method of Zernicke and Prins is because at small angles the effect of statistical fluctuations begins to be appreciable, as mentioned above. This would cause the scattered intensity to drop off more rapidly with decreasing angle, as is in fact

[20] I.C.T. 3, page 17.

[21a] R. S. Mulliken, Rev. Mod. Phys. **4**, 82 (1932).

[21b] Cf. Jeans, *Dynamical Theory of Gases*, p. 139 or Fowler, *Statistical Mechanics*, p. 234.

[22] E. O. Wollan, Proc. Nat. Acad. Sci. **17**, 475 (1931).

observed. As a matter of fact this experiment was first undertaken in the hope of detecting a rapid decrease in scattering at very small angles, due to statistical fluctuations. A system of Soller slits was constructed giving a maximum angular divergence of less than 15′ and it was possible to come within 30′ of the primary beam and yet not have the direct radiation enter the ionization chamber, but the scattered radiation was collected throughout such a small solid angle that measurement was hopeless and the experiment had to be revised.

Conclusion

The present experiment has shown that the effect of intermolecular interference is not negligible even in the case of a gas under moderate pressures. The scattering curves are very similar to those obtained for liquids and solids, the principal difference being that the main diffraction peak occurs at a smaller angle due to the greater mean molecular distance. We would thus conclude with Warren,[17] and with Gingrich and Warren[18] that such a decrease in scattering at small angles is due merely to the fact that there are a large number of scattering centers within a small space, rather than to any preferred grouping of the molecules, since the existence of such groups would be very unlikely in a gas so far from the liquid state.

In conclusion the author wishes to express his appreciation to Professor Arthur H. Compton for his interest in the work and the use of the Ryerson Physical Laboratory as well as for numerous suggestions and discussions during its progress.

An X-Ray Study of a Long X-Cut Quartz Crystal Vibrating Under the Transverse Piezoelectric Effect*

M. Y. Colby and Sidon Harris, *Department of Physics, The University of Texas*

(Received March 15, 1934)

The sixth order reflection from the (110) set of planes of a long X-cut quartz crystal of the $K\alpha$ radiation of Mo was photographed for the following conditions: (1) with the crystal non-oscillating, (2) with the crystal oscillating at its fundamental frequency under the transverse piezoelectric effect, and (3) with the crystal oscillating at its second harmonic frequency. From the microphotometer analysis of these lines it is shown that no increase in width of the lines reflected from the crystal oscillating at its fundamental frequency over the width of the lines reflected from the non-oscillating crystal is observed. This fact shows that there is no elastic deformation of the spacing of the (110) set of planes greater than 1.45×10^{-6} per unit dimension. This value is the limit of the sensitivity of the spectrograph and microphotometer used. However, an appreciable increase in intensity in the lines reflected from the crystal oscillating at its fundamental frequency over the lines reflected from the non-oscillating crystal is shown. A microphotometer analysis of Laue spots obtained by passing a rectangular beam of x-rays through the middle of the crystal when it was oscillating at its fundamental frequency confirms the prediction made by the authors in an article recently published in this journal. The results seem to indicate that any increase in intensity of the reflected x-rays from any portion of a quartz crystal produced by piezoelectric oscillations of the crystal is due almost entirely to a reduction of secondary extinction.

Introduction

SINCE Fox and Carr[1] reported a decided increase in the intensity of Laue spots obtained from a quartz crystal oscillating piezoelectrically along the direction of thickness of the plates caused by the longitudinal effect,[2] a number of investigators have conducted experiments with plates oscillating under this "thickness vibration" or more properly longitudinal effect; however, the authors are the only ones who have experimented with a long crystal vibrating under the transverse effect.[3, 4] From the interferometer experiments of Osterberg[5, 6] we now know that the strains in the plates

* This paper is an extract from the thesis presented for the degree of Doctor of Philosophy by Sidon Harris.

[1] Fox and Carr, Phys. Rev. **37**, 1622 (1931).

[2] The terminology here used is taken from *Piezoelectric Terminology* by W. G. Cady, Inst. Radio Eng. **18**, No. 12 (1930).

[3] Colby and Harris, Phys. Rev. **42**, 733 (1932).

[4] Colby and Harris, Phys. Rev. **43**, 562 (1933).

[5] Osterberg, Phys. Rev. **43**, 819 (1933).

[6] Osterberg, Rev. Sci. Inst. **5**, 183 (1934).

oscillating under the longitudinal effect are extremely complex and flexural, and that it is even doubtful if any standing waves parallel to the thickness dimension exist at all. It then seems probable that the large increased intensities of the Laue spots obtained under these conditions are produced by reduction of secondary extinction caused by the large inhomogeneous strains set up in the crystal, as first suggested by Langer.[7] Fox and Cork[8] failed to note any change in the lines reflected from the face of a plate oscillating under the longitudinal effect, but the authors[3] have succeeded in obtaining an effect on the lines reflected from the face of a long quartz crystal oscillating under the transverse effect. The failure of the Fox-Cork experiment to get any effect was due probably to the fact that the mode of oscillation of their plate was such that there existed approximately a node of pressure at the surface of the plate from which the x-ray beam was reflected. Hence, even if elastic deformations of the atomic plane spacings were taking place in other regions of the crystal, no widening of the lines obtained from this experiment could be expected. What reduction of secondary extinction that might have occurred at the point of reflection, caused by slight inhomogeneous strains in this region set up by the flexural vibrations, was probably obscured by an imperfect surface layer which had already reduced secondary extinction to nearly a minimum. In the authors' experiment,[3] a long crystal was used vibrating under the transverse effect; hence, a sinusoidal standing wave may be assumed with reasonable certainty. In the middle of the crystal where the x-rays were reflected, a loop of pressure existed clear through the crystal; hence, if any elastic deformations of the plane spacings were taking place, they would exist through this region of the crystal; also there would be a homogeneous strain through the crystal at this point, and therefore some displacement of the Zwicky blocks should be expected in the middle region of the crystal, if such blocks exist at all. Now if there is merely an elastic deformation of the spacings of the (1 1 0) set of planes and no rocking of the proposed blocks, the reflected line should show an increase in width but no appreciable increase in intensity. And if no appreciable elastic deformations are taking place, but a rocking of the blocks is taking place, then an increase in intensity and no appreciable increase in width of the lines should be expected. In the earlier experiment,[3] the authors detected both a widening of the lines and an increase in intensity. One purpose of the present work was to investigate further this result. By oscillating the crystal at its second harmonic, thereby producing a node of pressure through the middle of the crystal (the region from which the x-ray beam was reflected), it was found that the widening of the line is due solely to the jumping of the crystal in its mounting; however, the appreciable increase in intensity in the line reflected from the crystal when it was oscillating at its fundamental frequency was again observed. Thus it seems that the effect is due entirely to a reduction of secondary extinction produced by the rocking of the proposed Zwicky blocks.

In another paper,[4] the authors obtained practically no increase in the intensity of Laue spots obtained by passing an x-ray beam through the middle of the long crystal when it was oscillating at its fundamental frequency under the transverse effect; that is, no increase as far as the eye could detect. This result is due to the fact that in this experiment, homogeneous strain is present which does not reduce secondary extinction nearly as much as inhomogeneous strain which occurred in the other experiments in which the longitudinal effect was employed. Another purpose of this work was to examine these spots with a microphotometer, and see if the prediction made in the earlier paper[4] was correct.

Experimental Procedure

The crystal is an X-cut crystal of $100\times6\times2$ millimeter dimensions, with the 100 millimeter dimension parallel to the Y or mechanical axis, and the 2 millimeter dimension parallel to the X or electric axis. The electric field was applied across the X direction. The fundamental frequency of oscillation of the crystal is 27,400 cycles per second. With the spacing of the (1 1 0)

[7] Langer, Phys. Rev. **38**, 573 (1931).
[8] Fox and Cork, Phys. Rev. **38**, 1420 (1931).

set of planes given by Bradley and Jay[9] and the accepted value of the $K\alpha$ radiation of Mo, it was found that the sixth order reflection of this radiation from this set of planes could be obtained at a Bragg angle of 60.3°. By simple trigonometry it can be shown that the displacement ΔS of a line on the film caused by a change Δd in the spacing of the reflecting planes may be expressed as follows:

$$\Delta S = 2r \cdot \tan\theta \cdot \Delta d/d, \qquad (1)$$

where r is the film to crystal distance, which was 200 millimeters in this case, and θ is the usual Bragg angle. It was possible to detect a change of 0.01 millimeter in the width of a line from the microphotometer analysis; therefore a change as small as 1.45×10^{-5} per unit dimension of the spacing of the (1 1 0) set of planes could be detected.

The crystal U can be seen in its hard rubber mounting J in Fig. 1. When the crystal was oscillated at its fundamental frequency, the two top plates R' and R were connected to the binding post N, and the two similar bottom plates were connected in like fashion to the post N'. These terminals were connected across a large air condenser which was in a tuned circuit inductively coupled to the out-put of an amplifier, which was connected across the out-put of a standard Western Electric oscillator. When the crystal was oscillated at its second harmonic the plate R' was connected with the opposite bottom plate to one binding post, and the plate R was similarly connected with the other bottom plate to the remaining binding post.

Three exposures were made on the same film, one with the crystal not oscillating, one with the crystal oscillating at its fundamental frequency, and one with the crystal oscillating at its second harmonic frequency. Any effect on the line reflected from the crystal when it was oscillating at its second harmonic frequency may be attributed to the motion of the crystal as a whole in its mounting parallel to the 2 millimeter direction, as a node of pressure exists clear through the region from which the x-rays are reflected, and no deformations of the plane spacings or movements of the supposed blocks could possibly occur in this region. The motion of the crystal parallel to the 100 mm dimension in its mounting will have no effect on the width or intensity of the spectral line reflected from the face of the crystal. Thus, by comparing the widths of the lines reflected from the crystal when it is oscillating at its fundamental frequency and when it is oscillating at its second harmonic frequency, the true effect on the line produced by either the motion within the crystal of the grating space, or by the motion of the proposed Zwicky blocks may be determined accurately.

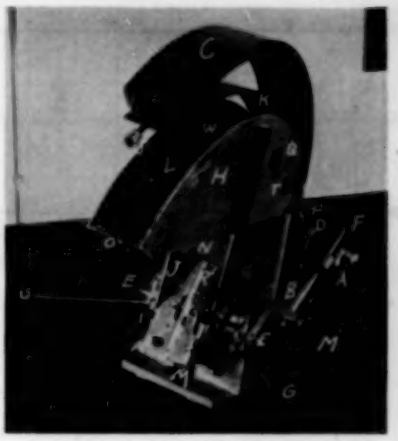

FIG. 1. The backward reflecting Bragg spectrograph shown with the quartz crystal U in its mounting J. R and R', brass plates forming the condenser through which the electric field is applied; N and N', terminals of the condenser; EE, shaft on which the crystal is rocked; I, protractor for setting the crystal; G, base of spectrograph; M, set screws for height adjustment. Arm B, follower F, cam A, and worm and pinion D, part of the arrangement for rocking the crystal during exposure. H, film holder; L, lead screen; W, window in screen; K, spring for holding film; G, light tight cover. P, screws for holding H in position; Q and T, threaded holes for other positions of H.

The crystal mounting J (Fig. 1) was accurately centered on the pointed ends of the rods E. The crystal was rocked through an angle of 5° during exposure by means of the shaft B, follower F, cam A, worm and pinion D, and a shaft (not shown in the figure) which connected the worm gear arrangement with the armature of a motor through a reduction gear. The film was placed in the holder H, over the lead screen L. The window W permitted the reflected radiation to strike the film at the proper position. The film was held fast by the spring K, and the cover C fitted over the holder, thus shielding

[9] Bradley and Jay, Proc. Roy. Soc. London **A45**, 507 (1933).

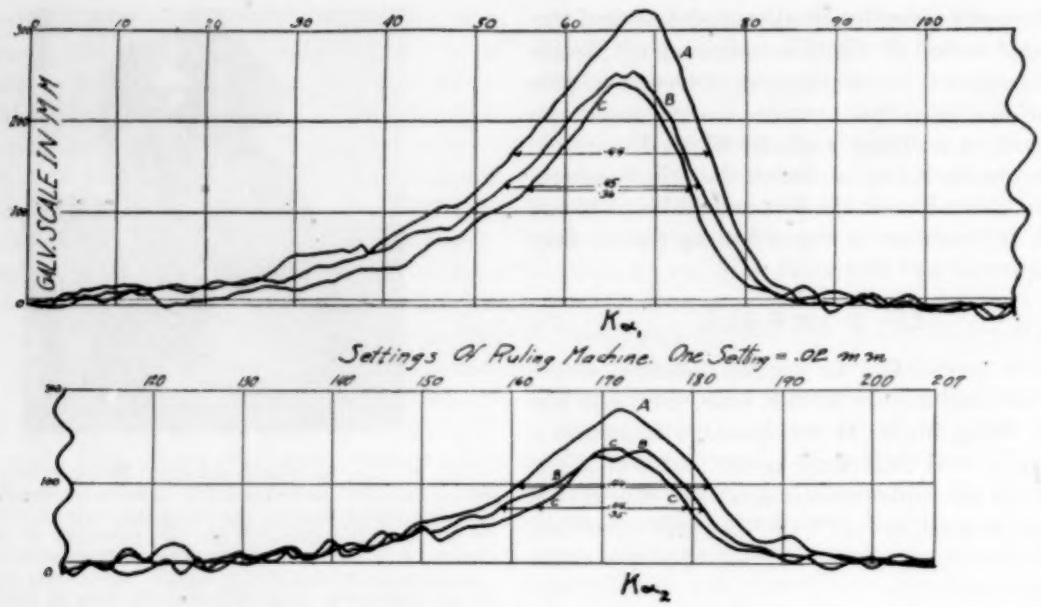

FIG. 2. Photograms of the three doublets obtained by the sixth order reflection from the (1 1 0) set of planes of the $K\alpha$ radiation of Mo. *A*, photogram of doublet obtained when crystal was oscillating at its fundamental frequency under the transverse effect; *B*, photogram of doublet obtained when the crystal was oscillating at its second harmonic frequency; *C*, photogram of doublet obtained when crystal was not oscillating.

the film from light. The holder was held in position by the screws *P*. The holes *Q* and *T* are for other positions of the holder. The spectrograph fits onto a track in a standard G.E. diffraction apparatus. The height of the spectrograph is adjusted by the screws *M*, shown on the base *G* of the instrument.

An exposure of sixteen hours was necessary to make each picture. The doublet obtained was highly resolved but quite weak. However, very satisfactory photograms were obtained by running the pictures through a fine structure photometer which was especially designed to reduce grain effects. This instrument has been described elsewhere.[10]

EXPERIMENTAL RESULTS

Fig. 2 shows the photograms of the three doublets. Curve *A* is the photogram of the doublet reflected from the crystal when oscillating at its fundamental frequency, curve *B* is the photogram of the doublet reflected from the crystal when it was oscillating at its second harmonic frequency, and curve *C* is the photogram of the doublet reflected from the crystal when it was not oscillating. It is seen that the curve *B* is 0.09 mm wider than curve *C*, but of approximately the same amplitude. This result shows that the increase in width of the line is due solely to the jumping of the crystal in its mounting. Any difference in the amplitude of the curves *B* and *C* may be attributed to the variations in the operation of the x-ray tube. It is clearly shown that the width of curves *A* and *B* are approximately the same within the accuracy of the experiment. Hence, no variation of the grating constant takes place during oscillation; at least no variation which is greater than 1.45×10^{-5} per unit dimension. The fact that the amplitude of the lines shown in curve *A* are greater than the amplitude of the lines shown in curves *B* and *C*, shows that secondary extinction was reduced on the face of the crystal in the vicinity of the middle when the crystal was oscillating at its fundamental frequency, but was not reduced in this region when the crystal was oscillating at its second harmonic. This fact shows that strain existed through the middle of the crystal when it was vibrating at its fundamental frequency, but that no appreci-

[10] Sidon Harris, Rev. Sci. Inst. **4**, 598 (1933).

able strain existed in this section when the crystal was oscillating at its second harmonic. The crystal was resonating vigorously during both exposures; the total average change in length per unit length along the 100 mm direction was calculated from microscope readings and found to be 6×10^{-4}. If the strain along X through the middle of the crystal can be taken as equal to the strain along Y as the authors[11] have found to be the case in static conditions, an increase in line width of 0.42 mm would be expected from the line reflected from the crystal when oscillating at its fundamental frequency, if the spacing of the (1 1 0) set of planes changed in a one to one ratio with the outside dimension of the crystal in the X direction. As no increase, not even as small as 0.01 mm was detected, it is to be supposed that most of the strain inside the crystal along the X direction must surely occur in the π-planes of Zwicky, and not in the p-planes, whose spacing effects the position of the reflected line on the film. This evidence would be a strong support of Zwicky's theory if it were definitely known that the dynamic ratio of X strain to Y strain were unity. Experiments to determine this dynamic ratio are now in progress in this laboratory. However, until this ratio for dynamic conditions is determined, the result presented immediately above is added as merely an interesting possibility. As the strain through the middle of the crystal described in this experiment is homogeneous when the crystal is oscillating at its fundamental frequency, naturally the reduction of secondary extinction in the middle region is not as great as in the cases where inhomogeneous strain acts on the reflecting surfaces of the crystal. In order to observe this relatively small decrease in secondary extinction, the surface of the crystal irradiated by x-rays, was etched lightly with hydrofluoric acid in order to remove the imperfect surface layer produced by polishing.

X-ray photographs were also made by sending a beam of x-rays from a slit source through the middle of the crystal when it was oscillating at its fundamental frequency, and when it was not oscillating. The photograms of the transmission lines thus obtained are shown in Fig. 3. Curve A is the photogram of the line obtained from the crystal when it was oscillating at its fundamental frequency, and curve B is the photogram of the line obtained from the crystal when it was not oscillating. Curve A is wider than curve B because the lines were not reflected from the same set of planes. The crystal was in a horizontal position when the line corresponding to curve A was taken, and in a vertical position when the line corresponding to curve B was taken. The films were given the same exposure and development. As the source of x-rays was a slit instead of the usual pinhole used in making transmission pictures, only the lines of the principal spectrum were sharp. The sharpest line was chosen for the photogram in each case. The fact that one of the spots is wider than the other should have no effect on the comparison of the relative intensities of the components. It is seen that the component reflected from the polished face of the crystal

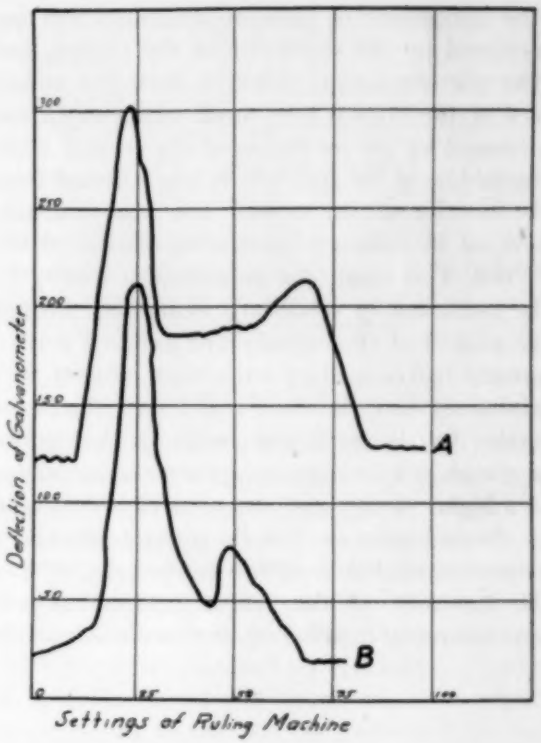

FIG. 3. Photograms of transmission lines obtained by passing a rectangular beam of x-rays through the middle of the crystal. A, photogram of line obtained when crystal was oscillating at its fundamental frequency; B, photogram of line obtained when crystal was not oscillating.

[11] Colby and Harris, J. Opt. Soc. Am. **24**, 217 (1934).

(the component of greatest intensity) was not increased by the oscillation of the crystal, and that the component reflected from the etched face of the crystal (the weak component) was increased by the oscillation of the crystal, while the middle of the spot which was reflected from the interior of the crystal was approximately doubled in intensity by the oscillation of the crystal. This result can be explained readily by the reduction of secondary extinction through the middle of the crystal. The polished surface already had secondary extinction reduced to a minimum, and therefore could be reduced no further by the oscillation; while on the surface of the etched face, secondary extinction existed to a higher degree and was appreciably reduced by the oscillation; and in the interior, secondary extinction existed to such a marked degree that the intensity of the reflected radiation was approximately doubled by the oscillation of the crystal. This result was predicted by the authors[4] in a recent publication in this journal.

In conclusion it may be said that the increased intensities of the components of the transmission lines, and the increased intensities of the reflected lines, together with the fact that the high resolving power spectrograph showed no increase in width of the reflection lines, show conclusively that any increased intensity in the radiation reflected from any portion of a quartz crystal oscillating piezoelectrically may be attributed almost entirely to a reduction of *secondary* extinction. This reduction of secondary extinction can be brought about only by the motion of some type of secondary structure block such as has been proposed by Zwicky as existing in crystals.

The authors wish to express their appreciation to Mr. L. H. Gruber, technician, for making the spectrograph used in this work.

Variation of the Dielectric Constant of Rochelle Salt Crystals with Frequency and Applied Field Strength

ANTHONY ZELENY AND JOSEPH VALASEK, *University of Minnesota*

(Received August 1, 1934)

The dielectric constant of Rochelle salt crystals perpendicular to the a axis at 0°C was measured over the frequency range of 30 to 30×10^6 cycles/sec. Following a fairly uniform decline from 62,000 at 30 cycles to 220 at 10^7 cycles, the dielectric constant drops abruptly to negative values (inductive reactance) at 14×10^7 cycles. This frequency is independent of the size and mounting of the crystal and thus appears to be critical for this crystalline material.

THE dielectric properties of Rochelle salt crystals are as unique as the magnetic properties of iron. In fact, the ferromagnetic analogy can be applied with considerable success, as has been pointed out by Valasek,[1] Müller[9] and others. Experimental measurements show a very high dielectric constant accompanied by hysteresis, and demonstrate the existence of two "Curie points," respectively, at −15°C and +23°C. Measurements of the dielectric constant of the substance are difficult because the results are very sensitive to the presence of even a slight layer of modified crystal or binding material between the crystal and the electrodes. The older measurements[1,2,3,6] all give values which are too low because of this effect. In the more recent work of Sawyer and Tower,[5] Errera,[7] Kobeko and Kurtschatov,[8] and of Busch,[4] improved electrodes are described which give better results. The present paper describes the results obtained in extending the measurements

[1] Valasek (a) Phys. Rev. **19**, 478 (1922); (b) Phys. Rev. **23**, 114 (1924); (c) Phys. Rev. **15**, 537 (1920); (d) Science **65**, 235 (1927).
[2] Cady, Rep. Nat. Res. Council, May 1918.
[3] Anderson, Rep. Nat. Res. Council, April 1918.
[4] Busch, Helvetica Physica Acta **6**, 315 (1933).
[5] Sawyer and Tower, Phys. Rev. **21**, 269 (1930).
[6] Frayne, Phys. Rev. **21**, 348 (1923).
[7] Errera, Phys. Zeits. **32**, 368 (1931).
[8] Kobeko and Kurtschatov, Zeits. f. Physik **66**, 192 (1930).
[9] Müller, Phys. Rev. **44**, 854 (1933).

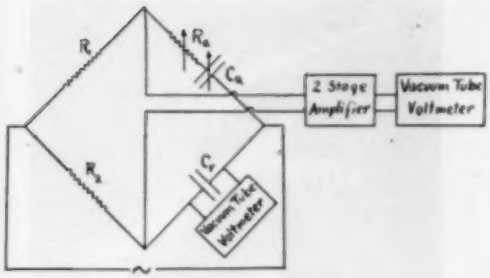

FIG. 1. Capacitance bridge.

with the newer type of electrodes to very high frequencies. The crystal was cut so that its faces were at right angles to the *a* axis, since it is only in this direction that the unusual dielectric properties exist.

METHOD OF MEASUREMENT AND APPARATUS

Two types of measuring circuits were used, a capacitance bridge for the lower frequencies (30–75,000 cycles) and a resonance circuit for the higher frequencies (75,000–30,000,000 cycles).

In the capacitance bridge, Fig. 1, R_1 and R_2 are equal resistances, C_a is a standard variable condenser (50–1,000,000$\mu\mu$f), R_a is a variable non-inductive resistance (0–100,000 ohms) and C_r a condenser whose dielectric is a plate of the crystal under observation.

It has been shown by Kobeko and Kurtschatov[5] that the potential gradient within a Rochelle salt crystal when used as the dielectric of a condenser is approximately uniform. The crystal condenser and its leakage, therefore, may be represented by a pure capacitance C in parallel with a non-inductive resistance R. Since R_1 at balance equals R_2, the impedance Z_p of the crystal, that is, of C and R in parallel, must equal the impedance Z_s of R_a and C_a in series. The impedance of R and C in parallel is

$$Z_p=(R/j\omega C)/(R+1/j\omega C).$$

The impedance of R_a and C_a in series is

$$Z_s=R_a+1/j\omega C_a.$$

Since at balance Z_p equals Z_s,

$$R_a+1/j\omega C_a=(R/j\omega C)/(R+1/j\omega C).$$

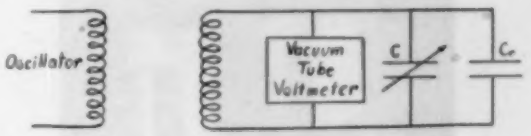

FIG. 2. Resonance circuit.

Equating the real and the imaginary parts of the above, and solving for C and R, it is found that:

$$C=C_a/(1+\omega^2R_a^2C_a^2)$$

and

$$R=R_a+1/\omega^2C_a^2R_a^2.$$

The open-circuit voltage across the crystal, measured by a vacuum-tube voltmeter, gives the electrostatic field strength to which the crystal is subjected during the measurements.

The resonance circuit method is a substitution method of the type used by Frayne.[6] The difference at resonance, Fig. 2, in the two settings of the standard air condenser, C, when C_r is disconnected and connected, is the capacitance C_r. In this circuit the vacuum-tube voltmeter indicates the voltage across the crystal as well as resonance.

The types of electrodes used were (1) the mercury-Rochelle salt solution type, Fig. 3, similar to those used by Kobeko and Kurtschatov[5] and (2) the silver-plated type, Fig. 4, in which the silver was evaporated and allowed to condense on the surface of the crystal in a vacuum. The crystal plates varied in thickness from 2 to 8 mm and the surfaces were usually 3 cm square. The electrodes were several millimeters smaller. After preparing the condenser, the crystal was given an impervious coating of celluloid dissolved in amyl acetate.

The temperature of the crystal was maintained at 0°C because at this temperature the dielectric constant is high and has a low temperature coefficient.[1, 6]

RESULTS

Fig. 5 shows typical curves for the dependence of the dielectric constant on frequency, for each of the two types of electrodes used, at 0°C and a potential gradient of 8.75 volts/cm.

The values of the dielectric constant changed from about 62,000 at 30 cycles to approximately

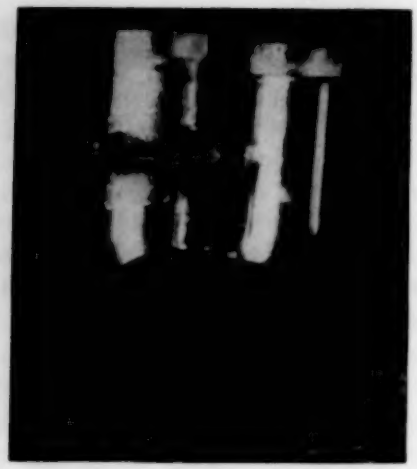

FIG. 3. Rochelle salt crystal condenser with mercury-salt solution electrodes.

FIG. 4. Rochelle salt crystal condenser with silver plated electrodes.

220 at 10^7 cycles when the mercury-salt solution electrodes were used and from about 3000 at 30 cycles to 100 at about 10^7 cycles with the silver-plated electrodes.

At a frequency of about 14×10^6 cycles a critical point was reached, after which the reactance of the crystal became inductive and remained that to the experimental limit of 30×10^7 cycles. In some cases it rose and fell again very steeply as shown in Fig. 5 before remaining negative. This critical point was independent of the physical dimensions of the crystal and of the type of electrodes used. It is accordingly of a different nature from those observed by Frayne and Errera at about 60,000 cycles.

These latter variations in the dielectric constant are due to the well-known fact that in a piezoelectric crystal the polarization produced by an applied alternating field is very appreciably altered by the accompanying piezoelectric polarization due to the deformation of the crystal. Especially large variations which resemble optical anomalous dispersion curves occur at the resonance frequencies. These frequencies depend on the dimensions of the crystal and on the velocity of sound in the crystalline medium. In our experiment the large damping and low field strength apparently prevented appreciable resonance effects of this type. According to the dimensions of our crystals these should have been located at about 50,000 cycles. The critical frequency we observed at 14×10^6 cycles was independent of the dimensions of the crystal. If it is due to any resonance effect, it must be ascribed to an internal structure of about 0.17 mm in width.

The rather large decline of the dielectric constant in the frequency range 30 to 100,000 cycles is no doubt related to the large residual-charge effect discussed by Valasek.[1b]

The large decrease in the values obtained for the dielectric constant when using the silver-plated electrodes and other electrodes with the probable exception of mercury, may be explained by assuming that during the process of silver-plating the surface of the crystal may become slightly dehydrated and that this thin dehydrated film has a low dielectric constant. From a well-known formula in electrostatics, the dielectric constant of two dielectrics in series is

$$K=K_1K_2(a_1+a_2)/(a_1K_2+a_2K_1),$$

where K_1 and a_1 are the dielectric constant and thickness, respectively, of one of the dielectrics, the crystal in this case, and K_2 and a_2 are the dielectric constant and thickness, respectively, of the other dielectric, the film. If the ratio of

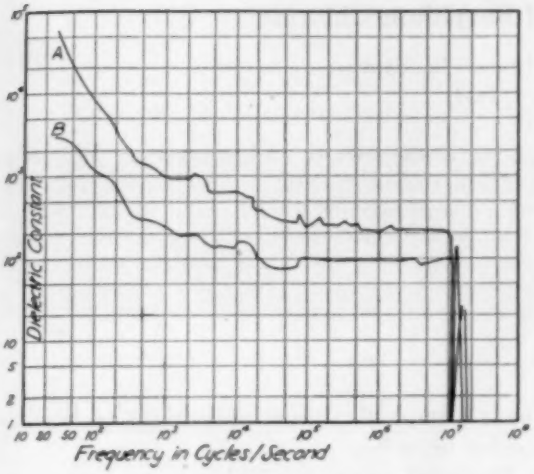

FIG. 5. Variation of dielectric constant with frequency of Rochelle salt crystal cut perpendicular to its a axis. Curve A is for mercury-salt solution electrodes and curve B for silver-plated electrodes; $t = 0°C$, potential gradient across crystal = 8.75 volts/cm.

K_1 to K_2 is very large, as is the case here, even with thin films the effective dielectric constant, K, will be considerably reduced from the large dielectric constant K_1.

With low frequencies the mercury-salt solution electrodes give higher values for the dielectric constant than other electrodes that have been tested. When these contacts are new and properly made the film effect may be assumed to be nearly eliminated. The silver-film electrodes are of value in that they form a crystal condenser whose capacitance apparently remains constant if the condenser is imbedded in some moisture proof insulating material.

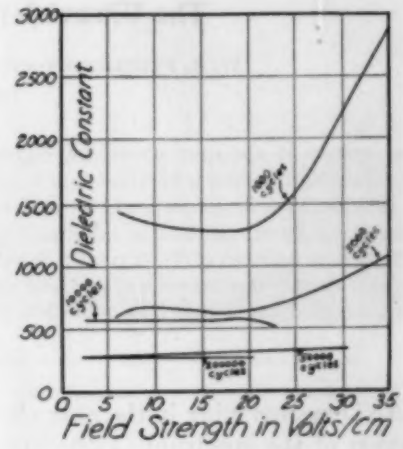

FIG. 6. Variation of dielectric constant with applied electrostatic field at various frequencies.

The dielectric constant is also a function of the field strength. For low field strengths and at low frequencies the observed variation is shown in Fig. 6. At higher frequencies and at low field strengths, the dielectric constant is very nearly independent of the field strength. At high field strengths such as 300 volts/cm or greater, and at low frequencies, Kobeko and Kurtschatov[8] found that the dielectric constant decreased with an increase in field strength.

This study was made possible by a grant from the Research Funds of the Graduate School, University of Minnesota. It is a pleasure to thank our assistants, Messrs. O. Norgorden and L. E. Norton, for constructing the apparatus and making the measurements reported in this paper.

The Ultraviolet Bands of Beryllium Chloride

W. R. FREDRICKSON AND MARTIN E. HOGAN, JR., *Syracuse University*

(Received July 7, 1934)

A band system in the near ultraviolet region (3468–3700A) is obtained by using a beryllium arc in an atmosphere of chlorine. Four heads are found for each band, the ${}^{S}R_{21}$ heads being about one-third as intense as the other heads. The system is due to a ${}^{2}\Pi-{}^{2}\Sigma$ transition with the ${}^{2}\Pi$ state an intermediate one between case **a** and case **b**. A complete rotational analysis is impossible but from the spacing of the lines in certain branches, $B' \leqq 0.8$ and $A/B \leqq 31$. The isotope effect for chlorine is observed in -1 and $+1$ sequences and the ${}^{S}R_{21}$ head of the (0,0) band. From the heats of dissociation, it appears that the electronic excitation is due to the ${}^{1}D \rightarrow {}^{1}P$ transition in the beryllium atom.

A BAND system lying in the near ultraviolet region of the spectrum (3468–3700A) was obtained by using a beryllium arc in an atmosphere of chlorine at reduced pressure. Fig. 1 shows the bands as obtained in the third order with a twenty-one foot grating. The bands are located in three groups, *a*, *b* and *c*, which form the -1, 0 and $+1$, sequences, respectively. The *b* group, which is by far the most intense, shows the three ${}^{S}R_{21}$ branches of the (0,0), (1,1) and the (2,2) bands. The other sequences (see the *a* group) also show indications of heads of similar branches.

The heads of the $BeCl^{35}$ bands are arranged in a square array in Table I. As in the case of beryllium fluoride,[1] it is possible to obtain the customary vibrational formula only for the Q_1 heads, but by adding the $\theta(v'+\frac{1}{2})(v''+\frac{1}{2})$ term[2] to the vibrational formula, expressions can be obtained which fairly well represent the R_1 and R_2 heads. The vibrational equations are as follows:

$$R_1 : \nu = 28{,}030.55 + 813.64(v'+\tfrac{1}{2}) - 1.96(v'+\tfrac{1}{2})^2 - 839.38(v''+\tfrac{1}{2}) + 7.78(v''+\tfrac{1}{2})^2 - 6.03(v'+\tfrac{1}{2})(v''+\tfrac{1}{2}),$$

$$R_2 : \nu = 28{,}008.03 + 809.06(v'+\tfrac{1}{2}) - 2.33(v'+\tfrac{1}{2})^2 - 831.14(v''+\tfrac{1}{2}) + 6.52(v''+\tfrac{1}{2})^2 - 5.54(v'+\tfrac{1}{2})(v''+\tfrac{1}{2}),$$

$$Q_1 : \nu = 27{,}970.46 + 824.19(v'+\tfrac{1}{2}) - 6.03(v'+\tfrac{1}{2})^2 - 846.58(v''+\tfrac{1}{2}) + 5.11(v''+\tfrac{1}{2})^2.$$

By adding the calculated $\theta(v'+\frac{1}{2})(v''+\frac{1}{2})$ term to the R_1 and R_2 heads given in Table I, the square array given in Table II is obtained. It can be seen from the ΔG values that this correction accounts for the wide variation in ΔG values given in Table I.

Rotational Data

The overlapping of the branches in a sequence made a complete rotational analysis impossible even with a plate taken in the fourth order with a twenty-one foot grating, but many lines near the head of the ${}^{S}R_{21}$ branch of the (0,0) band and a few near the head of the R_1 branch of the same band could be measured and assigned with certainty. In the former branch, it was possible to measure thirty-one lines and in the latter, thirteen lines. Assigning consecutive integral values of M to the lines of each group, with $M=0$ for the middle lines, the following equations were obtained for the lines by the method of least squares.

$${}^{S}R_{21} : \nu = 28{,}075.105 + 1.0024\,M - 0.0180826\,M^2,$$

$$R_1 : \nu = 28{,}006.426 + 0.909285\,M - 0.01754745\,M^2.$$

It was observed on the third and fourth order plates that there was a weak head located 0.98^{-1} cm to the red of the ${}^{S}R_{21}$ head. This weak head is undoubtedly the ${}^{S}R_{21}$ head of the corresponding $BeCl^{37}$ band. From the separation of the two heads, it is possible to obtain some

[1] Jevons, Proc. Roy. Soc. London **A122**, 211 (1929).
[2] Jevons, *Report on Band Spectra of Diatomic Molecules*, page 57.

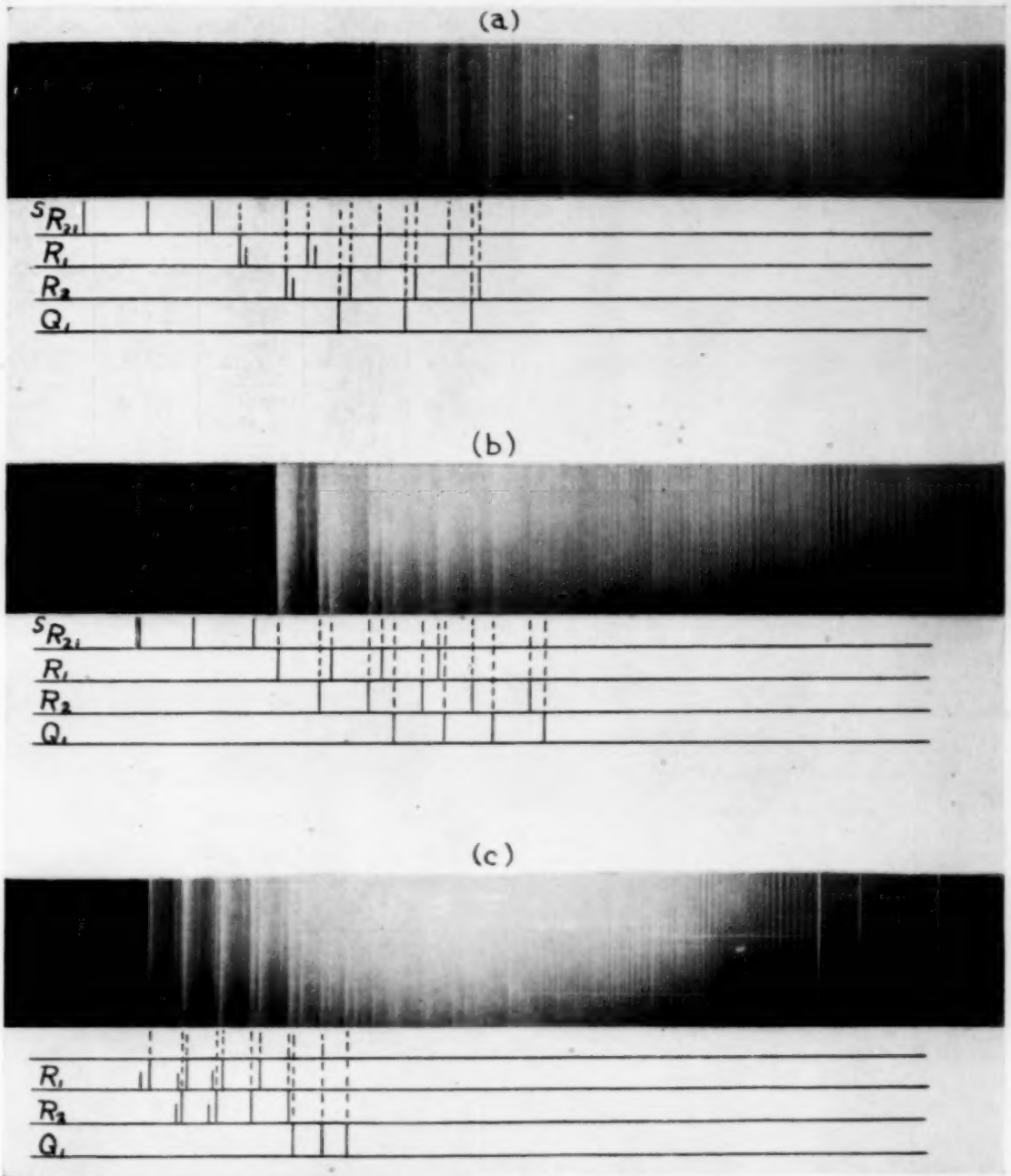

FIG. 1. The ultraviolet bands of beryllium chloride taken in the third order of a 21 foot grating, indicating the heads shown in the square array. The long lines refer to $BeCl^{35}$ heads and the short lines refer to $BeCl^{37}$ heads.

TABLE I. *Vibrational assignment of the $BeCl^{35}$ heads.*

v'	v''	0	$\Delta G''$	1	$\Delta G''$	2	$\Delta G''$	3	$\Delta G''$	4
0	SR_{21}	28088.59		———						
	R_1	28017.62	826.91	27190.17						
	R_2	27996.68	821.50	27175.18						
	Q_1	27959.04	836.04	27123.00						
1	SR_{21}	———		28058.96		———				
	R_1	28824.17	832.80	27991.37	817.40	27173.97				
	R_2	28798.44	827.02	27971.42	813.47	27158.95				
	Q_1	28771.17	836.42	27934.75	826.09	27108.66				
2	SR_{21}			———		28032.55				
	R_1			28788.18	823.36	27964.82	807.97	27156.85		
	R_2			28763.37	818.66	27944.71	802.66	27142.05		
	Q_1			28734.87	826.10	27908.77	816.07	27092.70		
3	SR_{21}					———		———		———
	R_1					28751.16	814.21	27936.95	798.93	27138.02
	R_2					28726.55	807.88	27918.67	794.61	27124.06
	Q_1					28698.99	815.93	27883.06		———
4	SR_{21}							———		———
	R_1							28710.82	802.05	27908.77
	R_2							28689.27	798.94	27894.33
	Q_1							———		———

TABLE II. *Vibrational assignment of R_1 and R_2 heads after the addition of the $\theta(v'+\frac{1}{2})(v''+\frac{1}{2})$ term.*

R_1 Heads

v' \ v''	0	$\Delta G''$	1		2		3		4	$\Delta G'$
0	28019.13		27195.24							
		823.89								809.64
1	28828.70		28004.96		27196.62					
		823.74		808.34						805.42
2			28810.83		28002.57		27209.90			
				808.26		792.67				801.38
3					28804.29		28010.94		27232.99	
						793.35		777.95		796.37
4							28805.79		28030.88	
								774.91		

R_2 Heads

v' \ v''	0	$\Delta G''$	1		2		3		4	$\Delta G'$
0	27998.04		27179.26							
		818.78								804.44
1	28802.52		27983.66		27179.35					
		818.86		804.31						799.74
2			28783.77		27978.71		27189.65			
				805.06		789.06				795.55
3					28774.15		27985.31		27214.30	
						788.84		774.01		789.69
4							28776.49		28002.51	
								773.98		

idea as to where the ν_2 origin might be. Applying the isotope relation

$$\Delta\nu = \nu' - \nu = (\rho - 1)(\nu_e) + (\rho^2 - 1)(\nu_R),$$

where $\rho = (\mu/\mu')^{\frac{1}{2}} = 0.99455$ and $\nu_e = \omega'(v' + \frac{1}{2}) - \omega''(v'' + \frac{1}{2})$. Assuming ω values from either the R or the Q branches, $\nu_e = -12$ cm^{-1} and $\nu_R = 105$ cm.

This calculation places the ν_2 origin about $\nu = 27{,}985$ cm^{-1}. Translating the above $^sR_{21}$ equation by substituting $M = J - 49$, we obtain the expression

$$^sR_{21} : \nu = 27{,}982.58 + 2.774J - 0.0180826J^2.$$

Comparing this expression with the simplified theoretical expression for the $^sR_{21}$ branch

$$\nu = \text{Constant} + 3B'J + (B' - B'')J^2 \cdots,$$

we find $B_2' = 0.925$ and $B'' = 0.943$.

Since the least squares expression for the lines of the strong R branch is very similar to that of the $^sR_{21}$, it seems most probable that these lines should be assigned to the R_1 branch. This interpretation would mean that here the R_1 and the R_2 branches cross as do the corresponding P branches in the calcium hydride band at λ6920A.[3] Assuming then, that the origin for this branch is close to the Q_1 head, we obtain by substituting $M = J - 33$ in the above least squares expression

$$R_1 : \nu = 27{,}957.3 + 2.067J - 0.01754745J^2.$$

Again, comparing this equation with the simplified theoretical expression for the R_1 branch, we have $B_1' = 0.689$ and $B'' = 0.707$.

The disagreement between the B_1' and B_2' values is extremely large and, yet, from the method of calculation it is to be expected. If a similar procedure is applied to the calcium hydride bands, we find there also a large disagreement between the B's obtained from the $^0P_{12}$ and P_2 branches,[4] but that the average value is approximately the one reported.

If the same procedure of averaging the B values be adopted for the BeCl bands above, a value of $B' \leqq 0.8$ is obtained. Then assuming that the electronic separation of the $^2\Pi$ state to be that of the two origins, 25 cm^{-1}, we find that $V = A/B = 31$.

Isotope Effect

Each strong band in the -1 and $+1$ sequence is accompanied by a weak head due to $BeCl_{37}$. In the -1 sequence the weak head falls inside the band and accurate measurements cannot be made except on the first heads. The average displacement of these heads is $= -4$ cm^{-1}. In the $+1$ sequence better measurements can be obtained but here too one can rely only on the measurements of the first heads in the group. An example of how the isotope shifts vary can be seen from the following:

(0,1) band $R_1 : \Delta\nu = 4.08$,
$R_2 : \Delta\nu = 4.31$.

(1,0) band $R_1 : \Delta\nu = -4.21$,
$R_2 : \Delta\nu = -3.70$.

This variation in shift can be qualitatively explained by assuming that the R_1 branch turns far from the origin and the R_2 not so far from the origin. In the (0,1) band, the rotational isotopic shift is opposite in direction to that due to the vibration, and hence, the R_1 shift should be less than the R_2. In the (1,0) band, however, the reverse is true for there both the rotational and vibrational shifts are negative and, hence, we should expect R_1 to have a larger displacement than the R_2.

Discussion

The number and position of the band heads indicates that the system is due to a $^2\Pi \rightarrow {}^2\Sigma$ electronic transition. Also from the facts that the $^sR_{21}$ branches have only about one-third the intensity of the other branches and that $Y = 31$, it is evident that the $^2\Pi$ state is an intermediate case between case **a** and case **b**.

As can be seen from the typical Fortrat diagrams of the $^2\Pi \rightarrow {}^2\Sigma$ transitions given by Mulliken[5] and Jevons,[3] in a case **a** type band the branches in the $^2\Pi_{1/2} \rightarrow {}^2\Sigma$ and the $^2\Pi_{3/2} \rightarrow {}^2\Sigma$ parts are similarly placed. Thus, the $^sR_{21}$ and R_1, R_2 and Q_1, Q_2 and P_1, P_2 and $^0P_{12}$, have similar appearance. In the case **b** type, however, the R_2 and R_1, Q_2 and Q_1, P_2 and P_1, branches

[3] Jevons, reference 2, page 165.

[4] Calculating from the $^0P_{12}$ branch, $B_1' = 5.44$ and from the P_2 branch $B_2' = 3.70$. The average is 4.57 which is in fair agreement with the reported value, 4.49.

[5] Mulliken, Rev. Mod. Phys. 3, 134, 138 (1931).

tend to coalesce. In an intermediate case, as shown by the calcium hydride diagram, the branches start out as in case **a** and then with increasing J values, tend toward case **b**. The beryllium chloride bands appear to follow the calcium hydride diagram and this might explain why the R_1 and R_2 branches have the $(v'+\frac{1}{2})(v''+\frac{1}{2})$ coefficients that they do. The R_1 branch turns at about $J=59$ and therefore should have a large coefficient, but the R_2 branch must turn at a relatively much lower J value and thus have a much smaller coefficient. The fact that both branches have practically the same coefficients may be due to the coalescing effect of the case **b** type; consequently, the R_1 branch tends to be drawn in and have a smaller coefficient than expected and the R_2 branch tends to be drawn out and have a larger coefficient.

The heats of dissociation of the upper and lower states, calculated in the customary way from the vibrational formula for the Q_1 heads, are 3.47 and 4.33 volts, respectively. From these values and that of the constant term in the vibrational formula, the atomic excitation comes out to be 2.59 volts which is in fair agreement with the $^1D \rightarrow P^1$ separation in beryllium of 2.70 volts. Hence, it is concluded that the electronic configurations in the upper and lower states are Be—$(2s)(3d)^1D$+Cl—$3p^5 \cdot {}^2P$ and Be—$(2s)(2p)^1P$+Cl—$3p^5 \cdot {}^2P$.

A. E. Parker[6] has recently reported another $^2\Pi \rightarrow {}^2\Sigma$ BeCl band system which lies in the yellow-green region of the spectrum. Neither state of this system is common to the ones given above but it seems quite certain that this yellow-green system has the same final state dissociation products and arises from the electronic transition of $^1S - P^1$ in the beryllium atom.

The authors wish to thank Dean Henry G. Gale and Dr. George Monk of the University of Chicago for permitting one of us to use the large grating in the Ryerson Laboratory.

[6] A. E. Parker, Phys. Rev. **45**, 752 (1934), and also in private communication.

The Vibrational Spectrum of Water Vapor

LYMAN G. BONNER, *Gates Chemical Laboratory, California Institute of Technology*

(Received June 27, 1934)

The nonlinear triatomic molecule of the type XY_2 has been treated and the expression for the energy of vibration has been obtained when second, third and fourth powers of the coordinates are considered in the potential function. The higher powers of the coordinates have been introduced by the use of first and second order perturbation theory. A method has also been outlined for treating the more complicated types of kinetic energy expressions by a perturbation method. Using the results of this treatment there have been evaluated for the water molecule, from the known spectrum, the primary binding constants and vibration frequencies for infinitesimal amplitudes. Finally, a prediction of the infrared vibration spectrum of the symmetrically substituted heavy water has been made.

INTRODUCTION

RECENTLY Adel and Dennison[1] have published a quite thorough treatment of the linear triatomic molecule of the CO_2 type, and have obtained the energy expression when higher powers of the coordinates are considered in the potential function. In this paper it is proposed to discuss the nonlinear molecule of the H_2O type from a similar standpoint. Some of the results of this treatment have already been published.[2] In the present paper the method will be more completely presented and further results will be discussed.

The present case is somewhat complicated by the fact that the kinetic energy expression is of such a form that it cannot be treated rigorously. However, it is hoped that this difficulty has been successfully surmounted by using a perturbation method.

It is desired in this article to find the form of the energy expression when the deviation of the potential field from that of a harmonic oscillator is considered. Third and fourth powers of the coordinates will be included in the potential

[1] A. Adel and D. M. Dennison, Phys. Rev. **43**, 716 (1933).
[2] L. Bonner, Phys. Rev. **45**, 496 (1934).

function. In addition, expressions will be found for the true mechanical frequencies of the molecule for infinitesimal amplitudes of vibration.

A brief outline of the method employed may now be given. First, the classical normal coordinates will be found, which, for infinitesimal amplitudes of vibration, reduce the kinetic and potential energies to sums of squares. The wave equation will then be written in terms of three coordinates having a simple significance in the molecule. The potential energy must, however, be expressed in terms of coordinates giving displacements from the equilibrium configuration, and a transformation to these displacement coordinates must be made. The normal coordinates will next be introduced and the Hamiltonian separated into three parts. The first of these will be solved rigorously, and the other two applied as perturbations.

This leads to the desired energy expression and to expressions for the mechanical frequencies of the molecule. The known spectrum of water vapor will then be used to evaluate certain of the constants of this molecule. Finally, a prediction will be made of the spectrum of the symmetrically substituted heavy water.

Classical Treatment

The kinetic energy expression for the nonlinear triatomic molecule has been given by Cross and Van Vleck;[3] and is, for the present case of a symmetric molecule,

$$T=\tfrac{1}{2}(\mu_1-A\mu_2^2r_2^2\sin^2\alpha)\dot{r}_1^2+\tfrac{1}{2}(\mu_1-A\mu_2^2r_1^2\sin^2\alpha)\dot{r}_2^2+\tfrac{1}{2}Ar_1^2r_2^2(\mu_1^2-\mu_2^2\cos^2\alpha)\dot{\alpha}^2$$
$$+(-\mu_2\cos\alpha+A\mu_2^2r_1r_2\sin^2\alpha)\dot{r}_1\dot{r}_2+A\mu_2r_1r_2\sin\alpha(\mu_1r_1-\mu_2r_2\cos\alpha)\dot{r}_1\dot{\alpha}$$
$$+A\mu_2r_1r_2\sin\alpha(\mu_1r_2-\mu_2r_1\cos\alpha)\dot{r}_2\dot{\alpha}.$$

$$1/A=\mu_1(r_1^2+r_2^2)-2\mu_2r_1r_2\cos\alpha,\qquad \mu_1=m(M+m)/(M+2m),\qquad \mu_2=m^2/(M+2m).$$

Here r_1 and r_2 represent the O−H distances, α is the angle between these two bonds, and m and M are, respectively, the masses of H and of O. For the present the potential energy expression may be taken to include all terms quadratic in the coordinates, and may be written

$$V^0=\tfrac{1}{2}a\{(\Delta r_1)^2+(\Delta r_2)^2\}+\tfrac{1}{2}b(\Delta\alpha)^2+c\Delta r_1\Delta r_2+d\Delta\alpha(\Delta r_1+\Delta r_2).$$

Displacement coordinates may now be substituted for the above r_1, r_2 and α, as follows

$$r_1=R+\rho,\qquad r_2=R+\sigma,\qquad \alpha=\beta+\varphi,$$

where R and β are the equilibrium values. If, in the coefficients of the dotted terms in T, the displacements in the coordinates may be considered negligible compared with the equilibrium values, the usual treatment by means of normal coordinates may be carried out. This gives expressions for the λ's, which are proportional to the fundamental frequencies, and also gives the substitutions which reduce T and V to sums of squares. These expressions are given below, where the ω's are the frequencies and the y's are the normal coordinates.

$$\lambda_1^2=4\pi^2\omega_1^2=(\mu_1-\mu_2\cos\beta)(a-c)/(\mu_1^2-\mu_2^2),$$

$$\lambda^2_{2,3}=4\pi^2\omega^2_{2,3}=R^{-2}(\mu_1^2-\mu_2^2)^{-1}\{b(\mu_1-\mu_2\cos\beta)+\tfrac{1}{2}R^2(\mu_1+\mu_2\cos\beta)(a+c)-2dR\mu_2\sin\beta\}$$
$$\pm R^{-2}(\mu_1^2-\mu_2^2)^{-1}[\{b(\mu_1-\mu_2\cos\beta)+\tfrac{1}{2}R^2(\mu_1+\mu_2\cos\beta)(a+c)-2dR\mu_2\sin\beta\}^2$$
$$-2R^2(\mu_1^2-\mu_2^2)\{b(a+c)-2d^2\}]^{\frac{1}{2}}.$$

λ_2^2 is taken with the positive sign.

$$\rho=y_1+y_2+y_3,\qquad \sigma=-y_1+y_2+y_3,$$
$$\varphi=\frac{-2d+\lambda_2^2R\mu_2\sin\beta}{b-\tfrac{1}{2}\lambda_2^2R^2(\mu_1+\mu_2\cos\beta)}y_2+\frac{-2d+\lambda_3^2R\mu_2\sin\beta}{b-\tfrac{1}{2}\lambda_3^2R^2(\mu_1+\mu_2\cos\beta)}y_3.$$

[3] P. C. Cross and J. H. Van Vleck, J. Chem. Phys. 1, 350 (1933).

Wave Mechanical

The assumption made above of constant coefficients in T introduces a certain amount of error, and it is desired to show here how this uncertainty may be considerably reduced, and a closer approximation obtained.

We may write the wave equation for the system under consideration in terms of the original coordinates, r_1, r_2 and α, following the method of Podolsky.[4] This gives:

$$\mu_1\left(\frac{\partial^2\psi}{\partial r_1^2}+\frac{\partial^2\psi}{\partial r_2^2}\right)+\frac{1}{Ar_1^2r_2^2}\frac{\partial^2\psi}{\partial\alpha^2}+2\mu_2\cos\alpha\frac{\partial^2\psi}{\partial r_1\partial r_2}-2\mu_2\sin\alpha\left(\frac{1}{r_2}\frac{\partial^2\psi}{\partial r_1\partial\alpha}+\frac{1}{r_1}\frac{\partial^2\psi}{\partial r_2\partial\alpha}\right)$$
$$+\frac{A}{r_1}(\mu_1^2r_2^2-2\mu_1\mu_2r_1r_2\cos\alpha+\mu_2^2r_1^2)\frac{\partial\psi}{\partial r_1}+\frac{A}{r_2}(\mu_1^2r_1^2-2\mu_1\mu_2r_1r_2\cos\alpha+\mu_2^2r_2^2)\frac{\partial\psi}{\partial r_2}$$
$$+\frac{8\pi^2(\mu_1^2-\mu_2^2)}{h^2}(W-V)\psi=0.$$

If, as before, we substitute in this expression the equilibrium positions plus the displacement coordinates, we obtain expressions involving $(R+\rho)^{-1}$, sin $(\beta+\varphi)$, etc. Although a rigorous treatment of this wave equation is impossible, a sufficiently close approximation to the true solution may probably be obtained by expanding these expressions in powers of the displacement coordinates, and neglecting all powers higher than the second. The justification of this procedure is that, at least for moderately small values of the vibrational quantum numbers, these coordinates are small in comparison with the equilibrium distances. The expressions for the normal coordinates obtained above may now be substituted, and another transformation made to remove multiplying constants, after which the wave equation takes the form:

$$\left(\frac{4\pi^2\omega_1}{h}+\frac{\omega_1}{\omega_2}a_{12}x_2^2+\frac{\omega_1}{\omega_3}a_{13}x_3^2\right)\frac{\partial^2\psi}{\partial x_1^2}+\left(\frac{4\pi^2\omega_2}{h}+\frac{\omega_2}{\omega_1}a_{21}x_1^2+a_{22}x_2^2+\frac{\omega_2}{\omega_3}a_{23}x_3^2\right)\frac{\partial^2\psi}{\partial x_2^2}$$
$$+\left(\frac{4\pi^2\omega_3}{h}+\frac{\omega_3}{\omega_1}a_{31}x_1^2+\frac{\omega_3}{\omega_2}a_{32}x_2^2+a_{33}x_3^2\right)\frac{\partial^2\psi}{\partial x_3^2}+b_{12}x_1x_2\frac{\partial^2\psi}{\partial x_1\partial x_2}+b_{13}x_1x_3\frac{\partial^2\psi}{\partial x_1\partial x_3}+b_{23}x_2x_3\frac{\partial^2\psi}{\partial x_2\partial x_3}$$
$$+c_1x_1\frac{\partial\psi}{\partial x_1}+c_2x_2\frac{\partial\psi}{\partial x_2}+c_3x_3\frac{\partial\psi}{\partial x_3}+\frac{8\pi^2}{h^2}(W-V)\psi=0,$$

where the a's, b's, and c's are constants involving the equilibrium positions, the binding constants, and the ω's. Analytical expressions for these constants will not be given, since they are quite complicated and their contribution to the energy in the present case, is small. All other powers of the x's are rejected in the coefficients, and those given are the only ones which have nonvanishing diagonals in the Hermitian matrix. The advantage of the normal coordinate substitution is that this reduces to second order magnitude the contributions of terms such as $\partial^2\psi/\partial x_1\partial x_2$ which cannot be treated rigorously and must be applied as perturbations.

We will now assume that the Hamiltonian, H, may be expanded in a power series in γ, a parameter of smallness.

$$H=H^0+\gamma H'+\gamma^2H''$$

corresponding to the expansion

$$W=W^0+\gamma W'+\gamma^2W''.$$

In H^0 we will include V^0 and those terms from the wave equation which have constant coefficients. H' contains all possible terms of V cubic in the coordinates, and H'' contains, in addition to the

[4] B. Podolsky, Phys. Rev. **32**, 812 (1928).

quartic terms of V, the terms from the wave equation containing the coordinates explicitly. If we assume the potential function to possess the same symmetry as the molecule it follows that X_1, being an odd function of the r's, may appear in V only to even powers. The terms in the expansion of H may now be written:

$$H^\circ = -\frac{h}{2}\left\{\omega_1\frac{\partial^2}{\partial x_1^2}+\omega_2\frac{\partial^2}{\partial x_2^2}+\omega_3\frac{\partial^2}{\partial x_3^2}-\omega_1x_1^2-\omega_2x_2^2-\omega_3x_3^2\right\},$$

$$\gamma H' = h\{ex_2^3+fx_3^3+gx_1^2x_2+ix_1^2x_3+jx_2^2x_3+kx_2x_3^2\},$$

$$\gamma^2H'' = -\frac{h^2}{8\pi^2}\left\{\left(\frac{\omega_1}{\omega_2}a_{12}x_2^2+\frac{\omega_1}{\omega_3}a_{13}x_3^2\right)\frac{\partial^2}{\partial x_1^2}+\left(\frac{\omega_2}{\omega_1}a_{21}x_1^2+a_{22}x_2^2+\frac{\omega_2}{\omega_3}a_{23}x_3^2\right)\frac{\partial^2}{\partial x_2^2}\right.$$
$$+\left(\frac{\omega_3}{\omega_1}a_{31}x_1^2+\frac{\omega_3}{\omega_2}a_{32}x_2^2+a_{33}x_3^2\right)\frac{\partial^2}{\partial x_3^2}+b_{12}x_1x_2\frac{\partial^2}{\partial x_1\partial x_2}+b_{13}x_1x_3\frac{\partial^2}{\partial x_1\partial x_3}+b_{23}x_3x_3\frac{\partial^2}{\partial x_2\partial x_3}$$
$$\left.+c_1x_1\frac{\partial}{\partial x_1}+c_2x_2\frac{\partial}{\partial x_2}+c_3x_3\frac{\partial}{\partial x_3}\right\}+h\{lx_1^4+mx_2^4+nx_3^4+px_1^2x_2^2+qx_1^2x_3^2+sx_2^2x_3^2\}.$$

The zeroth order equation separates, and may be solved at once, leading to the energy expression

$$W^\circ_{V_1V_2V_3} = h\omega_1(V_1+\tfrac{1}{2})+h\omega_2(V_2+\tfrac{1}{2})+h\omega_3(V_3+\tfrac{1}{2})$$

in which the V's are the vibration quantum numbers. The ψ's are then the regular Hermite functions of argument x_i. If W' is the first order perturbation energy, we have the expression

$$W'_{V_1V_2V_3} = \int H'\psi^2_{V_1V_2V_3}d\tau$$

and for the second order energy W''

$$W''_{V_1V_2V_3} = \int H''\psi^2_{V_1V_2V_3}d\tau+\sum{}'_{V_1'V_2'V_3'}\frac{\{\int\psi_{V_1V_2V_3}H'\psi_{V_1'V_2'V_3'}d\tau\}^2}{W^\circ_{V_1V_2V_3}-W^\circ_{V_1'V_2'V_3'}}.$$

Since the method of obtaining the necessary matrix elements of the Hermite functions is well known, it need not be gone into here and only the results will be given.

For the total energy of the system we obtain an expression of the form

$$W_{V_1V_2V_3} = h\{X_0+X_1V_1+X_2V_2+X_3V_3+X_{11}V_1^2+X_{22}V_2^2+X_{33}V_3^2+X_{12}V_1V_2+X_{13}V_1V_2+X_{23}V_2V_3\},$$

where the coefficients X_{ij} are given by the following equations:

$$X_0 = \tfrac{1}{2}(\omega_1+\omega_2+\omega_3)+\frac{h}{16\pi^2}\left\{\frac{\omega_1}{\omega_2}\frac{a_{12}}{2}+\frac{\omega_1}{\omega_3}\frac{a_{13}}{2}+\frac{\omega_2}{\omega_1}\frac{a_{21}}{2}+\frac{\omega_2}{\omega_3}\frac{a_{23}}{2}+\frac{\omega_3}{\omega_1}\frac{a_{31}}{2}+\frac{\omega_3}{\omega_2}\frac{a_{32}}{2}-\frac{a_{22}}{4}-\frac{a_{33}}{4}\right.$$
$$\left.-\frac{b_{12}}{2}-\frac{b_{13}}{2}-\frac{b_{23}}{2}+c_1+c_2+c_3\right\}+\tfrac{1}{4}(3l+3m+3n+p+q+s)-\frac{11e^2+g^2+k^2+6eg+6ek+2gk}{8\omega_2}$$
$$-\frac{11f^2+i^2+j^2+6fi+6fj+2ij}{8\omega_3}-\frac{g^2}{4(2\omega_1+\omega_2)}-\frac{i^2}{4(2\omega_1+\omega_3)}-\frac{j^2}{4(2\omega_3+\omega_2)}-\frac{k^2}{4(2\omega_2+\omega_2)},$$

$$X_1=\omega_1+\frac{h}{16\pi^2}\left\{\frac{\omega_1}{\omega_2}a_{12}+\frac{\omega_1}{\omega_3}a_{13}+\frac{\omega_2}{\omega_1}a_{21}+\frac{\omega_3}{\omega_1}a_{31}\right\}+\tfrac{1}{2}(3l+p+q)-g\frac{g+3e+k}{2\omega_2}-i\frac{i+3f+j}{2\omega_3}$$
$$-\frac{3g^2}{8(2\omega_1+\omega_2)}-\frac{g^2}{8(2\omega_1-\omega_2)}-\frac{3i^2}{8(2\omega_1+\omega_3)}-\frac{i^2}{8(2\omega_1-\omega_3)},$$

$$X_2=\omega_2+\frac{h}{16\pi^2}\left\{\frac{\omega_1}{\omega_2}a_{12}+\frac{\omega_2}{\omega_1}a_{21}+\frac{\omega_2}{\omega_3}a_{23}+\frac{\omega_3}{\omega_2}a_{32}+a_{22}\right\}+\tfrac{1}{2}(3m+p+s)-\frac{15e^2+6eg+6ek}{4\omega_2}-\frac{j^2+3fj+ij}{2\omega_3}$$
$$-\frac{g^2}{4(2\omega_1+\omega_2)}-\frac{g^2}{4(2\omega_1-\omega_2)}-\frac{3j^2}{8(2\omega_2+\omega_3)}-\frac{j^2}{8(2\omega_2-\omega_3)}-\frac{k^2}{4(2\omega_3+\omega_2)}-\frac{k^2}{4(2\omega_3-\omega_2)},$$

$$X_3=\omega_3+\frac{h}{16\pi^2}\left\{\frac{\omega_1}{\omega_3}a_{13}+\frac{\omega_2}{\omega_3}a_{23}+\frac{\omega_3}{\omega_1}a_{31}+\frac{\omega_3}{\omega_2}a_{32}+a_{33}\right\}+\tfrac{1}{2}(3n+q+s)-\frac{15f^2+6fi+6fj}{4\omega_3}-\frac{k^2+3ek+gk}{2\omega_2}$$
$$-\frac{i^2}{4(2\omega_1+\omega_3)}-\frac{i^2}{4(2\omega_1-\omega_3)}-\frac{j^2}{4(2\omega_2+\omega_3)}-\frac{j^2}{4(2\omega_2-\omega_3)}-\frac{3k^2}{8(2\omega_3+\omega_2)}-\frac{k^2}{8(2\omega_3-\omega_2)},$$

$$X_{11}=\frac{3}{2}l-\frac{g^2}{2\omega_2}-\frac{i^2}{2\omega_3}-\frac{g^2}{8(2\omega_1+\omega_2)}+\frac{g^2}{8(2\omega_1-\omega_2)}-\frac{i^2}{8(2\omega_1+\omega_3)}+\frac{i^2}{8(2\omega_1-\omega_3)},$$

$$X_{22}=\frac{h}{16\pi^2}a_{22}+\frac{3}{2}m-\frac{15e^2}{4\omega_2}-\frac{j^2}{2\omega_3}-\frac{j^2}{8(2\omega_2+\omega_3)}+\frac{j^2}{8(2\omega_2-\omega_3)},$$

$$X_{33}=\frac{h}{16\pi^2}a_{33}+\frac{3}{2}n-\frac{15f^2}{4\omega_3}-\frac{k^2}{2\omega_2}-\frac{k^2}{8(2\omega_3+\omega_2)}+\frac{k^2}{8(2\omega_3-\omega_2)},$$

$$X_{12}=\frac{h}{8\pi^2}\left(\frac{\omega_1}{\omega_2}a_{12}+\frac{\omega_2}{\omega_1}a_{21}\right)+p-\frac{3eg}{\omega_2}-\frac{ij}{\omega_3}-\frac{g^2}{2(2\omega_1+\omega_2)}-\frac{g^2}{2(2\omega_1-\omega_2)},$$

$$X_{13}=\frac{h}{8\pi^2}\left(\frac{\omega_1}{\omega_3}a_{13}+\frac{\omega_3}{\omega_1}a_{31}\right)+q-\frac{gk}{\omega_2}-\frac{3fi}{\omega_3}-\frac{i^2}{2(2\omega_1+\omega_3)}-\frac{i^2}{2(2\omega_1-\omega_3)},$$

$$X_{23}=\frac{h}{8\pi^2}\left(\frac{\omega_2}{\omega_3}a_{23}+\frac{\omega_3}{\omega_2}a_{32}\right)+s-\frac{3ek}{\omega_2}-\frac{3fj}{\omega_3}-\frac{j^2}{2(2\omega_2+\omega_3)}-\frac{j^2}{2(2\omega_2-\omega_3)}-\frac{k^2}{2(2\omega_3+\omega_2)}-\frac{k^2}{2(2\omega_3-\omega_2)}.$$

In spite of the apparent complexity of these expressions, they are readily solved for the ω's, leading to the result

$$\omega_1=X_1-X_{11}-\tfrac{1}{2}X_{12}-\tfrac{1}{2}X_{13},\qquad \omega_2=X_2-X_{22}-\tfrac{1}{2}X_{12}-\tfrac{1}{2}X_{23},\qquad \omega_3=X_3-X_{33}-\tfrac{1}{2}X_{13}-\tfrac{1}{2}X_{23}.$$

These equations for the ω's in terms of experimentally determinable quantities are perhaps the most important result of this analysis, since it is from these that the zeroth order binding constants in the potential energy expression are evaluated, and it is about these constants that the greatest interest centers.

Application to the Spectrum of Water Vapor

We have now obtained an expression which should fit the known vibrational energy levels of triatomic molecules to a fair degree of accuracy. We have also obtained expressions giving the true mechanical frequencies of the molecule in terms of the coefficients in this energy expression. It is desirable to check the validity of the energy formula over as wide a range as

possible in order to determine its general usefulness and the degree of reliability to be attached to the results. For this purpose the spectrum of water vapor is at present most favorable. In the case of water seventeen infrared and visible vibration-rotation bands are known, and have been measured with great care. In addition the recent work of R. Mecke,[5] Baumann and Mecke,[6] and Freudenberg and Mecke[7] on the rotational analysis of these bands should give the positions of the band centers with considerable accuracy.

The figures for the band centers have been taken from Mecke's paper, and nine of the best known bands, distributed throughout the spectrum, have been selected to determine the coefficients X_{ij}. X_0 cannot, of course, be determined in this way, since the given band positions are differences between the given energy level and the ground level.

In Table I are given the positions of the bands,

TABLE I. *Positions of vibrational bands.*

Designation $V_1\ V_2\ V_3$			Position (cm^{-1}) obs.	calc.	Designation $V_1\ V_2\ V_3$			Position (cm^{-1}) obs.	calc.
0	0	1	1595.5	1595.5*	1	2	1	12151.22	12149.8
0	0	2	3152.0	3152.0*	3	0	1	12565.01	12565.0*
0	1	0	(3600)	3604.6	1	3	0	13830.92	13830.8*
1	0	0	3756.5	3756.5*	3	1	0	14318.77	14318.8*
1	0	1	5332.3	5331.0	1	3	1	15347.91	15348.6
1	1	0	7253.0	7255.0	3	1	1	15832.47	15832.4*
1	1	1	8807.05	8810.6	1	3	2	16821.61	16827.4
1	2	0	10613.12	10613.1*	1	4	0	16899.01	16908.1
3	0	0	11032.36	11032.5*	3	2	0	17495.48	17464.7

* Indicates the band centers used in evaluating the constants.

observed and calculated, together with the designation of each in terms of the vibrational quantum numbers.

The fundamental (0, 1, 0) is not observed due to heavy overlying of that region by neighboring stronger bands, but is predicted at about 3600 cm^{-1} from combination relations. The value given above of 3604.6 cm^{-1} confirms this, and gives a more reliable figure for the actual frequency.

The check here is satisfactory, within experimental error for all cases but the last two. There is considerable doubt as to the complete correctness of the rotational analysis of these two bands, which appear very weakly in the solar spectrum. This agreement between the observed and calculated values of the band centers justifies the use of the coefficients X_{ij} in further calculation. The values of the X's which have been calculated are:

$$X_1 = 3796.0\ cm^{-1}, \qquad X_{11} = -39.5\ cm^{-1},$$
$$X_2 = 3674.8\ cm^{-1}, \qquad X_{22} = -70.2\ cm^{-1},$$
$$X_3 = 1615.0\ cm^{-1}, \qquad X_{33} = -19.5\ cm^{-1},$$
$$X_{12} = -106.1\ cm^{-1},$$
$$X_{13} = -21.0\ cm^{-1},$$
$$X_{23} = -18.9\ cm^{-1}.$$

If these quantities are substituted in the formulae of the previous section, we obtain for the ω's

$$\omega_1 = 3899.0\ cm^{-1}, \qquad \omega_2 = 3807.5\ cm^{-1},$$
$$\omega_3 = 1654.5\ cm^{-1}.$$

We are now in a position to calculate the zeroth order force constants in the potential function, from the normal coordinate expressions given earlier. However, we have only three relations from which to calculate the four constants therein assumed. The reasonable assumption may therefore be made that the constant d is small in comparison with a, b and c, and has, in this case, been taken equal to zero. The values for the equilibrium positions of the molecule have been obtained from Freudenberg and Mecke's[7] extrapolation to the vibrationless state, and were

$$\beta = 104°\ 36' \quad \text{and} \quad R = 0.9558\text{A}.$$

The equations may now be solved and we obtain

$$a = 8.233 \times 10^5\ \text{dynes/cm},$$
$$b/2R^2 = 0.376 \times 10^5\ \text{dynes/cm},$$
$$c = -0.0757 \times 10^5\ \text{dynes/cm}.$$

b is divided by $2R^2$ to give dimensional similarity.

The above values of the force constants are in fair agreement with those obtained by Van Vleck and Cross[8] by an entirely different, and somewhat less accurate method. It is also of interest to note that the constants a and b may be obtained with fair accuracy from the relation

[5] R. Mecke, Zeits. f. Physik **81**, 313 (1933).
[6] Baumann and Mecke, Zeits. f. Physik **81**, 445 (1933).
[7] Freudenberg and Mecke, Zeits. f. Physik **81**, 465 (1933).
[8] J. H. Van Vleck and P. C. Cross, J. Chem. Phys. **1**, 357 (1933).

proposed by Badger[9] between force constant and internuclear distance.

Three of the nine relations given by the X's have now been used, and it should be possible to calculate six higher order constants in the potential expression. However, it seems scarcely worth while to do this, since the additional information concerning the nature of the function would be small. It seems desirable to leave this until the nature of the interaction between rotation and vibration has been studied.

Prediction of the Spectrum of Heavy Water

It may be assumed for the present that the equilibrium positions and force constants of the water molecule are unchanged by the introduction of the hydrogen isotope of mass two. If this assumption be made we may calculate the mechanical frequencies and convergence factors of the symmetrical heavy water. Putting the changed masses in the normal coordinate expressions for the ω's given above, we find the following values

$$\omega_1 = 2865.4 \text{ cm}^{-1}, \qquad \omega_2 = 2764.7 \text{ cm}^{-1},$$
$$\omega_3 = 1209.7 \text{ cm}^{-1}.$$

The ratios of these three frequencies to the corresponding frequencies for ordinary water are rather close to 1.37. Making use of this fact, it is possible to calculate approximate values for the X_{ij}. It will be assumed that the force constants l–s appearing in H'' are small compared with the higher order constants, and that the contributions of the terms from the kinetic energy perturbation are negligible. Further, it should be noticed that due to the substitutions previously made the coefficients e–k of H' must be multiplied by terms of the order of ω^1 before the real force constants are obtained. These assumptions, then, make the factors X_{11}, X_{22}, etc., but not X_1, X_2, X_3, homogeneous functions of the order ω^2. Using the average value of the ratio of ω's given above, we see that we may expect these X's for ordinary water to be approximately $(1.37)^2$ or 1.78 times the same constants for heavy water. From these six values, and the values of the ω's, X_1, X_2 and X_3 may be readily calculated. This gives

$$X_1 = 2810 \text{ cm}^{-1}, \qquad X_{11} = -21.2 \text{ cm}^{-1},$$
$$X_2 = 2694 \text{ cm}^{-1}, \qquad X_{22} = -37.7 \text{ cm}^{-1},$$
$$X_3 = 1188 \text{ cm}^{-1}, \qquad X_{33} = -10.5 \text{ cm}^{-1},$$
$$X_{12} = -56.9 \text{ cm}^{-1},$$
$$X_{13} = -11.3 \text{ cm}^{-1},$$
$$X_{23} = -10.1 \text{ cm}^{-1}.$$

The positions of the three fundamentals so calculated are 2790, 2655 and 1180 cm^{-1}, respectively. These figures fit the band observed by Casselman[10] at 4.2μ very closely as being the first overtone of ν_3. It should be observed that there has been as yet no completely satisfactory proof that the potential function for a bond involving heavy hydrogen is the same as that for the same bond with ordinary hydrogen. In consequence, any prediction of the spectrum of heavy water is a risky procedure, and the above values are to be taken as merely provisional.

In conclusion I wish to express my thanks to Professor Richard M. Badger who proposed this problem and who has assisted in its prosecution with valuable aid and advice.

[9] R. M. Badger, J. Chem. Phys. **2**, 128 (1934).

[10] A. L. Casselman, Phys. Rev. **45**, 221 (1934).

The Infrared Spectra of the Chlorine Derivatives of Ethylene C_2H_4

TA-YOU WU,* *University of Michigan*

(Received July 23, 1934)

The infrared absorption spectra of the molecules $C_2H_3Cl_3$, cis $C_2H_2Cl_2$, trans $C_2H_2Cl_2$, C_2HCl_3, C_2Cl_4 are studied in the region between 2 and 25μ. The difference of the spectra of the two symmetric isomers is shown. An attempt is made to analyze the absorption bands observed together with the Raman spectra into the fundamental vibrations of these molecules.

INTRODUCTION

AT present the spectra of two molecules of the ethylene type, namely, ethylene and nitrogen tetroxide, are known. Next in simplicity come the chlorine derivatives of ethylene, C_2H_3Cl, cis $C_2H_2Cl_2$, trans $C_2H_2Cl_2$, C_2HCl_3, C_2Cl_4.[1] The Raman spectra of these molecules are known.[2] Of special interest is the work of Bonino and Brüll[3] who showed that the two symmetric isomers have distinctly different Raman spectra. From the difference of their geometric symmetry, one would expect their infrared absorption spectra to be different also. A study of the infrared spectra of these molecules will therefore be of some interest. As some fundamental vibrations of molecules are active in infrared absorption but are inactive in Raman scattering because of symmetry properties of the molecules, the combined data of infrared and Raman spectra may be necessary for obtaining all the fundamental vibrations of the molecules. Until now the only infrared data on these molecules are the absorption curve of C_2Cl_4 obtained by Coblentz[4] for the liquid state. In this work the vapors of these compounds were studied.

EXPERIMENTAL

In this investigation, the C_2HCl_3, C_2Cl_4, $C_2H_2Cl_2$ were obtained from the Eastman Kodak Laboratory. The cis and trans dichloroethylenes $C_2H_2Cl_2$ were separated by repeated fractional distillation, the original sample being very rich in the cis form (b.p. 60°C).[5] Another sample of the trans $C_2H_2Cl_2$ was kindly furnished by Mr. G. A. Stone who obtained an enriched portion by heating the sample in a closed tube at 240°C for twelve hours in the course of experiments on the transformation of one isomer into another. As the amount of trans $C_2H_2Cl_2$ was small, it had not been possible to obtain pure trans $C_2H_2Cl_2$ which is free from the cis form. However, by varying the amount of the cis form there is no difficulty in distinguishing between the spectra of the two forms.

The vinyl chloride C_2H_3Cl was obtained by boiling a mixture of ethylene chloride $C_2H_4Cl_2$ (1.2 dichloroethane) with sodium hydroxide solution and alcohol. The vinyl chloride generated was separated in a fractionating column.

For the preliminary survey over the whole region from 2 to about 25μ, the recording spectrometer described by Randall and Strong[6] fitted with a 60° KBr prism was used. A big cell with KBr windows contained the substance at its saturated vapor pressure at room temperature and the radiation from a Nernst glower traversed a path of about 60 cm in the cell. Thus it is not likely that any fundamental band in this region may have been overlooked. For study of the individual bands, a prism-grating spectrometer was used. Shorter cells of 10 cm long with KBr or NaCl windows contained the vapor at the desired pressure for the mapping of the envelopes of the bands.

---

* Now at National University of Peking. The work was done when holding a China Foundation Fellowship.

[1] The asymmetric isomer $CH_2 : CCl_2$ cannot be investigated on account of its ready polymerization under the action of light.

[2] Kohlrausch, *Smekal-Raman Effekt.* (1931).

[3] Bonino and Brüll, Zeits. f. Physik **58**, 194 (1929); Atti. accad. lincei **13**, 275 (1931).

[4] Coblentz, *Investigations on Infrared Spectra* (1905).

[5] There has been quite some confusion in the literature as to whether the high b.p. 60°C or the low b.p. 48°C is the cis form. By dielectric constant measurement, it is shown that the high b.p. form has a permanent moment, and hence is the cis isomer.

[6] Randall and Strong, Rev. Sci. Inst. **2**, 585 (1931).

TABLE I. *Infrared and Raman spectra of C_2H_3Cl. s, m, w denote that the band is strong, medium, weak in intensity.*

Infrared absorption band in cm^{-1}	3130 (s)		1616 (s)	1390 (s)		1300 (s)	1160 (m)	1053 (s)	910 (s)	935 (s)	719 (s)	617 (s)		
Raman scattering in cm^{-1}	3134 (s)	3036 (s)	1608 (m)		1355 (m)	1271 (m)	1186 (?)	1048 w	909 w		715 (m)	610 w	535 w	400 (s)

As the rotational lines of these molecules are too close to be easily resolved, no attempt was made to obtain the fine structure of the bands and the width of the slits of the spectrometer was so adjusted that it included a spectral interval of about 1.5–2 wave numbers in the different regions of the spectrum.

(1) Vinyl chloride

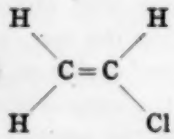

Nine regions of absorption are located at 3.2μ, 6.2μ, 7.2μ, 7.7μ, 8.62μ, 9.5μ, 10.8μ, 13.9μ, 16.2μ. Of all these, the band at 8.62μ is of medium intensity, while all the others are very intense. The band at 10.8μ is a very broad one and examination under different vapor pressures indicates that there are two bands close to each other with maxima at 10.7μ and 11.0μ. As the molecule is highly unsymmetric, little information will be obtained from the contour of the bands and they have not been examined with the grating spectrometer. A comparison of the infrared and the Raman spectra is given in Table I.

(2) Cis $C_2H_2Cl_2$

Six regions of intense absorption are observed with centers at 3.240μ, 6.28μ, 7.67μ, 11.7μ, 14.4μ and 17.55μ. The envelopes of these bands are given in Fig. 1.

(3) Trans $C_2H_2Cl_2$

Five regions of intense absorption are located with centers at 3.236μ, 8.35μ, 10.91μ, 12.20μ, 16.15μ. The envelopes of these bands are given in Fig. 2.

The infrared and the Raman spectra of these two isomers are given in Table II for comparison.

TABLE II. *Infrared and Raman spectra of cis and trans $C_2H_2Cl_2$.*

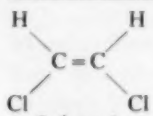 Infrared	(cis) Raman	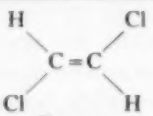 Raman	(trans) Infrared
	3161 ?	3141	
3087 s	3079 s	3079 s	3090 s
1591 s	1586 s	1581 s	
1303 s		1271 s	
	1186 s		1200 s
857 s			917 s
	714 s	846 s	
694 s			820 s
570 s	568 s	763 s	
	407 s		620 s
	173 s	251	

(4) Trichloroethylene

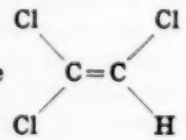

Seven regions of intense absorption are located with centers at 3.230μ, 6.4μ, 7.97μ, 10.63μ, 11.77μ, 12.76μ, 15.80μ. The envelopes of the bands and the comparison with the Raman spectra are given in Fig. 3 and Table III, respectively. The band at 6.4μ has not been examined with the grating spectrometer, for its overlapping with the strong absorption by water vapor in the atmosphere makes this difficult.

(5) Tetrachloroethylene C_2Cl_4

There are only 4 intense bands in the whole region between 2 and 25μ. They have centers at 10.95μ, 12.48μ, 12.80μ, 13.3μ. The bands at 5.6μ, 7.5μ, 9.0μ observed by Coblentz[3] for the

TABLE III. *Infrared and Raman spectra of C_2HCl_3.*

Infrared absorption bands in cm^{-1}	3096 m		1590 m			1250 m		940 s	850 s	784 s		633 s				
Raman lines in cm^{-1}		3082 s	1586 s	1385 s	1242 s		1226 w	947 w	845 w	786 m	765	628 s	449 m	381 s	274 s	212 s	165 s

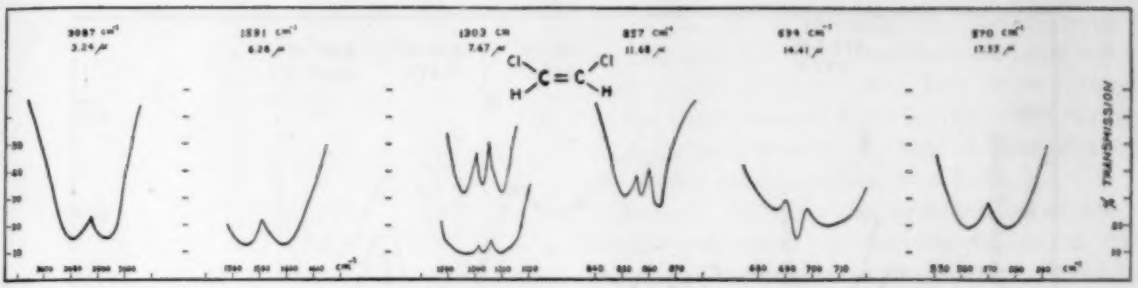

FIG. 1. Infrared absorption bands of cis $C_2H_2Cl_2$.

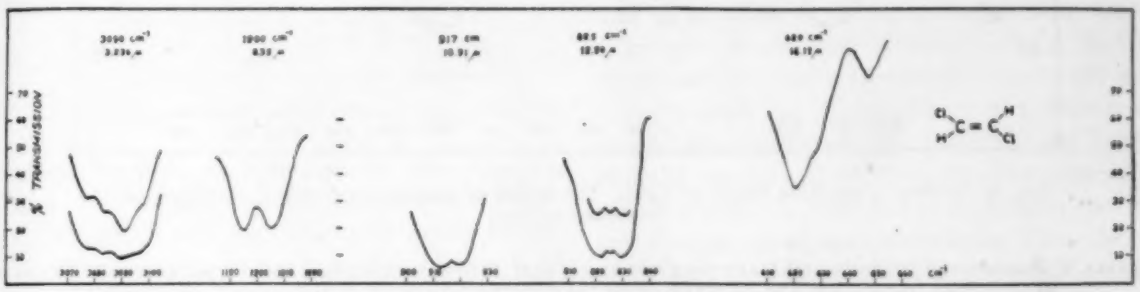

FIG. 2. Infrared absorption bands of trans $C_2H_2Cl_2$.

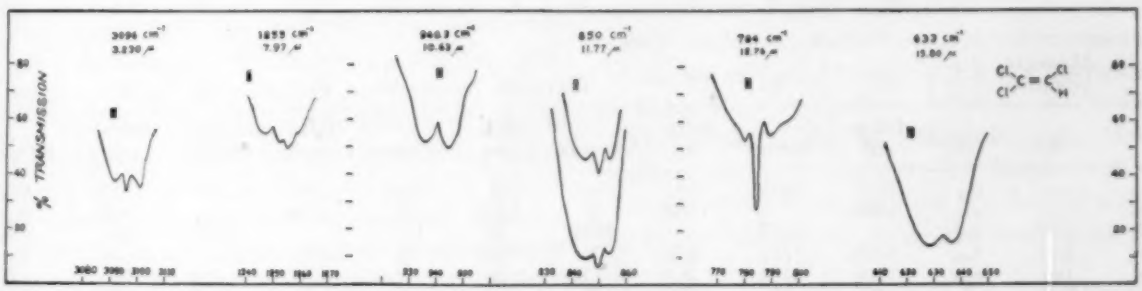

FIG. 3. Infrared absorption bands of C_2HCl_3. The width of spectrometer slits used in mapping the different bands is indicated by the shaded strips.

liquid cannot be found with radiation travelling 60 cm of path of saturated C_2Cl_4 vapor at room temperature, while the bands at 10.95μ, 12.48μ, 12.80μ show about 70 percent absorption for a path of 10 cm at 2 cm pressure. Thus it is unlikely that any one of the bands at 5.6μ, 7.5μ, 9.0μ is a fundamental band. (See Table IV and Fig. 4.)

TABLE IV. *Infrared and Raman spectra of C_2Cl_4.*

Infrared absorption in cm^{-1}		913 s	802 s	782 s	755 m					
Raman lines in cm^{-1}	1570 s					512 m	447 s	383 w	341 m	234 s

DISCUSSION

While the molecules C_2H_3Cl and C_2HCl_3 have no simple symmetry, and all the twelve fundamental vibrations are expected to be active both in infrared absorption and in Raman scattering, it is not so with cis $C_2H_2Cl_2$, trans $C_2H_2Cl_2$ and C_2Cl_4. Assuming the forms of these molecules to be that of the ethylene type[7]

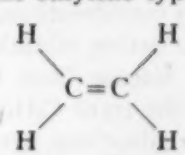

[7] The form of these molecules seems to be well established by the electron interference measurements of Weirl, Ann. d.

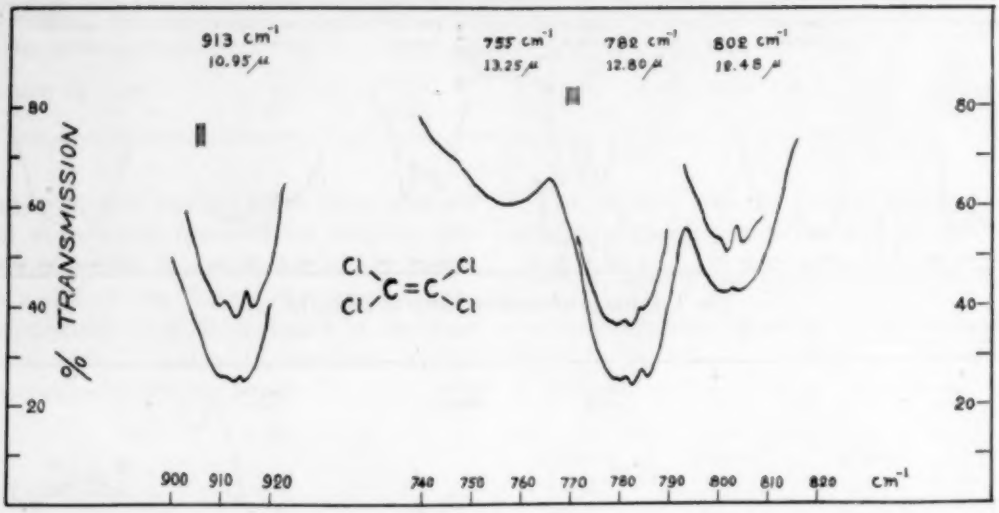

FIG. 4. Infrared absorption bands of C_2Cl_4. The width of spectrometer slits is indicated by the shaded stripes.

TABLE V. *Fundamental frequencies of the chlorine derivatives of* C_2H_4. The crosses indicate inactive infrared and inactive or weak Raman frequencies. The notations under the columns (S) and (M) are those of Sutherland[9] and Mecke, respectively.

Modes of vibration			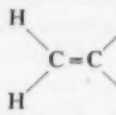		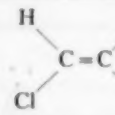		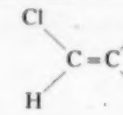		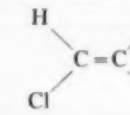		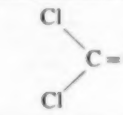	
	(S)	(M)	Infra-red	Raman	Infra-red	Raman	Infra-red	Raman	Infra-red	Raman	Infra-red	Raman
ν_1	(ν_2)	ν_{CH}	1615	1608	1591	1586	X	1581	1590	1586	X	1570
ν_2	(ν_1)	ν_{CH}	1390		1303	X	1200	X	1250		913	X
ν_3	(ν_4)	δ_{CH}		1355		1186	X	1271		1241	X	446
ν_4	(ν_3)	δ_{CH}	1300	1271	857	X	917	X				X
ν_5	(ν_8)	ν_{CCl}	1160	1186	X	714	X	763		384	X	235
ν_6	(ν_7)		617	610	X	X		X		449	X	X
ν_7	(ν_6)	ν_{CH}	3130	3134		X	X	3141	3096		X	X
ν_8	(ν_5)	ν_{CH}		3036	3087	3079	3090	X		3082	862	X
ν_9	(ν_{10})	δ_{CH}	910	909		X	X	846	850	845	X	X
ν_{10}	(ν_9)	δ_{CH}	719	715	570	568	620	X	633	628	755	X
ν_{11}	(ν_{12})	δ_{CCl_2}	1053	1048	X	X	X	X	940	947	X	X
ν_{12}	(ν_{11})	δ_{CCl_2}	935		694	X	820	X	784	786	782	X

one can easily obtain the selection rules in infrared absorption and Raman scattering for these molecules, as given in Table V. The twelve modes of vibrations are represented in Fig. 5.

From symmetry considerations, the cis $C_2H_2Cl_2$ should have nine active vibrations in infrared absorption, five intense lines in the Raman spectrum; while the trans $C_2H_2Cl_2$ should have six infrared active vibrations, five intense Raman lines. C_2Cl_4, possessing a higher symmetry, should have only five infrared active vibrations and three[8] intense Raman lines.

The assignment given in the table is partly based on mechanical considerations, partly on the shape of the envelopes of the individual bands, and on considering their relation with the

Physik 13, 453 (1932) and R. W. Dormte, Chem. Phys. 1, 566 (1933).

[8] For C_2Cl_4, the vibrations ν_7, ν_9, ν_{11} will be active in Raman scattering, according to the considerations of Placzek, Leipziger Vorträge (1931), but they are very weak and will probably not be observed experimentally. Similarly such weak lines are here considered inactive for cis and trans $C_2H_2Cl_2$.

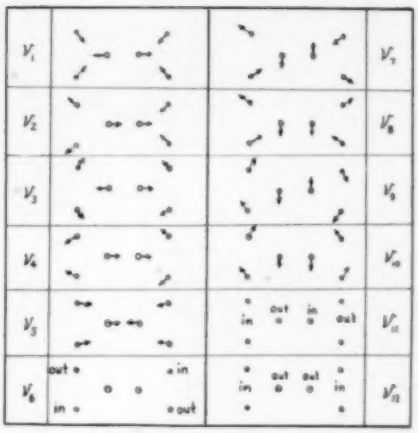

FIG. 5. Fundamental vibrations of ethylene type molecules.

Raman spectra as indicated by the selection rules. The intensity of the four observed bands of C_2Cl_4 shows that they are fundamental bands; the other active one has not been observed up to 25μ. It is possible that it lies beyond 25μ. The scarcity of lines in the Raman spectrum and the intensities of the 1570, 446, 235 cm^{-1} lines show that they are the three active frequencies ν_1, ν_3, ν_5. From electron diffraction data[7] one finds that the principal moments of inertia of C_2Cl_4 stand roughly in the ratio 2 : 1 : 1 and one would not expect the envelopes of the bands to exhibit distinct doublet structure or intense Q branch. This agrees with the observed envelopes where the insufficiently resolved maxima might not be real. This makes the distinction between ν_2, ν_4, ν_8, ν_{10} inpracticable. Assuming ν_2 is 913 cm^{-1}, a calculation for ν_4 from a relation among ν_1, ν_2, ν_3, ν_4, ν_5 obtained on the simplifying assumption that only neighboring atoms act on each other[9] gives $\nu_4 \sim 385$. This is very rough, as the force constant between the two C carbons so calculated does not agree with that obtained by similar considerations from C_2H_4.

For cis $C_2H_2Cl_2$, the principal moments of inertia calculated on electron diffraction data stand approximately in the ratio 1 : 6.5 : 7.5. Reference to Dennison's diagram[10] shows that ν_1, ν_2, ν_8, ν_{10} would possess a doublet structure and ν_3, ν_4, ν_7, ν_9 would possess something like a Q branch. In the case of trans $C_2H_2Cl_2$, as the directions of changes of electric moment do not coincide with the principal axes of moments of inertia, the above considerations no longer apply, and the assignment of the active frequencies is mainly guided by reference to its Raman spectra and the spectra of the cis molecule. The scheme in Table V may be regarded as tentative; a final assignment can be made only with the aid of additional data on the combination and harmonic bands of these molecules.

On similar considerations, the fundamental vibrations of C_2H_3Cl and C_2HCl_3 are also given in Table V.

The writer wishes to acknowledge his deep appreciation to Professor H. M. Randall whose courtesy in extending him the privilege of working in this Laboratory makes this study possible.

[9] G. B. B. M. Sutherland, Proc. Roy. Soc. **A141**, 342 (1933).
[10] D. M. Dennison, Rev. Mod. Phys. **3**, 280 (1931).

The Nuclear Mechanical Moment of Cobalt

KENNETH R. MORE, *Department of Physics, University of California, Berkeley*

(Received July 6, 1934)

The hyperfine structure of the lines λλ4191, 4234, 6082, 6231, 6450 and 6592 of the arc spectrum of cobalt has been studied. The number of components and the interval ratios give a value of $I=7/2$. The nuclear magnetic moment is estimated to be of the order of 2 to 3 small magnetons.

INTRODUCTION

THE nuclear spin of cobalt ($Z=27$, $M=59$) has been reported by Grace[1] to be probably 7/2. This value was based on a study of partially resolved hyperfine structure of the lines λ3454, $3d^84s\ {}^4F_{9/2}-3d^84p\ {}^4G_{11/2}$; λ3466, $3d^74s^2\ {}^4F_{9/2}-3d^74s4p\ {}^4G_{11/2}$ and λ3909, $3d^74s^2\ {}^4F_{9/2}-3d^74s4p\ {}^6G_{11/2}$. A value of $I=5/2$ was set as the lower limit while a value of $I=9/2$ was considered to be possible. In an attempt to determine the nuclear moment more definitely the hyperfine-structure patterns of λλ4191, 4234, 6082, 6231, 6450 and 6592 have been examined. The nuclear spin is found to be 7/2. During the course of the present investigation Kopfermann and Rasmussen[2] published a note on the hyperfine structure of the lines λλ4234 and 4268, from which they found that $I=7/2$. Their results on λ4234 are in agreement with those obtained in the present investigation.

EXPERIMENTAL

The Co I spectrum was excited in a liquid air cooled Schüler tube the hollow cathode of which was made from a cobalt rod. Argon was introduced into the tube and the pressure varied until the discharge took place entirely in the base of the tube. Discharge currents of the order of 0.2 amp. were used.

The spectrum was photographed with a three-prism flint glass spectrograph and silvered Fabry-Pérot etalons. Eastman 33 plates were used for the violet portion of the spectrum and Eastman hypersensitive panchromatic plates which were sensitized with ammonia were used for the red region. Exposure times varied from ten minutes to five hours.

RESULTS

A reproduction of a portion of a plate taken with 7.5 mm etalons is given in Fig. 1. Many of the lines are resolved into several components. Of the clearly resolved lines with uniformly degrading intensities and intervals the ones arising from transitions between levels for which $J>7/2$ show eight components. The number of components in a line arising from levels for which $J>I$ is $2I+1$ if the splitting of one of the levels is large compared with that of the other. If the

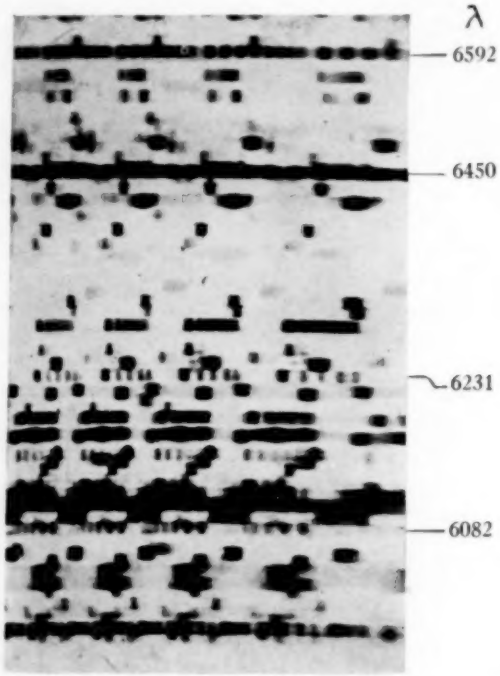

FIG. 1. Reproduction of a plate showing hyperfine structure in the red region of the Co I spectrum.

[1] N. S. Grace, Phys. Rev. **43**, 762 (1933).
[2] H. Kopfermann and E. Rasmussen, Naturwiss. **22**, 291 (1934).

levels have splittings of the same order of magnitude the off-diagonal components appear, giving more than $2I+1$ components. In such cases the intervals and intensities do not vary uniformly. The lines λλ4234, 6082 and 6592, for which $J>7/2$, show eight components of uniformly degrading intensities and intervals. This leads to the value $I=7/2$.

The mechanical moment is also determined by the application of the Landé interval rule to the hyperfine-structure intervals of any fine-structure level for which $J>1/2$. While the intervals in a line are not the same as the intervals in one of the levels from which the line arises unless the other level involved is not split, the interval ratios are nearly the same if the splitting in one level is large compared with that in the other. The intervals and interval ratios observed, together with the theoretical interval ratios for spins of 5/2, 7/2 and 9/2, are given in Table I. The theoretical values are not given for spins of 3 and 4 because integral spins have not been found for other elements of odd mass number. For several of the lines, however, the ratios observed are nearer to the theoretical values for $I=7/2$ than to those for $I=3$ or $I=4$. For most of the lines only the first four intervals can be measured with sufficient accuracy to warrant giving the interval ratios. In all cases the overall splitting is measured and its ratio to the first interval compared with the theoretical ratio.

In the following the different lines will be discussed in some detail.

λ4191, $3d^74s^2\ {}^4F_{9/2}-3d^74s4p\ {}^6F_{9/2}$, shows a flag type pattern degrading toward the red. This indicates that ${}^6F_{9/2}$ is split normally and that ${}^4F_{9/2}$ is relatively sharp. This is to be expected because the ${}^6F$ term arises from a configuration with an unbalanced s electron. In this line only the first interval and the overall splitting could be measured because of the presence of an overlapping line in the center of the pattern.

λ4234, $3d^74s^2\ {}^4F_{9/2}-3d^74s4p\ {}^6F_{11/2}$, definitely shows at least seven components and almost certainly eight. The pattern is degraded toward the red indicating that ${}^6F_{11/2}$ is split normally.

λ6082, $3d^74s4p\ {}^4F_{9/2}-3d^84s\ {}^4F_{9/2}$, shows eight components degraded toward the violet. The splitting is attributed to the $4s4p\ {}^4F_{9/2}$ level, which would thus be normal, because this is

TABLE I. *Hyperfine-structure intervals and interval ratios.*

Intervals observed cm^{-1}	Interval ratios observed	Theoretical interval ratios $I=5/2$	$I=7/2$	$I=9/2$
	λ4191	$3d^74s^2\ {}^4F_{9/2}-3d^74s4p\ {}^6F_{9/2}$		
0.116	100	100	100	100
		Overall splitting		
0.504	434	400	437	500
	λ4234	$3d^74s^2\ {}^4F_{9/2}-3d^74s4p\ {}^6F_{11/2}$		
0.137	100	100	100	100
0.120	87.7	87.5	88.9	90.0
0.109	79.6	75.0	77.8	80.0
0.095	69.4	62.5	66.7	70.0
0.08	58	50.0	55.6	60.0
		Overall splitting		
0.650	475	375	467	540
	λ6082	$3d^74s4p\ {}^4F_{9/2}-3d^84s\ {}^4F_{9/2}$		
0.111	100	100	100	100
0.097	87.4	85.7	87.5	88.9
0.083	74.8	71.1	75.0	77.8
0.071	64.0	57.1	62.5	66.7
0.06				
0.04				
		Overall splitting		
0.490	442	357	437	500

Intervals observed cm^{-1}	Interval ratios observed	Theoretical interval ratios $I=5/2$	$I=7/2$	$I=9/2$
	λ6231	$3d^84s\ {}^4P_{1/2}-3d^74s4p\ {}^4D_{3/2}$		
0.117	100	100	100	100
0.095	81.5	75.0	80.0	83.3
0.095	81.5	75.0	80.0	83.3
0.072	61.1	50.0	60.0	66.7
	λ6450	$3d^84s\ {}^4P_{5/2}-3d^74s4p\ {}^4D_{7/2}$		
0.145	100	100	100	100
0.124	85.5	83.3	85.7	87.5
0.104	71.7	66.7	71.4	75.0
0.083	57.2	50.0	57.1	62.5
		Overall splitting		
0.581	402	333	400	437
	λ6592			
0.106	100			
0.097	91.5			
0.088	83.0			
0.079	74.5			
0.072	67.9			
0.061	57.5			
0.04	38			

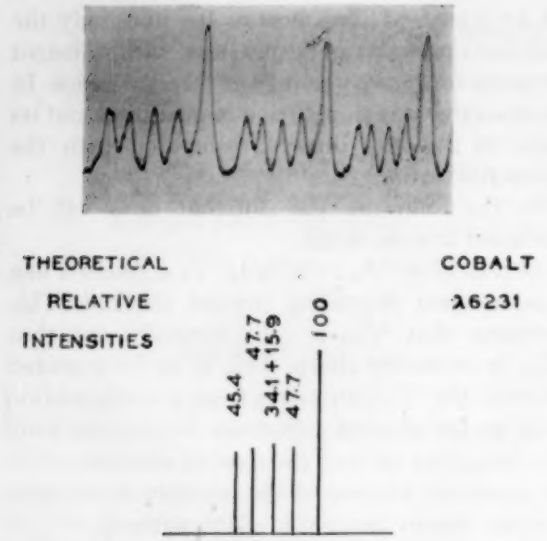

FIG. 2. Photometer curve of the hyperfine structure of λ6231.

consistent with the partially resolved structure found for λ3527, $3d^74s^2\ {}^4F_{9/2}-3d^74s4p\ {}^4F_{9/2}$, and with the structure of λλ4191 and 4234 already discussed.

λ6231, $3d^84s\ {}^4P_{1/2}-3d^74s4p\ {}^4D_{3/2}$, consists of five components. Both levels are split, the upper one being normal and the lower inverted, with the splitting of the lower level equal to the second interval of the upper. A photometer curve of this line and the pattern to be expected theoretically from the above interpretation are given in Fig. 2. The relative intensities of the components were determined by the method used by Anderson[3] in his work on the nuclear moment of lanthanum. The results agree with the theoretical values, thus checking the interpretation of the structure. The overall splittings of the levels are 0.284 cm^{-1} and 0.095 cm^{-1} for the $^4D_{3/2}$ and $^4P_{1/2}$ levels, respectively.

λ6450, $3d^84s\ {}^4P_{5/2}-3d^74s4p\ {}^4D_{7/2}$, shows several components degraded toward the red. It is certain that there are more than six components. Only the first four intervals could be measured because of the presence of an overlapping line in the tail of the pattern. The splitting is attributed to the $^4D_{7/2}$ term which would thus be normal.

λ6592 is an unclassified line for which the J values are not known. It consists of eight components, as is shown by the photometer curve in Fig. 3. Thus either I or J equals 7/2. The interval ratios are very high indicating that $I+J$ is at least 20/2. Since the results from the other lines show that $I=7/2$, definitely excluding any value as high as 11/2, the J value must be high and $I=7/2$.

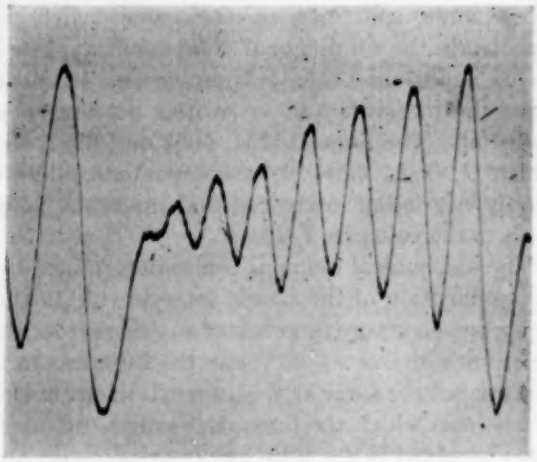

FIG. 3. Photometer curve of the hyperfine structure of λ6592.

It is thus concluded from a study of the hyperfine-structure patterns observed in the Co I spectrum that the nuclear mechanical moment of cobalt is given by $I^*h/2\pi$, where $I^*=[I(I+1)]^{\frac{1}{2}}$ and $I=7/2$.

The determination of the nuclear magnetic moment by the application of the Bacher-Goudsmit equations to the observed splittings is very inaccurate because even if all the splitting of a line is attributed to one level, it is not known what portions of the splitting are due to the s, p and d electrons. There is definite evidence that the p and d electrons, as well as the s electron, contribute an appreciable amount to the splitting. It is possible however to make an estimate of the magnitude of the magnetic moment by assuming that all the splitting is due to the s electron. If the splitting observed in λ4234 is assigned to the upper level, $3d^74s4p\ {}^6F_{11/2}$, the value of the magnetic moment is found to be 3.5 small magnetons. If there is a small splitting in the lower level the splitting in the upper level would be slightly larger or smaller than the line splitting, depending on whether the splitting of the lower level is normal or inverted. This would change the value of the magnetic moment

[3] O. E. Anderson, Phys. Rev. **45**, 685 (1934).

slightly from the value given. The other lines for which J is high give values that agree reasonably well with the above value. There seems to be little doubt but that the value found is high because an appreciable part of the splitting observed is due to the p and d electrons, while for purposes of calculation it was assumed to be due to the s electron only. Estimations of the contributions of the p and d electrons, by analogy with the results obtained in the different lines in cobalt as well as in other elements, would set as a probable value of the nuclear magnetic moment of cobalt 2 to 3 small magnetons.

In concluding I wish to thank Professor H. E. White for many valuable discussions of this problem.

The Nuclear Magnetic Moment of Lanthanum

O. E. ANDERSON, *Department of Physics, University of California, Berkeley*

(Received July 20, 1934)

The hyperfine structure of some twenty-five lines has been investigated in order to determine the absolute overall widths of each member of the $5d^26s\ {}^4F$ levels. From these a nuclear g-factor of 0.719 and a magnetic moment of 2.5 small magnetons have been computed. The Landé interval rule applied to the hyperfine structure of a three-electron configuration was found to hold. It was found that the interaction energy between the s electron and the nucleus as given by the Bacher-Goudsmit equations is not sufficient to account for the observed intervals but that the interaction energy between the d electrons and the nucleus must also be considered.

AS reported earlier,[1] the hyperfine structure of the arc spectrum of lanthanum has been investigated in order to determine the nuclear mechanical moment. All three of the independent methods, maximum number of components in a line involving sufficiently high J values, relative intervals of the hyperfine structure levels and relative intensities of the components, gave good agreement with $I=(7/2)h/2\pi$. In this investigation the h.f.s. separations, chiefly in the metastable ^4F levels, have been determined and from these absolute values the g-factor and hence the nuclear magnetic moment have been evaluated. Also it is possible from these values of the h.f.s. intervals to determine to what extent the Landé interval rule and the Bacher-Goudsmit equations apply to a three-electron configuration.

In their preliminary work, Meggers and Burns[2] found that the $5d^26s\ {}^4F$ levels of lanthanum showed wide h.f.s. whereas the normal state $5d6s^2\ {}^2D$ was relatively sharp. The widths of some twenty-five lines have now been measured in order to determine the width of each of the ^4F levels. These lines are given by transitions from the triad of quartets $^4D°$, $^4F°$ and $^4G°$ arising from the electronic configuration $5d^26p$ to the metastable $5d^26s\ {}^4F$ levels.

The apparatus and experimental procedure are explained in detail in the previous paper.[1] The plates were calibrated for intensity measurements by the use of a step-slit as described earlier. The overall width of each line was carefully measured in several orders in each pattern, then corrected for dispersion and the average value adopted.

From flag patterns, i.e., patterns in which the intensities and intervals degrade uniformly, only the sum or difference of the energy level widths can be determined very accurately unless the absolute width of one of the levels is known. To assume that one level is sharp because many components in a uniformly degrading line are clearly resolved can easily introduce an error as high as 15 percent in the value of the computed level. Hence to determine accurately the widths of the levels of a multiplet, detailed measurements must be made on at least one line which has the off-diagonal components resolved. Most of the lines measured in this investigation degrade uniformly or are only partially resolved. Fortunately, however, two lines in which the off-diagonal components are clearly resolved fix the absolute width of one of the ^4F levels.

---

[1] O. E. Anderson, Phys. Rev. **45**, 685 (1934).
[2] W. F. Meggers and K. Burns, J. O. S. A. and R. S. I. **14**, 449 (1927).

Experimental Results

Twenty-five lines involving the ^4F levels were carefully measured and the average value of each is given in Table I. The wave-lengths and classification are taken from the analysis of the arc spectrum by Russell and Meggers.[3] In the column headed "remarks" is given the number of clearly resolved components in the line, the "+" sign indicating that there is a smeared tail which could contain at least one and in some cases several more components.

In the notation adopted, the symbol Δ denotes the separation in cm^{-1} between the first and the last h.f.s. levels in a fine-structure level and it precedes the term symbol, e.g., $\Delta^4F_{9/2} = +0.55$ cm^{-1} is the overall width of the $^4F_{9/2}$ level from its lowest to its highest h.f.s. level. A positive Δ indicates that the h.f.s. levels are normal and a negative Δ that they are inverted. If the components of a line degrade towards the violet (e.g., λ5212), Δ of the lower level $-\Delta$ of the upper level is positive and *vice versa* if they degrade towards the red (e.g., λ5106), this difference is negative. Actually the Δ difference does not give the entire width of the line in some cases but since all the measurements were made from the first main component to the point where the tailing off is complete, the measured overall width gives the Δ difference in all cases accurately to within 0.02 cm^{-1} and in most cases more accuratelv.

Table I. *Overall widths of spectrum lines.*

		Remarks
λ5212	$\Delta^4F_{9/2}-\Delta^4D^\circ_{7/2} = +0.58$ cm^{-1}	7+components
5047	$\Delta^4F_{7/2}-\Delta^4D^\circ_{7/2} = +0.45$	5+
5791	$\Delta^4F_{9/2}-\Delta^4F^\circ_{9/2} = +0.47$	5+
5588	$\Delta^4F_{7/2}-\Delta^4F^\circ_{9/2} = +0.31$	2+
6007	$\Delta^4F_{9/2}-\Delta^4F^\circ_{7/2} = +0.37$	4+
5789	$\Delta^4F_{7/2}-\Delta^4F^\circ_{7/2} = +0.25$	3+
5177	$\Delta^4F_{7/2}-\Delta^4D^\circ_{5/2} = +0.38$	5+
5051	$\Delta^4F_{5/2}-\Delta^4D^\circ_{5/2} = +0.16$	2+
5789	$\Delta^4F_{7/2}-\Delta^4F^\circ_{7/2} = +0.25$	3+
5631	$\Delta^4F_{5/2}-\Delta^4F^\circ_{7/2} = 0.0$	1(sharp)
5935	$\Delta^4F_{7/2}-\Delta^4F^\circ_{5/2} = +0.24$	3+
5769	$\Delta^4F_{5/2}-\Delta^4F^\circ_{5/2} = +0.03$	1+
6617	$\Delta^4F_{7/2}-\Delta^4G^\circ_{7/2} = +0.23$	3+
6411	$\Delta^4F_{5/2}-\Delta^4G^\circ_{7/2} = 0.0$	1(sharp)
5145	$\Delta^4F_{5/2}-\Delta^4D^\circ_{3/2} = +0.14$	2+
5056	$\Delta^4F_{3/2}-\Delta^4D^\circ_{3/2} = -0.23$	3+
5769	$\Delta^4F_{3/2}-\Delta^4F^\circ_{5/2} = +0.03$	1+
5658	$\Delta^4F_{5/2}-\Delta^4F^\circ_{5/2} = -0.35$	2+
5856	$\Delta^4F_{5/2}-\Delta^4F^\circ_{3/2} = +0.17$	4+
5741	$\Delta^4F_{3/2}-\Delta^4F^\circ_{3/2} = -0.22$	2+
6693	$\Delta^4F_{3/2}-\Delta^4G^\circ_{5/2} = -0.17$	2+
6543	$\Delta^4F_{3/2}-\Delta^4G^\circ_{5/2} = -0.55$	9(exact)
6600	$\Delta^4F_{5/2}-\Delta^4P^\circ_{5/2} = -0.23$	2+
6454	$\Delta^4F_{3/2}-\Delta^4P^\circ_{5/2} = -0.62$	4+
5106	$\Delta^4F_{3/2}-\Delta^4D^\circ_{1/2} = -0.27$	5(exact)
6250	$\Delta^4F_{9/2}-\Delta^4G^\circ_{11/2} = +0.49$	7+
6394	$\Delta^4F_{7/2}-\Delta^4G^\circ_{9/2} = +0.30$	5+

[3] H. N. Russell and W. F. Meggers, Bur. Stand. J. Research 9 (RP497) (1932).

Table II. *Relative widths of adjacent ^4F levels.*

		Average
$\Delta^4F_{9/2}-\Delta^4F_{7/2}$	0.13, 0.16, 0.12	0.14 cm^{-1}
$\Delta^4F_{7/2}-\Delta^4F_{5/2}$	0.22, 0.25, 0.21, 0.23	0.23
$\Delta^4F_{5/2}-\Delta^4F_{3/2}$	0.37, 0.38, 0.38, 0.39, 0.39	0.38

The values given in Table II are obtained by taking the difference of the widths of the lines in brackets in Table I. These give the relative widths of adjacent levels in the ^4F multiplet. As soon as the absolute width of any one of these levels is determined, this table gives quite accurately the absolute values of the remaining three. From λλ5106 and 6543, $\Delta^4F_{3/2}$ can be evaluated. Immediately the widths of the remaining ^4F levels and the $^4D^\circ$, $^4F^\circ$ and $^4G^\circ$ levels are fixed. The Δ values in Table III therefore depend on the average value of $\Delta^4F_{3/2}$ as determined from λλ5106 and 6543.

Table III. *Absolute intervals between line components.*

	5106 (15 mm sep.)						
Abs.	0.085	0.064	0.068	0.041	cm^{-1}		
Rel.	5.00	(3.77)	4.00	2.41			
	6250 (8 mm sep.)						
Abs.	0.111	0.097	0.083	0.068	0.058	0.043	0.028
Rel.	8.00	6.94	5.95	4.90	4.14	3.08	2.00
	6543 (15 mm sep.)						
Abs.	0.106	0.081	0.089	0.083			
Rel.	6.00	(4.58)	5.05	(3.58)			
	(6.54)	5.00	(5.51)	3.91			
	6543 (7.5 mm sep.)						
Abs.	0.106	0.078	0.085	0.066	0.067	0.054	0.049 0.032
	6454 (12 mm sep.)						
Abs.	0.205	(first to third component)					

By using etalons with a resolving power of 500,000, λ5106, as shown in Fig. 1, is resolved into five components. The intervals and the

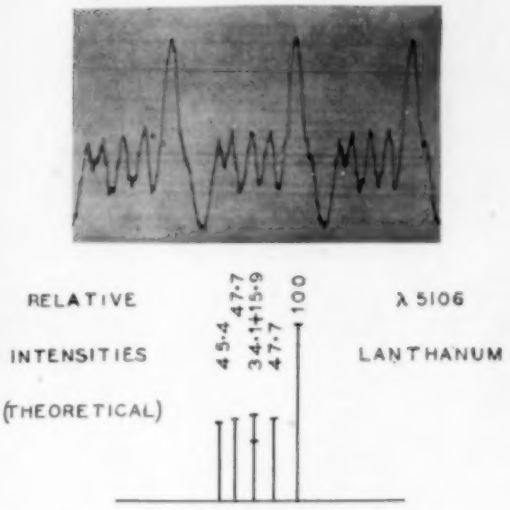

FIG. 1. Microphotometer curve and theoretical intensities of components of λ5106.

intensities of the components indicate that $\Delta^4D_{1/2}^\circ = 0.063$ cm^{-1} and $\Delta^4F_{3/2} = -0.208$ cm^{-1}. The calculated theoretical and observed intensities agree to within 4 percent. The fourth interval of λ5106, see Table III, is smaller than would be expected. Undoubtedly the peak of the fifth component is shifted towards the center of the pattern by the overlapping of the fourth component.

The overall width of $^4F_{3/2}$ can be again evaluated from λ6543, $^4F_{3/2} - {}^4G_{5/2}^\circ$, shown in Fig. 2. This line shows nine resolved components. The measured intervals and visual estimates of the intensities of the components are in good agreement with $\Delta^4F_{3/2} = -0.194$ cm^{-1} and $\Delta^4G_{5/2}^\circ = +0.355$ cm^{-1}. The eight intervals of this line are given in Table III; however, their accuracy cannot be great since the values are taken from only the two orders nearest the center of the pattern where the dispersion is changing rapidly. By using a 15 mm separator and taking an average over many orders a more accurate determination of the first four intervals was obtained. These intervals, given in Table III, along with the overall width of the line, were used to determine the values given above for $\Delta^4F_{3/2}$ and $\Delta^4G_{5/2}^\circ$.

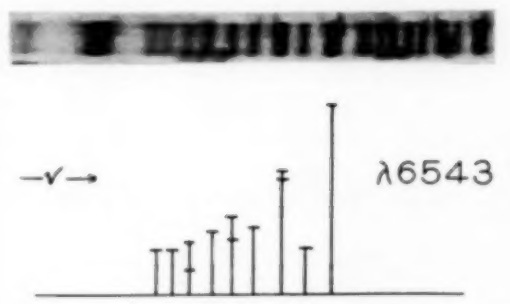

FIG. 2. Etalon pattern and theoretical pattern of λ6543.

Hence both λ5106 and λ6543 indicate that the overall width of $^4F_{3/2}$ is -0.20 ± 0.008 cm^{-1}. Measurements on the partially resolved λ6454 indicate close agreement with this same value. By using an average value $\Delta^4F_{3/2} = -0.20$ cm^{-1}, the absolute values of the remaining members of the multiplet can now be evaluated very accurately (see Table IV). These are also given in Fig. 3, with the energy levels marked "observed."

TABLE IV. *Overall widths of levels.*

$\Delta^4F_{3/2} = +0.55$	$\Delta^4D^\circ_{1/2} = -0.04$	$\Delta^4F^\circ_{9/2} = +0.09$	$\Delta^4G^\circ_{11/2} = +0.06$
$\Delta^4F_{1/2} = +0.41$	$\Delta^4D^\circ_{3/2} = +0.03$	$\Delta^4F^\circ_{7/2} = +0.17$	$\Delta^4G^\circ_{9/2} = +0.11$
$\Delta^4F_{5/2} = +0.18$	$\Delta^4D^\circ_{5/2} = +0.04$	$\Delta^4F^\circ_{5/2} = +0.16$	$\Delta^4G^\circ_{7/2} = +0.18$
$\Delta^4F_{7/2} = -0.20$	$\Delta^4D^\circ_{7/2} = +0.07$	$\Delta^4F^\circ_{3/2} = +0.01$	$\Delta^4G^\circ_{5/2} = +0.35$

THEORETICAL DISCUSSION

From the known intervals of the h.f.s. energy levels, the nuclear g-factor and magnetic moment can now be calculated. Assuming that all the interaction energy is due to the penetrating 6*s* electron, the Bacher-Goudsmit equations[4] give the relative widths of the ^4F levels as shown in the first column of Fig. 3. Qualitatively these separations are also given by the vector diagrams as suggested by White.[5] By assuming $\Delta^4F_{9/2} = +0.55$ cm as correct, the splittings of the other members will be as shown. This results in $a' = 0.141$ cm^{-1} in the interaction energy equation $\Gamma_F' = a'I^*s^* \cos(I^*s^*)$. By using this a', the g-factor can be calculated as suggested by Goudsmit.

By taking the orbital interaction into consideration much better agreement with observation is obtained. We may assume to a first approximation that this additional interaction energy is given by $\Gamma_F'' = a''L^*I^* \cos(L^*I^*)$. Now by assuming $\Delta^4F_{3/2} = -0.20$ cm^{-1} and $\Delta^4F_{9/2}$

[4] S. Goudsmit and R. F. Bacher, Phys. Rev. **34**, 1499 (1929).
[5] H. E. White, Phys. Rev. **34**, 1404 (1929).

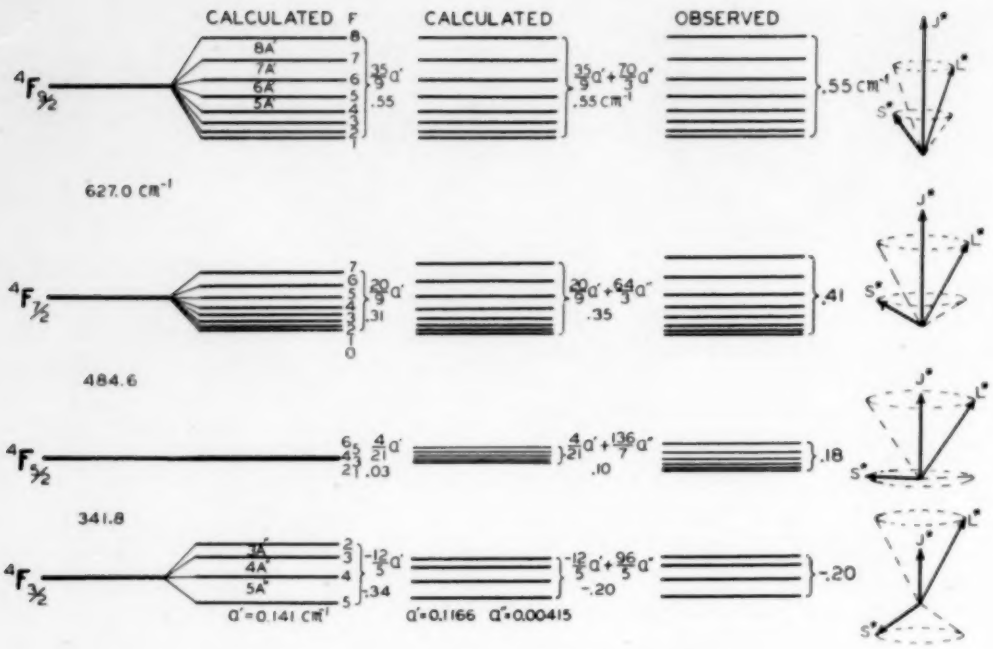

FIG. 3. Hyperfine structure in the ^4F levels.

$= +0.55$ cm^{-1} as correct, a' and a'' can be calculated. The new values computed for $\Delta^4F_{5/2}$ and $\Delta^4F_{7/2}$ are shown in the second column of Fig. 3.

Although the agreement is considerably better in this latter case, it is not yet as good as one would desire it to be. Undoubtedly, a quantum-mechanical treatment applied to the $5d^26s$ configuration will result in still closer agreement between the observed and calculated intervals. Nevertheless, from the latter value of a', a fairly good estimate of the nuclear g-factor and the magnetic moment can be made. Substituting $a' = 0.117$ cm^{-1} in Eq. (5) of Goudsmit's paper,[6] results in $g = 0.719$ and hence a magnetic moment for lanthanum of 2.5 small magnetons.

The relative values of the intervals in several lines, Table III, show that the Landé interval rule as applied to h.f.s. arising from a three-electron configuration holds to within the limits of error in this experiment. The results also show that the coupling of the penetrating $6s$ electron with the nucleus is not sufficient to account for the h.f.s. in the ^4F multiplet and that the other interactions are large enough to be taken into account.

In concluding I wish to thank Professor H. E. White for suggesting the problem and for the many helpful suggestions that he has given in connection with this work and also Professor F. A. Jenkins for many suggestions pertaining to the intensity work.

[6] S. Goudsmit, Phys. Rev. **43**, 638 (1933).

Nuclear Magnetic Moments and Their Origin

ALFRED LANDÉ, *Ohio State University*

(Received June 27, 1934)

The origin of the nuclear moments is in most cases one proton or one neutron only. The analysis of hyperfine structure leads to the following magnetic moments: proton ~ 2.0 magnetons and neutron ~ -0.6 magneton.

THE purpose of this article is to give a report on the theoretical interpretation of the observed mechanical momenta j (in units $h/2\pi$) and magnetic moments μ (in units $he/4\pi mc = 1$ nuclear magneton) of various nuclei throughout the periodic system. The theory was outlined already in a letter to the *Physical Review*[1] and applied to a group of cases. Meanwhile Tamm and Altschuler[2] extended our scheme to a new group of cases. The basic idea is this: *One* particle only, one proton or one neutron, is responsible for the total spin and the magnetic properties of the whole nucleus, the rest of it forming closed shells in general. The observed vector j is thus composed in general by the orbit l and the spin s of one particle only. Since s is known to be $\frac{1}{2}$ for the proton as well as for the neutron, l can be only $j \pm \frac{1}{2}$; hence there is no arbitrariness in this 2-vector model. This model fails, however, in some cases. The exceptions can be accounted for by the supplementary assumption of Tamm and Altschuler that here two neutrons line up their spins to $s=1$ instead of forming a closed shell $s=0$. The arbitrariness of this additional third vector $s=1$ is greatly reduced by assuming that it reappears in all cases. This theory is in contradiction to that of H. Schueler[3] who starts from the beginning with a 3-vector model taking the core as the third vector. Although Schueler uses the basic idea that one proton or one neutron is mainly responsible for j and μ beside the core, he ascribes, for instance, to the neutron a magnetic moment of -1.65 magnetons instead of Tamm-Altschulers and our value of about -0.5 or -0.6.

The theory is based on a division of all nuclei into four types belonging to different charge numbers Z and mass numbers M.

Type 1: Z even, M even. Nuclei of this type are most abundant. They consist of an *even* number of protons and an *even* number of neutrons. Since they show no mechanical momentum j and no magnetic moment μ at all we suppose them to consist of closed shells.

Type 2: Z odd, M odd. This type differs from the first one by one additional *proton* only. We suppose then that this one proton, by its orbit l and its spins, is responsible for the j and μ of the whole nucleus.

Type 3: Z even, M odd. This type differs from type 1 only by one additional *neutron*. We suppose then that this one neutron is responsible for the j and μ of the whole nucleus.

Type 4: Z odd, M even: This type differs from the closed shell type 1 by one additional neutron plus one proton. In general this type is unstable and occurs only in four instances H_2^1, Li_6^3, B_{10}^5, N_{14}^7, among them the deuton. Since here two different particles are cooperating it is not possible to obtain a unique interpretation of their j and μ values. Conversely the deuton would be the most inadequate object for an analysis of the properties of its two components. If one wants to know about the proton one has to inquire higher nuclei of type 2, and to know about the neutron one has to inquire type 3.

In some cases Tamm and Altschuler assume that one pair of neutrons does not form a closed shell. One has thus:

Type 2': Z odd, M odd, differing from the closed shell type 1 by one proton plus two neutrons. The latter are supposed to form $j_{2n}=1$ out of $s_{2n}=1$ and $l_{2n}=1$ in all cases.

Type 3': Z even, M odd, differing from type 1 by three neutrons forming $s_{3n}=\frac{3}{2}$.

[1] A. Landé, Phys. Rev. **44**, 1028 (1933).
[2] I. Tamm and S. Altschuler, Academy U.R.S.S. **1**, 455 (1934); D. Inglis and A. Landé, Phys. Rev. **45**, 842 (1934).
[3] H. Schueler, Zeits. f. Physik **88**, 323 (1934). A thorough discussion of the experimental g-values is given in Schueler's paper.

The theoretical g-values of type 2 and 3 are both taken from the generalized g-formula

$$g = g_l \frac{j(j+1)+l(l+1)-s(s+1)}{2j(j+1)} + g_s \frac{j(j+1)+s(s+1)-l(l+1)}{2j(j+1)}. \quad \text{(a)}$$

In *type 2* we put $s=\frac{1}{2}$, $l=j\pm\frac{1}{2}$, $g_l=1$. To fit the observation best one has to choose $g_s\sim 4$, according to a *magnetic moment of the proton of about* $4\cdot\frac{1}{2}=2$ *magnetons*. In *type 3* we put $s=\frac{1}{2}$, $l=j\pm\frac{1}{2}$, $g_l=0$. To fit the observation best we choose $g_s=-1.2$ according to a *magnetic moment of the neutron of* $-1.2\times\frac{1}{2}=-0.6$ *magneton*.

To calculate g in *type 2'* for $j_\tau j_{2\nu}$-coupling T. and A. first calculate separately g_τ for the proton and $g_{2\nu}$ for the neutron pair, and then insert g_τ and $g_{2\nu}$ into the formula

$$g = g_\tau \frac{j(j+1)+j_\tau(j_\tau+1)-j_{2\nu}(j_{2\nu}+1)}{2j(j+1)} + g_{2\nu} \frac{j(j+1)+j_{2\nu}(j_{2\nu}+1)-j_\tau(j_\tau+1)}{2j(j+1)}. \quad \text{(b)}$$

In most cases of type 2' there is an isotope of the same element belonging to type 2 where the two neutrons form still a closed shell. So $j_\tau s_\tau l_\tau$ and hence g_τ are fixed already. Furthermore we assume in all cases of type 2' $j_{2\nu}=s_{2\nu}=l_{2\nu}=1$, hence $g_{2\nu}=-0.6$. In *type 3'* one uses formula (a) with $s=\frac{3}{2}$ and $g_s=-1.2$ for 3 neutrons. This theory claims to represent the facts only in first order approximation. All finer traits brought about by the interaction of the one acting particle with the rest of the nucleus are neglected. It is significant nevertheless that the observed g-values can be well explained in this way, taking into account that the observed g-values claim at best 10 percent accuracy. For instance Goudsmit[4] calculated with his extrapolation formula the value $g=3.6$ for Tl and marked it even with the best grade A of accuracy, while Schueler[5] later decided for $g=2.94$ using the formula of Fermi-Segrè.[6] This may be kept in mind by judging the observed g-values graded B and C and the aim of getting better agreement between observation and theory by help of more complicated models.

To compare the theory with the observed g-values we give first the theoretical g-Tables I and II for various values of j and l. In Table I

TABLE I. *Theoretical g-values of type 2 (and type 2') using* $\mu_\tau=2.0$ *and* $\mu_\nu=-0.6$.

l \ j	1/2	3/2	5/2	7/2	9/2
0	4 *−2.133*				
1	0 *−0.8*	2 *1.306*			
2		0.4 *0.133*	1.6 *1.35*		
3			0.57 *0.44*	1.43 *1.28*	
4				0.67 *0.59*	1.33 *1.24*
5					0.73 *0.68*

TABLE II. *Theoretical g-values of type 3 (and type 3') using* $\mu_\tau=2.0$ *and* $\mu_\nu=-0.6$.

l \ j	1/2	3/2
0	−1.2	*−1.2*
1	+0.4 *−2.0*	−0.4 *−0.88*
2	*+1.2*	+0.24 *−0.24*
3		*+0.72*

the number in the upper left of each square represents type 2, where one proton alone is responsible for g and μ. The number in the lower right of each square in italics accounts for type 2', where according to T. and A. 2 neutrons participate with $s_{2\nu}=1$. In Table II the number in the upper left of each square represents type

[4] S. Goudsmit, Phys. Rev. **43**, 636 (1933).
[5] H. Schueler, Zeits. f. Physik **88**, 323 (1934).
[6] E. Fermi and E. Segrè, Zeits. f. Physik **82**, 729 (1933).

TABLE III. *Observed and theoretical g-values with $\mu_\tau = +2$ magnetons, $\mu_\nu = -0.6$ magneton.*

	j	g observed Schueler-Goudsmit		g theor.	coordination		
Li_7^3	3/2	2.19 (Breit)		2	$l_\tau = 1$		s_τ
Al_{21}^{13}	1/2	3.86	4.2 (B)	4	0		
$Cu_{63,\ 65}^{29}$	3/2	1.82	1.7 (B)	2	1		
Ga_{71}^{31}	3/2	1.82	1.7 (A)	2	1		
As_{75}^{33}	3/2		0.6 (?)	0.4	2		
Rb_{85}^{37}	5/2	0.6	0.5 (C)	0.57	3		
Rb_{87}^{37}	3/2	2.04	1.8 (C)	2	1		
Tn_{115}^{49}	9/2	1.10	1.2 (B)	1.33	4		$j = j_\tau$, $l_\tau = j_\tau \pm 1/2$; $= 1/2$ in type 2
Sb_{123}^{51}	7/2		0.7 (B)	0.67	4		
Cs_{133}^{55}	7/2	0.83		0.67	4		
$Tl_{203,\ 205}^{81}$	1/2!	2.94	3.6 (A)	4?	0?		
Bi_{209}^{83}	9/2	0.80	0.89 (A)	0.73	5		
Na_{23}^{11}	3/2	1.42		1.31	$l_\tau = 1$,	$j_\tau = 3/2$	$s_{3\nu} = l_{3\nu} =$ $j_{3\nu} = 1$ in type 2′
Ga_{69}^{31}	3/2	1.42		1.31	$l_\tau = 1$,	$j_\tau = 3/2$	
Sb_{121}^{51}	5/2	1.08	1.1 (B)	1.35	$l_\tau = 4$,	$j_\tau = 5/2$	
Au_{197}^{79}	3/2	0.15		0.133	$l_\tau = 2$,	$j_\tau = 3/2$	
Cd_{113}^{48}	1/2	−1.26	−1.33 (B)	−1.2	$l = 0$	$s = 1/2$	$s_\tau = 1/2$ in type 3, $s_{3\nu}$ in $= 3/2$ type 3′
Sn_{119}^{50}	1/2	−1.90		−2	1	3/2	
Ba_{137}^{56}	3/2	+0.63?		+0.72	3	3/2	
Hg_{199}^{80}	1/2		+1.10 (B)	+1.2	2	3/2	
Hg_{201}^{80}	3/2		−0.41 (B)	−0.4	1	1/2	
Pb_{207}^{82}	1/2		+1.20 (A)	+1.2	2	3/2	

3 where one neutron alone is responsible for j and μ. The lower right numbers in italics account for type 3′, where 3 neutrons line up their spins to $s_{3\nu} = \frac{3}{2}$. The theoretical g-values of Tables I and II are drawn as horizontal bars in Figs. 1 and 2, the normal types 2 and 3 a little more to the left than the abnormal types 2′ and 3′ for each single j. The observed g-values are represented by dots, or vertical dashes on account of their possible error of ±10 percent in most cases. The admission of the abnormal types is increasing the number of possible g-values considerably as compared with our original simple theory of types 2 and 3. Nevertheless there are so great distances between the possible g-values *for small* j that one still has a unique coordination of theory and experiment. On the other hand *for large* j the g-values of type 2′ come closer and closer to those of type 2; and in type 3′ only the cases $j = \frac{1}{2}$ and $j = \frac{3}{2}$ are realized at all.

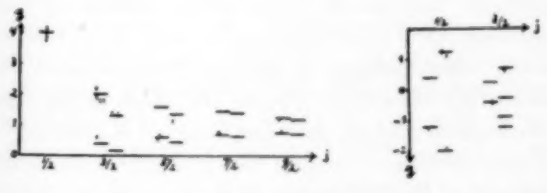

FIG. 1 and FIG. 2. Theoretical g-values of Tables I and II are drawn as horizontal bars.

Aside from every detailed interpretation there remains one main result: The proton has a magnetic moment of $\mu_\tau \sim 2$ and the neutron has a magnetic moment of $\mu_\nu \sim -0.6$, as proved by the hyperfine structure of higher nuclei. There are other determinations of μ_τ by Stern and Rabi, namely, 2.5 from molecular rays and 3.2 from atomic rays of hydrogen in inhomogeneous magnetic fields. The Rabi method in particular is a very direct and unobjectionable way of finding μ_τ, and one may wonder as to what is responsible for the difference between the two ray methods and the analysis of hyperfine structure.[7] No direct methods are known so far to determine the magnetic moment of the neutron. Scattering experiments seem to indicate that the neutron has no or only a very small magnetic moment.

[7] According to new ideas on the structure of the nucleus a proton may split up into a positron and a neutron, and the neutron may split up into an electron and a proton; then the latter proton may perhaps contain an electron and a positron less than the former proton and may also have a different magnetic moment, a very precarious hypothesis of course, which I do not want to propagate.

Table III gives a more detailed report of the g-values and their origin in various isotopes. It is of interest that the proton (type 2 and 2′) produces j and l-values that are small at the beginning of the periodic table and increase more and more with higher elements.[8] On the other hand the neutrons of type 3 and 3′ retain their small j and l-values throughout the periodic table. One may interpret this in the sense that the single proton is bound to the surface of the nucleus while the single neutrons are bound inside.

[8] Only Tl^{81} is an exception with $j=\frac{1}{2}$. This behavior makes us suspect that our scheme of type 2 and the g-formula (a) does not apply here. The experimental g-value of Tl is rather uncertain, too, depending on whether one applies the interpolation formulas of Goudsmit or of Fermi-Segrè. For these two reasons we have marked Tl in Table III with question marks and have not drawn it in Fig. 1.

Small-Angle Inelastic Scattering of Electrons in Helium, Hydrogen and Mercury

S. N. Van Voorhis, *Palmer Physical Laboratory, Princeton University*

(Received July 2, 1934)

The inelastic scattering of electrons by helium, hydrogen and mercury is measured for angles very close to the forward direction, ranging from 0° to 15° scattering. Those electrons are studied which have suffered losses of 21.1 volts, 12.6 volts and 6.7 volts, respectively, for the three gases. The initial energies range from 100 to 300 volts. The scattering per unit solid angle is found to reach a maximum at a fairly small angle and then decrease to a lower value at zero angle. The position of the maximum is a function of energy and not of momentum as predicted by the Born theory.

A PRELIMINARY report of some results on the inelastic scattering of electrons of medium energy in the region around the forward direction was made[1] at the New York meeting of the American Physical Society in 1933. Since that time Whiddington[2] and others have published results, first confirming and later failing to confirm the anomalies reported in the behavior of the scattering cross sections at very small angles. It was originally intended to continue the work with some changes in the apparatus, but this has not been possible, so the results already obtained are put on record. The gases used were helium, hydrogen and mercury, those electrons being studied which had lost 21.1 volts, 12.6 volts and 6.7 volts, respectively, in the three gases. The initial energies of the electrons were approximately 100 volts, 150 volts, 200 volts and 300 volts. The range of angles covered was about 0° to 15°.

The apparatus used is shown diagrammatically in Fig. 1. The source of electrons is a cylindrical, indirectly heated cathode. Immediately surrounding it is an electrode whose potential can be varied for focussing purposes. The main accelerating field is between the cathode and the anode. The anode is insulated from the main part of the apparatus, although at the same potential, in order that a galvanometer may be connected between them to measure the current leaving S_1. Scattering takes place in the region R. Scattered electrons go through slits S_2 and S_3 into the electrostatic analyzer,[3] A. Those of the proper energy go on through S_4 to the collector, where they are measured by a two-tube FP-54 amplifier. The dimensions of the slits are: lengths of all, 3 mm; widths, S_1, 0.15 mm, S_2, 0.14 mm, S_3, 0.28 mm, S_4, 0.27 mm. The radii of the plates of the electrostatic analyzer are 5 and 6 cm.

The part of the apparatus containing the cathode and anode is movable about an axis through O. Its movement is read on a divided circle, the readings of which, after the zero has been determined by letting the main beam pass through S_2 and S_3, give the angle of scattering of those electrons entering the analyzer. Gas is admitted to the apparatus at I and pumped out at

[1] S. N. Van Voorhis, Phys. Rev. **43**, 777A (1933).

[2] Whiddington, Emerson and Taylor, Nature **132**, 65 (1933); Poultney and Whiddington, Nature **133**, 685 (1934).

[3] Hughes and Rojansky, Phys. Rev. **34**, 284 (1929).

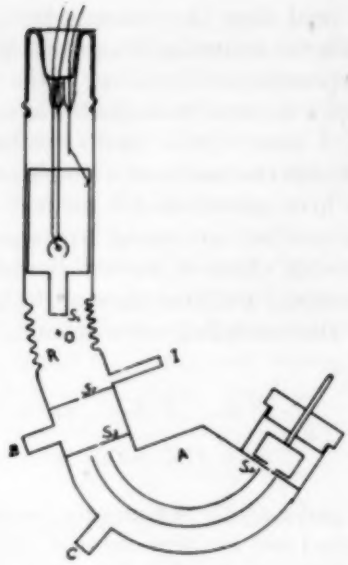

FIG. 1. Diagram of apparatus.

B between the slits and at *C* from the analyzer chamber. The pumping speeds are such that the pressure in the analyzer chamber is about 1/30 of that in the scattering region. Pressures are read on a McLeod gauge, which unfortunately had to be connected back in the gas supply system so that its readings are about twice the actual pressure in the scattering chamber. Since no attempt is made to determine absolute values of scattering cross sections, this does not matter. The pressures used range from 10^{-2} mm of Hg down in the case of hydrogen and helium. Mercury is admitted by placing ice instead of liquid air on a trap in the line to *I*.

The effective scattering volume was determined graphically. The slits S_2 and S_3 determine a wedge-shaped region from which electrons might enter the analyzer. The effective scattering volume is the intersection of this wedge and the initial beam. It was found that by proper adjustment of the potential of the focussing electrode, the beam coming out of S_1 could be made very closely parallel, the intensity half a degree away from the center of the beam being down by a factor of a thousand. Therefore the assumption was made that the initial beam is strictly parallel. The scattering volume was found to be proportional to $1/\sin\theta$, where θ is the angle of scattering, down to angles of 1 or 2 degrees, providing the apparatus is in perfect mechanical adjustment.

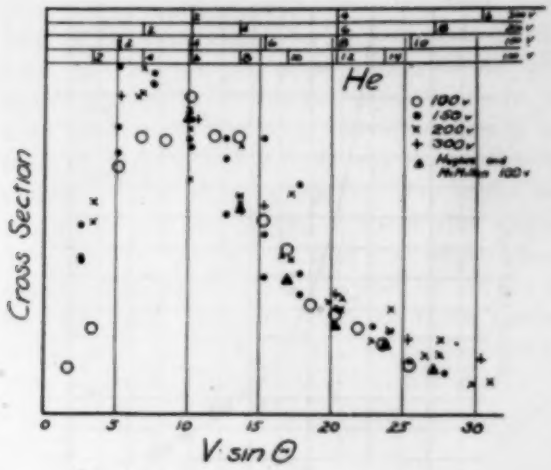

FIG. 2. Scattering in helium.

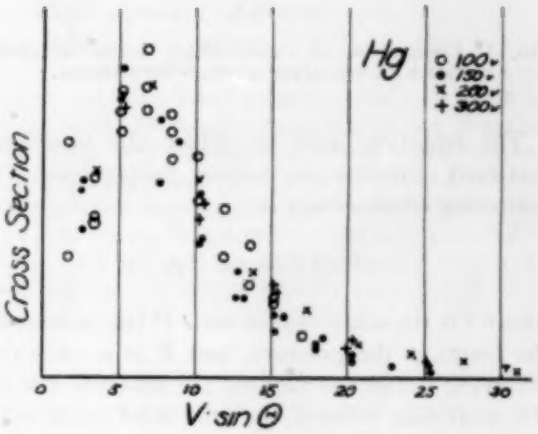

FIG. 3. Scattering in mercury.

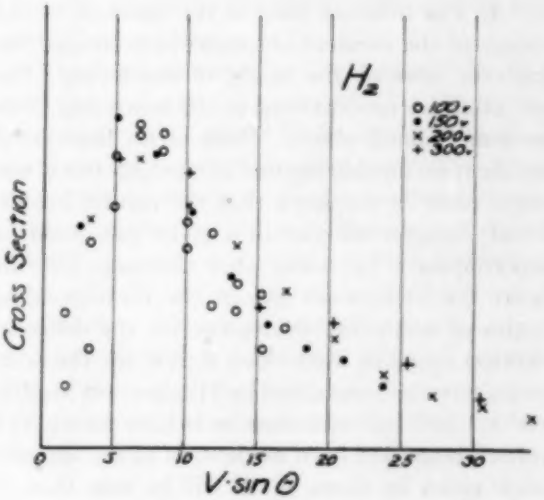

FIG. 4. Scattering in hydrogen.

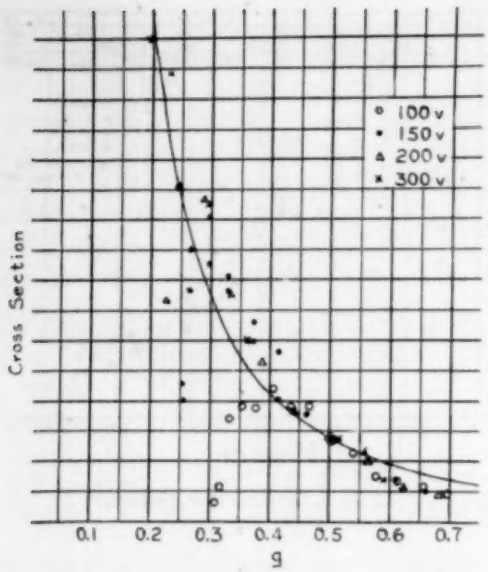

FIG. 5. Comparison of experimental scattering cross section with first approximation Born theory.

The equation used to reduce the observed scattered currents to values proportional to scattering cross section is

$$\sigma = (KI \sin\theta)/I^* p,$$

where I is the scattered current, I^* the current in the beam, p the pressure, and K is a constant involving numerical factors, the absolute size of the scattering volume, and the solid angle subtended by the collector at the scattering volume.

The results obtained are shown in Figs. 2, 3 and 4. The abscissa used is the product of the energy of the incident electrons in volts and the angle or sine of the angle of scattering. The ordinates are proportional to the scattering cross sections defined above. There is no theoretical justification for this method of plotting, but it was found early in the work that the results for different electron energies in a given gas could be superimposed by using this abscissa. On the figure for helium are shown the corresponding angles of scattering in degrees for the different electron energies used. Also shown are the scattering cross sections given by Hughes and McMillen[4] for 100 volt electrons in helium losing 21.1 volts. These have been made to fit at the smallest angle given by them, 6°. It will be seen that all the gases used show the common behavior of a maximum in the scattering at a small angle of from 2° to 6° depending on the energy of the electrons, followed by a decrease in scattering at zero angle.

In Fig. 5 some of the results for helium are compared with the results of a simple calculation using the first approximation method of Born.[5] This was carried out using hydrogenic wave functions with effective nuclear charges Z_1 and Z_2 for the initial and final state of the atom, and gives for the scattering cross section, for small values of g,

$$\sigma = \frac{2^{12}}{3}\frac{k_m}{k}\frac{Z_1 Z_2^3}{(2Z_1+Z_2)^6}\frac{\pi a^{\circ 2}}{g^2},$$

where k_m and k are $2\pi/h$ times the momentum of the scattered and incident electron, respectively, a° is the radius of the first Bohr orbit, and g is a quantity proportional to the momentum given to the atom in the encounter. It is given by

$$g = [(E^{\frac{1}{2}} - E'^{\frac{1}{2}})^2 + 4(EE')^{\frac{1}{2}} \sin^2\theta/2]^{\frac{1}{2}}$$

where E and E' are the energies of the electron before and after scattering expressed in terms of the Rydberg unit. The smooth curve in Fig. 5 is the expression const./g^2. The experimental results and the curve have been made to agree at $g = 0.5$. It will be seen that the agreement is good at angles greater than that at which the maximum of scattering is found, but that at smaller angles the results for different energies of incident electrons are definitely not in agreement with the curve. It does not seem to be clear whether or not the higher approximations of the Born theory could give such behavior.

The fact that the scattered current is proportional to the gas pressure was checked, but difficulty in reading the current in the beam prevented a check of the proportionality between it and the scattered current. It is very important in working in this region of angles, that the apparatus be lined up so that the region defined by the collecting slits S_2 and S_3, and the initial beam shall intersect on the axis of rotation. If this is not the case, the scattered currents on the two sides will not be equal, and in extreme cases, a false decrease in scattering in the forward direction will be produced. The apparatus used here was

[4] Hughes and McMillen, Phys. Rev. **44**, 20 (1933).

[5] Born, Zeits. f. Physik **38**, 803 (1926).

especially constructed to be in as good alignment as possible. Some difficulty was experienced in this work which was attributed to surface charges built up on small insulating patches. These produced random asymmetries in the scattered current, which, however, appeared and disappeared on both sides of the center. The results given here were taken when the disturbing effects were absent. It is not thought that mechanical misalignment is responsible for the results. The readings covered a space of two months, during which time the apparatus was taken apart and reassembled several times. Readings taken over this whole length of time were consistent. Also lack of alignment seem to be incapable of explaining the variation with voltage of the observed scattering. A further possible source of error lies in the fact that the apparatus is so built that the slit S_1 comes into the scattering volume at the smallest angles. This might increase the scattering volume above that calculated by the $1/\sin\theta$ rule, and also might allow electrons scattered by gas adsorbed on the slit to be registered. However, both of these causes would seem to make the scattering observed at these angles too large rather than too small.

Large Barkhausen Discontinuities and Their Propagation in Ni-Fe Alloys. II

RAYMOND E. REINHART, *Department of Physics, University of Kansas*

(Received July 9, 1934)

The relationships between longitudinal field, intensity of magnetization and velocity of propagation of large Barkhausen discontinuities have been investigated. For a constant velocity of propagation a linear relation has been found between intensity of magnetization and longitudinal field. The curves relating velocity and intensity of magnetization for a fixed value of longitudinal field resemble velocity-longitudinal field curves. The relationships between longitudinal field, circular field and the directions of strain axes have been investigated for pure nickel wire under combined torsional and tensile stresses. It has been found that only the component of field in the direction of maximum compression affects the velocity of propagation. The behavior of propagation phenomena for pure nickel is just the reverse of that observed for a 10 percent Ni-Fe alloy. This difference is probably related in some way to the difference in magnetostrictive properties of the two wires.

I. INTRODUCTION

IN a Letter to the Editor of the *Physical Review* the writer[1] reported briefly some further results concerning the propagation of large Barkhausen discontinuities in Ni-Fe alloy wires. These results included experimental investigations of the dependence of the velocity of propagation upon intensity of magnetization and also investigations of the relationship between longitudinal field, circular field, direction of maximum strain and velocity of propagation for pure nickel wire. The purpose of the present paper is to present more completely the experimental data regarding those results.

II. APPARATUS AND SYMBOLS

The apparatus used for velocity of propagation measurements was the same as for some previous investigations of propagation phenomena.[2] Intensity of magnetization measurements were made by a fixed point method in which the air field was completely balanced out by means of a variable mutual inductance in the primary and secondary circuits.

The symbols denoting the magnetic fields referred to in the following will be the same as those previously used.[2] These symbols are: H, the longitudinal magnetic field produced by a magnetizing solenoid; H_c the circular field (always specified at the surface of the wire) produced by sending a direct current through the wire; H_0, the critical field or the field corresponding to zero velocity of propagation.

The convention previously adopted[2] regarding the directions of the circular field relative to the strain axes will also be used here. This convention requires that a circular field in such a direction

[1] R. E. Reinhart, Phys. Rev. **45**, 342 (1934).

[2] R. E. Reinhart, Phys. Rev. **45**, 420 (1934).

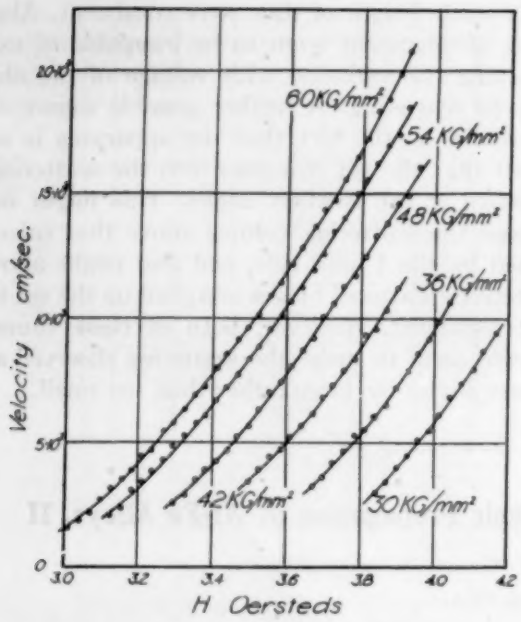

FIG. 1. A set of velocity-longitudinal field curves for various fixed values of tensile stress. The curves are for a cold drawn 10 percent Ni-Fe alloy wire.

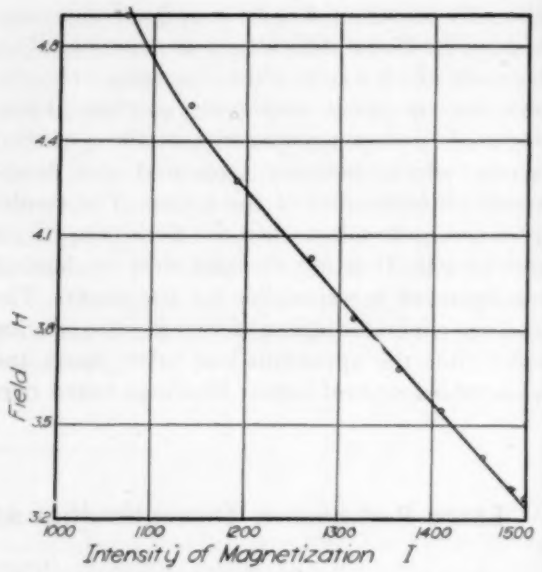

FIG. 2. A curve showing the relationship between longitudinal field and intensity of magnetization for a constant velocity of propagation. The curve is for a cold drawn 10 percent Ni-Fe alloy wire.

that its component along the direction of maximum elongation has the same sense as the component of longitudinal field in that direction will be considered positive.

III. RESULTS

A set of velocity-longitudinal field curves for various tensile stresses is shown in Fig. 1. These curves are for a cold drawn 10 percent Ni-Fe alloy wire 0.0334 cm in diameter. The striking thing about this set of curves is that the shift of the curves relative to the field axis with changes in tension tends definitely to saturate with tension. This behavior differs from that for 15 percent Ni-Fe Wires such as were used by Sixtus and Tonks.[3] They found for the 15 percent wire that the critical field strength H_0 varied approximately as the reciprocal of the tensile stress.

Hysteresis loops taken for the same 10 percent Ni-Fe wire and for the same tensile stresses as were the curves in Fig. 1 showed a similar behavior with increasing tensile stress. That is the change in height of the hysteresis loop with increase in tensile stress was found also to saturate with tension. This seemed to be a suggestion that the position of the velocity field curves relative to the field axis was a function of the intensity of magnetization. In order to investigate this point the relationship between longitudinal field and intensity of magnetization was determined for a constant velocity. The curve relating I and H is shown in Fig. 2. Since the curves in Fig. 1 are approximately parallel a curve similar to that in Fig. 2 should also be obtained between the critical field values or the field values for zero velocity and intensity of magnetization. The relation between I and H for a constant velocity is accurately linear except at lower values of I, i.e., for small tensile stresses.

For a 70 percent Ni-Fe wire the velocity field characteristics were found to shift very little with respect to the field axis with large changes in tensile stress.[4] It was found that the changes in intensity of magnetization for this wire, with changes in tensile stress were very small, only some three or four percent. A linear relationship between H and I for a constant velocity was also found for some pure nickel wires under combined torsion and tension. In the case of pure nickel, however, I decreases with increase in tensile

[3] K. J. Sixtus and L. Tonks, Phys. Rev. **37**, 930 (1931).

[4] Reference 2, p. 424.

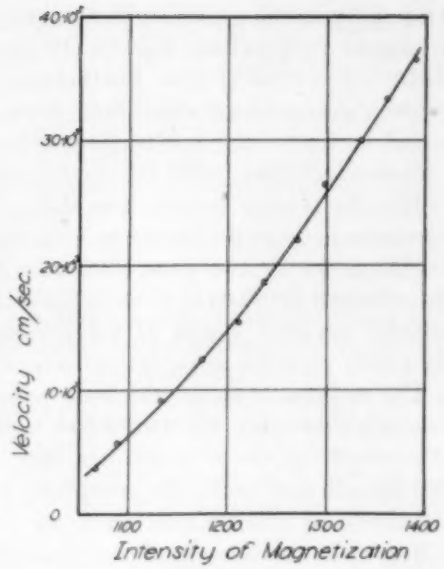

FIG. 3. A curve showing the manner of variation of velocity of propagation with intensity of magnetization for a constant longitudinal field.

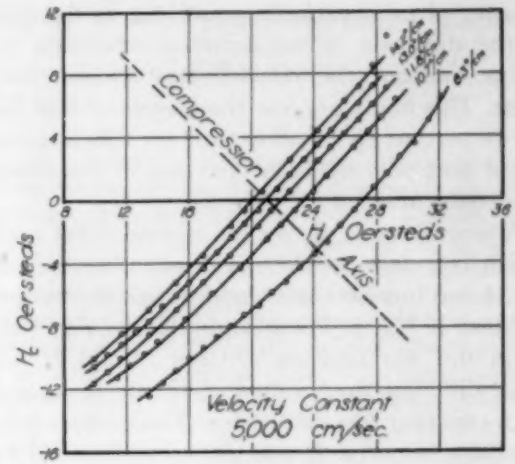

FIG. 4. A set of curves relating H and H_e for a constant velocity of propagation and for various fixed torsional stresses. The relationships are for a pure nickel wire.

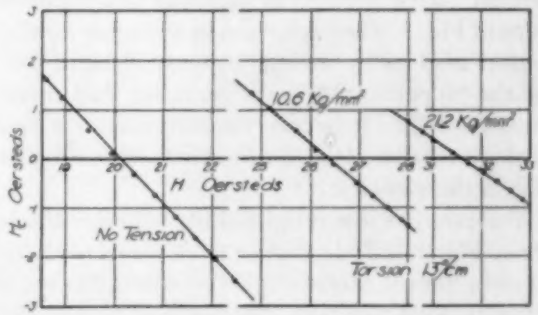

FIG. 5. A set of linear relationships between H and H_e for a constant torsional stress and for various fixed values of tensile stress. These relationships are for a pure nickel wire.

stress which requires that H be increased in order that the velocity of propagation remain constant, when the tension is increased. A linear relation was also found to exist between H and I for a given velocity for 15 percent Ni-Fe wire.

The relationship between velocity of propagation and intensity of magnetization was investigated for the 10 percent Ni-Fe wire. A typical curve showing the manner of variation of velocity with I is shown in Fig. 3. To obtain this curve H was held constant and I varied by means of changing the tensile stress. The curve thus obtained relating intensity of magnetization and velocity resembles closely those relating velocity and field in Fig. 1.

Some investigations into the relationships existing between H, H_e and applied stress, similar to those previously carried out for a 10 percent Ni-Fe wire,[5] were carried out for some commercially pure nickel wire 0.0321 cm in diameter. Before large discontinuities could be obtained with this wire it was found necessary to first subject it to a tensile stress somewhat beyond its elastic limit so that the length of the wire would increase some 15 percent. When this stress was removed and the wire subjected to torsional stress large discontinuities were obtained in which the change in magnetization was some 97 percent of the total change in magnetization between saturation in the two directions.

A set of curves showing the relationship between H and H_e for various fixed values of torsional stress and all for a constant velocity of 5000 cm/sec. is shown in Fig. 4. These curves are for a length of nickel wire treated as described above. In taking the data for the curves no tensile stress was applied beyond that just necessary to hold the wire straight along the axis of the magnetizing solenoid.

The point of significance in connection with the curves of Fig. 4 is that it is only the component of the resultant magnetic field along the direction of maximum compression which affects the

[5] Reference 2, p. 422 and 423, Figs. 3, 4 and 5.

velocity of propagation, i.e., so long as the field in the direction of maximum compression remains constant the velocity also remains constant. This finding is just the reverse of that for the 10 percent Ni-Fe alloy wire[6] for which it was found that only fields in direction of maximum elongation affected the velocity.

A second set of curves for a pure nickel wire, which corroborates the conclusion drawn from Fig. 4 and furnishes some additional information is shown in Fig. 5. The straight lines of Fig. 5 are again the relationships between H and H_c for three different fixed values of tensile stress and for a constant torsional stress. These linear relationships between H and H_c were obtained by eliminating velocity from velocity-circular field and velocity-longitudinal field curves in a manner similar to that carried out for the 10 percent Ni-Fe wire.[7] The straight line relationships of Fig. 5, when analyzed in a manner similar to that used for the analogous set of straight lines for the 10 percent Ni-Fe wire, again lead to the conclusion that it is only the component of field in the direction of maximum compression which affects the velocity.

The straight line relationships between H and H_c in Fig. 5 shift to higher field values with increasing tensile stress while the analogous set of straight lines for the 10 percent Ni-Fe wire shifted toward lower field values. This behavior demands, of course, that for a pure nickel wire under torsion an increase in tensile stress would cause the velocity-longitudinal field curves to shift to higher field values. For the 10 percent Ni-Fe wire the reverse is true. Furthermore the slope of the velocity-longitudinal field curves, for pure nickel under torsion and tension, decreases as the tension increases, while for the 10 percent Ni-Fe alloy the reverse is true. The shift of the characteristics in opposite directions with respect to the field axis for the two wires when the tensile stress is increased is to be expected because of the relationships between I and H for a constant velocity which were discussed in connection with Fig. 2. The changes in slope which the velocity-field characteristics for the two wires undergo when the tensile stress is varied are also to be expected since in pure nickel the compression axis is the direction in which a field produces a maximum effect upon the velocity of propagation and in the 10 percent Ni-Fe wire the axis of elongation is the important one.

The difference in behavior of propagation phenomena in the pure nickel and 10 percent Ni-Fe alloy wires seems to be related to their magnetostrictive properties, since these are opposite in sign. All wires having the same magnetostrictive properties do not, however, seem to have the same properties as regards propagation. The curves of Sixtus and Tonks[8] for a 25 percent Ni-Fe wire behave as does pure nickel which would seem to indicate a negative magnetostriction whereas magnetostriction is positive for this alloy.

[6] Reference 2, p. 421, Fig. 2.
[7] Reference 2, p. 423, Fig. 5.
[8] Reference 3, p. 954, Fig. 18.

Spectral Multiplets Belonging to Configurations of the Type d^k ms and d^k msns

ROBERT A. MERRILL, *Department of Physics, University of Wisconsin*

(Received July 27, 1934)

The Dirac vector model, as considered by Van Vleck, has been applied to calculate the energy values of configurations of the type d^k ms and d^k msns, in cases where the d^k core conforms to Russell-Saunder's coupling. The spin-orbit energy is not assumed small compared to the electrostatic energy coupling d^k to ms or d^k to ns. Johnson's formulas for the four vector problem have been used to set up a general secular determinant for configurations of the type d^k msns. The special cases where d^k msns may be treated as a three vector problem or as a case of Russell-Saunder's coupling are also considered. The following multiplets have been examined: Y I, $4d(^2D)5s6s$; Cu I, $3d^9(^2D)4s5s$; Zr I, $4d^2(^3F)5s6s$; Ni I, $3d^8(^3F)4s5s$; Co I, $3d^7(^4F)4s5s$; Fe I, $3d^6(^5D)4s5s$; and Ti I, $3d^2(^3F)4s6s$. The exchange integrals are considered as parameters and chosen to give the best fit with experimental data. The agreement with experiment for d^k msns is better, as it ought to be, with the four vector problem ($\mathbf{L}_d$, $\mathbf{S}_d$, $\mathbf{s}_m$, $\mathbf{s}_n$) than with the three vector problem ($\mathbf{L}_d$, $\mathbf{S}_{d+m}$, $\mathbf{s}_n$) which in turn agrees better with experiment than does the two vector problem ($\mathbf{L}_d$, $\mathbf{S}_{d+m+n}$), the case resulting from the assumption of Russell-Saunder's coupling. Configurations d^k ms (other than Houston's singlet-triplet case) have been examined as a three vector problem ($\mathbf{L}_d$, $\mathbf{S}_d$, $\mathbf{s}_m$). Some examples treated are: Ti II, $3d^2(^3F)5s$; Ni II, $3d^8(^3F)5s$; Co I, $3d^8(^3F)5s$; Co I, $3d^8(^3F)4s$; Pd II, $4d^8(^3F)6s$; Fe I, $3d^7(^4F)5s$; Co II, $3d^7(^4F)5s$.

§1. INTRODUCTION

THE convenience of the Dirac vector model in the study of complex spectra has been revealed by J. H. Van Vleck.[1] According to this model the electrostatic exchange energy of interaction between any two electrons will be proportional to the scalar product of their spin vectors. Van Vleck showed among other things that if s electrons are added to a d^k core for which the orbital and spin angular momenta of the core have a meaning, the resulting configurations may very easily be handled by the Dirac vector model. However, this would not be the case if anything other than s electrons were added to the d^k core.

§2. THE THREE VECTOR PROBLEM APPLIED TO d^k ms

For configurations of the type d^k ms we will consider the interaction of the three vectors $\mathbf{L}$, $\mathbf{S}_d$ and $\mathbf{s}_m$, where $\mathbf{L}$ and $\mathbf{S}_d$ refer to the orbital and spin angular momenta of the core, and $\mathbf{s}_m$ refers to the spin vector of the ms electron. The quantum number L will be the same for the d^k core as for the complete configuration d^k ms, since the orbital angular momentum l for s electrons equals zero. This vector method, illustrated in Fig. 1, is applicable only if L and S_d have a meaning; i.e., if the ion core d^k conforms to Russell-Saunder's coupling. Whether this is true may be tested by noting whether the d^k configuration follows Landé's interval rule or not. If it does, the spin S_d of the core d^k as well as the total spin S of the configuration d^k ms will be good quantum numbers. It will not be supposed that the spin-orbit energy of the core is small compared to the electrostatic energy coupling d^k to ms. The magnetic energy of interaction between the ms electron and the d^k core is neglected; or, in other words, we neglect (in the usual fashion) the coupling between a given orbit of the core and the spin of the ms orbit. Since Van Vleck[1] has shown that the electrostatic exchange energy of interaction of an ms electron with the d^k core is proportional to the scalar product of their respective spin vectors the Hamiltonian will be of the form,

$$\mathcal{H} = E + A(\mathbf{L}\cdot\mathbf{S}_d) + B_d(\mathbf{S}_d\cdot\mathbf{s}_m). \qquad (1)$$

The coefficient A is the Landé interval constant for d^k, and the coefficient B_d is numerically equal to twice the negative value of the exchange integral connecting ms with any electron of the core d^k. The additive constant E is the same for all states of the configuration. In this problem the secular determinant is of the second order; and it may be set up either by using Johnson's

[1] J. H. Van Vleck, Phys. Rev. **45**, 405 (1934).

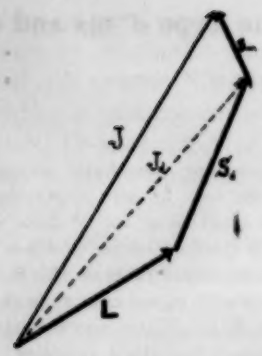

FIG. 1. Three vector problem for d^k ms.

formulas,[2] or by considering extreme cases of Russell-Saunder's coupling and then solving for the unknown perturbing term by Goudsmit's inspection method.[3] The secular equation leads to the following formula for the energy values;

$$|L-S_d|-\tfrac{1}{2}<J<L+S_d+\tfrac{1}{2}, \text{ where } J=J_d-\tfrac{1}{2}:$$

$$W=E+\tfrac{1}{2}\epsilon+\tfrac{1}{2}A[(J+\tfrac{1}{2})^2-L(L+1)-S_d(S_d+1)]$$
$$\pm\tfrac{1}{2}[\epsilon^2+(2A\epsilon/2S_d+1)((J+\tfrac{1}{2})^2$$
$$-L(L+1)+S_d(S_d+1))+A^2(J+\tfrac{1}{2})^2]^{\frac{1}{2}}, \quad (2)$$

$$J=|L+S_d|+\tfrac{1}{2}: \; W=E+ALS_d,$$

$$J=|L-S_d|-\tfrac{1}{2}: \; W=E-AS_d(L+1) \text{ for } L\geq S_d$$
$$=E-AL(S_d+1) \text{ for } L\leq S_d.$$

Here $\epsilon=-B_d(S_d+\frac{1}{2})=K_{md}(2S_d+1)$ is the separation between the multiplets with spins $S_d+\frac{1}{2}$ and $S_d-\frac{1}{2}$. The coefficient K_{md} is the exchange integral between ms and an electron of the ion core d^k.

When $k=1$ or $k=9$ configurations of the type d^k ms are included in the Houston singlet-triplet case and have been considered by others.[4] Goudsmit[3] and Johnson[2] examined configurations of the type $(^3P)ns$ when the (^3P) multiplets were regular. The inverted case will be elaborated by R. Schlapp in Proc. Edin. Phil. Soc. Condon and Shortley[5] treated three electron configurations of the type d^k ms where $k=2$. However, a general formula (2) inclusive of spin-orbit interaction for the energy states belonging to configurations of the type d^k ms (or a^k ms), when the core d^k (or a^k) has arbitrary L and S_d, apparently has not been published before.

§3. The Four Vector Problem Applied to d^k msns

In configurations of the type d^k msns it is only necessary to consider the interaction of the four vectors $\mathbf{L}$, $\mathbf{S}_d$, $\mathbf{s}_m$ and $\mathbf{s}_n$, where $\mathbf{s}_m$ and $\mathbf{s}_n$ represent, respectively, the spin vectors of the ms and ns electrons, while $\mathbf{S}_d$ is the total spin of the core d^k. This four vector problem illustrated in Fig. 2, is similar to the three vector problem applied to d^k ms, and all conditions required of the d^k core of d^k msns in the preceding section, §2, will be required of the d^k core of d^k msns in the present section. Again it will not be supposed that the spin-orbit energy of the core d^k is small compared to the electrostatic energy coupling d^k to ms or d^k to ns. The Hamiltonian will be of the form

$$\mathfrak{H}=E+A(\mathbf{L}\cdot\mathbf{S}_d)+B(\mathbf{S}_d\cdot\mathbf{s}_m)$$
$$+C(\mathbf{S}_d\cdot\mathbf{s}_n)+D(\mathbf{s}_m\cdot\mathbf{s}_n). \quad (3)$$

The matrix elements of the products in the Hamiltonian may be obtained from the formulas derived by Guttinger and Pauli[6] or from those

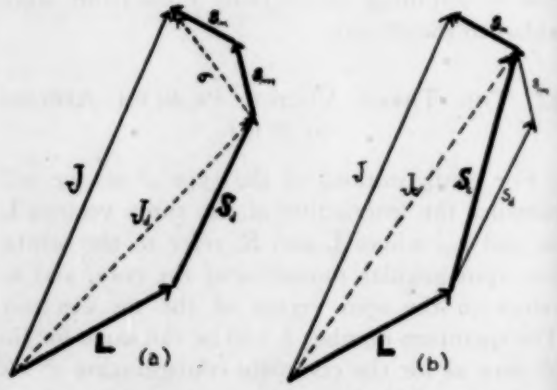

FIG. 2. (a) Four vector problem for d^k msns. (b) Three vector problem for d^k msns.

[2] M. H. Johnson, Jr., Phys. Rev. **38**, 1628 (1931).
[3] S. Goudsmit, Phys. Rev. **35**, 1325 (1930).
[4] W. V. Houston, Phys. Rev. **33**, 297 (1929); O. Laporte and D. R. Inglis, Phys. Rev. **35**, 1337 (1930); E. U. Condon and G. H. Shortley, Phys. Rev. **35**, 1342 (1930).
[5] E. U. Condon and G. H. Shortley, Phys. Rev. **37**, 1025 (1931).
[6] Guttinger and Pauli, Zeits. f. Physik **67**, 762 (1931).

given by Johnson.[2] Indeed the four vector problem for any two electron configuration treated by Johnson is very similar to that studied here. Johnson's vectors $\mathbf{l}_1$, $\mathbf{l}_2$, $\mathbf{L}$, $\mathbf{s}_1$, $\mathbf{s}_2$, $\mathbf{S}$ and $\mathbf{J}$ correspond, respectively, to the vectors $\mathbf{L}$, $\mathbf{S}_d$, $\mathbf{J}_d$, $\mathbf{s}_m$, $\mathbf{s}_n$, σ and $\mathbf{J}$ considered in this paper and illustrated in Fig. 2. The coefficient A is the Landé interval constant for the multiplet corresponding to the d^k configuration. The coefficients B, C and D of the interaction energies are numerically equal to twice the negative values of the respective exchange integrals.

§4. The Energy Matrix for d^k $msns$ Considered as a Four Vector Problem

The energy matrix for configurations of the type $d^k(^{2S_d+1}L)msns$ may be considered as a set of separate matrices in J as there are no components between states of different J values. From Johnson's formulas[2] the energy matrix for $L \geq S_d+1$ is

$J=L+S_d+1$

	$J_d=L+S_d$ $\sigma=1$
$J_d=L+S_d$ $\sigma=1$	$E+ALS_d+\frac{1}{2}S_d(B+C)+\frac{1}{4}D$

$J=L-S_d-1$

	$J_d=L-S_d$ $\sigma=1$
$J_d=L-S_d$ $\sigma=1$	$E-AS_d(L+1)+\frac{1}{2}S_d(B+C)+\frac{1}{4}D$

$J=L+S_d$

	$J_d=L+S_d$ $\sigma=1$	$J_d=L+S_d$ $\sigma=0$	$J_d=L+S_d-1$ $\sigma=1$
$J_d=L+S_d$ $\sigma=1$	$E+ALS_d-\frac{1}{2}\frac{S_d}{(L+S_d)}(B+C)+\frac{1}{4}D$	$\frac{1}{2}S_d\left[\frac{(L+S_d+1)}{(L+S_d)}\right]^{\frac{1}{2}}(B-C)$	$\frac{1}{2}\left[\frac{(L+S_d+1)LS_d}{(L+S_d)^2}\right]^{\frac{1}{2}}(B+C)$
$J_d=L+S_d$ $\sigma=0$	$\frac{1}{2}S_d\left[\frac{(L+S_d+1)}{(L+S_d)}\right]^{\frac{1}{2}}(B-C)$	$E+ALS_d-\frac{1}{4}D$	$-\frac{1}{2}\left[\frac{LS_d}{(L+S_d)}\right]^{\frac{1}{2}}(B-C)$
$J_d=L+S_d-1$ $\sigma=1$	$\frac{1}{2}\left[\frac{(L+S_d+1)LS_d}{(L+S_d)^2}\right]^{\frac{1}{2}}(B+C)$	$-\frac{1}{2}\left[\frac{LS_d}{(L+S_d)}\right]^{\frac{1}{2}}(B-C)$	$E-A(L+S_d-LS_d)+\frac{1}{2}\frac{(LS_d+S_d-L)}{(L+S_d)}(B+C)+\frac{1}{4}D$

$L+S_d>J>L-S_d$

	$J_d=J+1$ $\sigma=1$	$J_d=J$ $\sigma=1$	$J_d=J$ $\sigma=0$	$J_d=J-1$ $\sigma=1$
$J_d=J+1$ $\sigma=1$	$E+\frac{1}{2}Af(J+1)-\frac{1}{2}\frac{g(J+1)}{(J+1)}(B+C)+\frac{D}{4}$	$\frac{1}{2}h(J+1)\left[\frac{J}{(2J+1)}\right]^{\frac{1}{2}}(B+C)$	$\frac{1}{2}h(J+1)\left[\frac{J+1}{(2J+1)}\right]^{\frac{1}{2}}(B-C)$	0
$J_d=J$ $\sigma=1$	$\frac{1}{2}h(J+1)\left[\frac{J}{(2J+1)}\right]^{\frac{1}{2}}(B+C)$	$E+\frac{1}{2}Af(J)-\frac{1}{2}\frac{g(J)}{J(J+1)}(B+C)+\frac{1}{4}D$	$\frac{1}{2}\frac{g(J)}{[J(J+1)]^{\frac{1}{2}}}(B-C)$	$\frac{1}{2}h(J)\left[\frac{J+1}{(2J+1)}\right]^{\frac{1}{2}}(B+C)$
$J_d=J$ $\sigma=0$	$\frac{1}{2}h(J+1)\left[\frac{J+1}{(2J+1)}\right]^{\frac{1}{2}}(B-C)$	$\frac{1}{2}\frac{g(J)}{[J(J+1)]^{\frac{1}{2}}}(B-C)$	$E+\frac{1}{2}Af(J)-\frac{1}{4}D$	$-\frac{1}{2}h(J)\left[\frac{J}{(2J+1)}\right]^{\frac{1}{2}}(B-C)$
$J_d=J-1$ $\sigma=1$	0	$\frac{1}{2}h(J)\left[\frac{J+1}{(2J+1)}\right]^{\frac{1}{2}}(B+C)$	$-\frac{1}{2}h(J)\left[\frac{J}{(2J+1)}\right]^{\frac{1}{2}}(B-C)$	$E+\frac{1}{2}Af(J-1)+\frac{1}{2}\frac{g(J-1)}{J}(B+C)+\frac{1}{4}D$

where $f(J)=[J(J+1)-L(L+1)-S_d(S_d+1)]$
$g(J)=[J(J+1)-L(L+1)+S_d(S_d+1)]$
$h(J)=[(L+S_d+1-J)(L+S_d+1+J)(J-L+S_d)(J+L-S_d)/J^2]^{\frac{1}{2}}$

$J=L-S_d$

	$J_d=L-S_d+1$ $\sigma=1$	$J_d=L-S_d$ $\sigma=1$	$J_d=L-S_d$ $\sigma=0$
$J_d=L-S_d+1$ $\sigma=1$	$E-A[(L+1)(S_d-1)+S_d]-\frac{1}{2}\left[\frac{(L-S_d+1)-S_d(L-S_d)}{(L-S_d+1)}\right](B+C)+\frac{1}{4}D$	$\frac{1}{2}\frac{[S_d(L+1)(L-S_d)]^{\frac{1}{2}}}{(L-S_d+1)}(B+C)$	$\frac{1}{2}\left[\frac{S_d(L+1)}{(L-S_d+1)}\right]^{\frac{1}{2}}(B-C)$
$J_d=L-S_d$ $\sigma=1$	$\frac{1}{2}\frac{[S_d(L+1)(L-S_d)]^{\frac{1}{2}}}{(L-S_d+1)}(B+C)$	$E-AS_d(L+1)+\frac{1}{2}\frac{S_d}{(L-S_d+1)}(B+C)+\frac{1}{4}D$	$-\frac{1}{2}\frac{S_d(L-S_d)(B-C)}{[(L-S_d)(L-S_d+1)]^{\frac{1}{2}}}$
$J_d=L-S_d$ $\sigma=0$	$\frac{1}{2}\left[\frac{S_d(L+1)}{(L-S_d+1)}\right]^{\frac{1}{2}}(B-C)$	$-\frac{1}{2}\frac{S_d(L-S_d)(B-C)}{[(L-S_d)(L-S_d+1)]^{\frac{1}{2}}}$	$E-AS_d(L+1)-\frac{1}{4}D$

For the meaning of σ see Fig. 2. The matrices are the same for $L=S_d+\frac{1}{2}$ as those above except that then there is no matrix for $J=L-S_d-1$. If $L=S_d$, there is no $J=L-S_d-1$ matrix; and the matrix for $J=L-S_d$ is a second order matrix in which the second row and the second column in the corresponding matrix for $L \geq S_d+1$ have been deleted; the other matrices are the same as those

above. For $S_d > L$ the matrix is very similar to that for $L > S_d$. This matrix is not given here as no examples are considered in this paper where $S_d > L$.

§5. The Three Vector Problem Applied to d^k msns

In a few special cases the four vector problem may reduce to a three vector problem. This will be the case if $\mathbf{S}_d$ and $\mathbf{s}_m$ are legitimately quantized to a resultant $\mathbf{S}_{d+m} = \mathbf{S}_e$. Then the extended core d^k ms (to be distinguished from the true core d^k) will conform to Russell-Saunder's coupling and S_e will be a good quantum number. Thus the three vector problem will be valid only if the separation between the multiplets $d^k(^{2S_d+1}L)ms$ for the parent ion d^k ms is large compared to the separation between the multiplets d^k ms$(^{2S_d+2}L)ns$ or the multiplets d^k ms$(^{2S_d}L)ns$ for the configuration d^k msns. This requirement will be amplified in § 6. The three vector problem applied to d^k msns is illustrated in the second vector diagram in Fig. 2. The Hamiltonian will be of the form

$$\mathfrak{H} = E' + A_e(\mathbf{L}\cdot\mathbf{S}_e) + B_e(\mathbf{S}_e\cdot\mathbf{s}_m), \tag{4}$$

where A_e is the Landé interval constant for the d^k ms multiplet. The magnitude of the coefficient B_e is discussed in the following paragraph. The formula (2) for the energy values may be used if A, S_d and J_d there are replaced, respectively, by the Landé interval constant A_e, the spin quantum number S_e, and the orbital quantum number J_e of the extended core d^k ms for this three vector problem. However, mention should be made that the three vector problem applied to d^k ms is rigorous while the three vector problem applied to d^k msns is only an approximation to the four vector problem.

In order to examine the relationship between the three and the four vector problems applied to d^k msns we will make use of the kinematical interpretation of the components of the vector matrices.[7] $\mathbf{S}_d$ and $\mathbf{s}_m$ are considered quantized to a resultant $\mathbf{S}_e$; i.e., $\mathbf{S}_e = \mathbf{S}_d + \mathbf{s}_m$. This implies that $\mathbf{S}_d$ and $\mathbf{s}_m$ precess around $\mathbf{S}_e$ so fast that the components perpendicular to $\mathbf{S}_e$ are negligible. Hence the two electrostatic terms containing $\mathbf{s}_n$ in the Hamiltonian for the four vector problem, (3), become on the average

$$C\overline{(\mathbf{S}_d\cdot\mathbf{s}_n)} + D\overline{(\mathbf{s}_m\cdot\mathbf{s}_n)} = \frac{C(\mathbf{S}_d\cdot\mathbf{S}_e)(\mathbf{S}_e\cdot\mathbf{s}_n)}{\mathbf{S}_e^2} + \frac{D(\mathbf{s}_m\cdot\mathbf{S}_e)(\mathbf{S}_e\cdot\mathbf{s}_n)}{\mathbf{S}_e^2}$$

$$= \left[\frac{C[S_d(S_d+1) + S_e(S_e+1) - s_m(s_m+1)] + D[S_e(S_e+1) + s_m(s_m+1) - S_d(S_d+1)]}{2S_e(S_e+1)}\right](\mathbf{S}_e\cdot\mathbf{s}_n), \tag{5}$$

where we have substituted for the squares of the vectors $\mathbf{A}^2$ their equivalent diagonal terms $A(A+1)$, and have made use of the vector relation

$$\mathbf{S}_e^2 = (\mathbf{S}_d + \mathbf{s}_m)^2 = \mathbf{S}_d^2 + \mathbf{s}_m^2 + 2(\mathbf{S}_d\cdot\mathbf{s}_m), \qquad \text{etc.}$$

Setting s_m equal to its numerical value $\frac{1}{2}$, and letting S_e assume the two values $S_d + \frac{1}{2}$ and $S_d - \frac{1}{2}$ in (5) we find the two respective values for the coefficient B_e of $(\mathbf{S}_e\cdot\mathbf{s}_n)$ in (4)

$$[2S_dC + D]/(2S_d+1) \qquad \text{and} \qquad [2(S_d+1)C - D]/(2S_d+1). \tag{6}$$

The coefficient A_e is numerically equal to $2AS_d/(2S_d+1)$ for the $^{2S_d+2}L$ multiplet and to $2A(S_d+1)/(2S_d+1)$ for the ^{2S_d}L multiplet of the parent ion d^k ms, where A is the Landé interval constant for the multiplet belonging to the d^k configuration.

---

[7] See either, J. H. Van Vleck, *Electric and Magnetic Susceptibilities*, Oxford Press, 1930; or Pauling and Goudsmit, *The Structure of Line Spectra*, McGraw Hill, 1930.

§6. Comparison of Experimental Data with Calculations for d^k msns Configurations

There will in general be four spin multiplets belonging to the configuration d^k msns. This is illustrated in Fig. 3; dotted lines correspond to

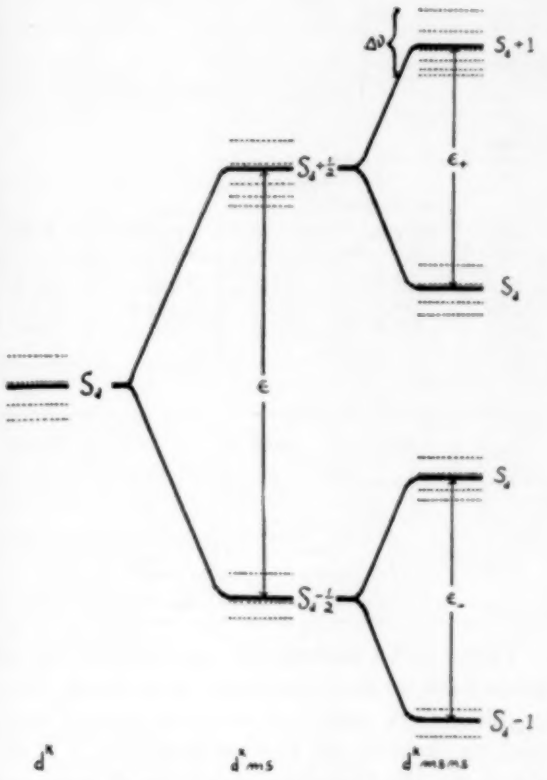

FIG. 3. Energy diagram illustrating the four spin multiplets belonging to the configuration d^k msns.

different J values in the spin multiplet. We may treat this configuration by any one of the following three procedures:

1. Russell-Saunder's coupling

If $\mathbf{S}_d$, $\mathbf{s}_m$ and $\mathbf{s}_n$ quantize to a resultant $\mathbf{S}$ and the multiplets are all separated by large intervals the complete configuration d^k msns would follow Russell-Saunder's coupling. That is, Russell-Saunder's coupling will be a good approximation in those cases where the interval ϵ_+, ϵ_-, or ϵ, between any two of the multiplets belonging to d^k msns is very much larger than the width of any one of the multiplets, say, $\Delta\nu$ in Fig. 3.

2. The three vector problem

This approximation will be good only if the interval ϵ_+ between the $S_d+\frac{1}{2}$ multiplets, or the interval ϵ_- between the $S_d-\frac{1}{2}$ multiplets is very small compared to the interval ϵ between the $S_d+\frac{1}{2}$ and $S_d-\frac{1}{2}$ multiplets. The multiplet width $\Delta\nu$ may be of the same order as ϵ_+, however.

3. The four vector problem

This procedure is rigorous regardless of the intervals between multiplets or of the respective widths of the multiplets. Indeed, even though ϵ_+ and ϵ_- be several times smaller than ϵ the three vector problem may not be substituted for this four vector problem as the interaction between the $S_d+\frac{1}{2}$ state and the $S_d-\frac{1}{2}$ state will still be large. It is to be particularly emphasized that Russell-Saunder's coupling (the two vector problem) is an approximation to the three vector problem which in turn is an approximation to the four vector problem, and that the approximate methods will be valid only in a very few special cases.

In all three procedures the d^k core is considered to conform to Russell-Saunder's coupling. The multiplets which have been examined by these three types of coupling are:

Y I, $4d(^2D)5s6s$; Cu I, $3d^9(^2D)4s5s$;

Zr I, $4d^2(^3F)5s6s$; Ni I, $3d^8(^3F)4s5s$;

Co I, $3d^7(^4F)4s5s$; and Fe I, $3d^6(^5D)4s5s$.

There are, of course, several ways of choosing the values of the parameters B, C and D in (3). If one should choose these parameters to fit the levels of different J values in one multiplet in d^k msns well, then the separations between the multiplets might very easily be of the wrong magnitudes. In other words a small change in value of one of the parameters B, C or D affects the J separations in any one multiplet very little, but has considerable effect on the relative separations between multiplets. Therefore an attempt has been made to adjust the values of these parameters as well as possible to give the right separations between multiplets. The usual procedure in roughly finding the first values of the parameters B, C and D was to compare the coefficients in the secular equation for any one value of J with the respective numerical co-

TABLE I.

Y II, $4d(^2D)5s$

J	^3D Term values		Separations		
	obs.	3V calc.	obs.	3V calc.	R–S
1	840.18	841.56	204.91	203.53	243.88
2	1045.09	*1045.09	404.79	406.17	365.82
3	1449.88	1451.26			
	^1D				
2	3296.27	*3296.27			

Y I, $4d(^2D)5s6s$

J	$(^2D)6s\ ^4D$ Term values				Separations				
	obs.	4V calc.	3V′ calc.	3V′ calc.*	obs.	4V calc.	3V′ calc.	3V′ calc.*	R–S
½	33148.3	33145.6	33124.0	33111.2	89.5	100.7	113.8	126.6	121.9
1½	33237.8	33246.3	*33237.8	*33237.8	173.7	186.3	200.0	191.8	203.2
2½	33411.5	33432.6	33437.8	33429.6	341.2	322.7	295.9	291.3	284.5
3½	33752.7	33755.3	33733.7	33720.9					
	^2D								
1½		35066.5	*35066.5			379.4	409.5		406.5
2½		35445.9	35476.2						
	^2D								
1½	36420.5	36432.0		*36420.5	10.5	43.8		417.9	
2½	36431.0	36475.8		36838.4					

efficients in the corresponding equation for the experimental term values for the same value of J. These first values were then varied one at a time and curves were plotted to obtain a general idea of the way the term values varied with the parameters. The values of the parameters given in Table VII are those which seem to give the best fit with experimental data. A change say of two percent in the value of one of the parameters B, C or D will produce only a very small change in the separations between the components belonging to different values of J in any one multiplet but may change the interval between any two multiplets by one or two percent. The value of the arbitrary parameter E in (3) is determined by the absolute value of the energy with respect to the normal state. The A value for all configurations has been chosen from the multiplet $d^k\,ms\,^{2S_d+2}L$ of the parent ion.[8]

Tables I–VI include (1) calculations for the parent ion $d^k\,ms$ considered as a three vector problem ("3V calc.") of the type treated in §2, and as a case of Russell-Saunder's ("R–S") coupling; (2) Calculations for the $d^k\,msns$ configuration considered as a four vector problem ("4V calc."), as a three vector problem ("3V′ calc."),[9] and as a case of true Russell-Saunder's coupling ("R–S"). For the latter case only the separations are tabulated. In some of the calculations the parameters were chosen to fit certain term values; these term values are preceded by an asterisk. The experimental term values have been taken from *Atomic Energy States* by Bacher and Goudsmit [10]

[8] If A_o is the Landé interval constant for the $d^k\,ms\,^{2S_d+2}L$ multiplet, then $A=A_o(2S_d+1)/2S_d$. The reason that the A value has not been chosen from the d^k configuration of the grandparent ion, i.e., the doubly ionized atom, is that in all cases, save for Zr, the corresponding multiplets have not been found experimentally. In Zr, the d^3 multiplet is obviously perturbed by near configurations and hence the A value chosen from this multiplet could not possibly be the right A value to use in the calculations.

[9] The prime attached to the V is to indicate that the core in this case is the extended core $d^k\,ms$ and not d^k as in the three vector problem applied to $d^k\,ms$.

[10] Bacher and Goudsmit, *Atomic Energy States*, McGraw Hill, 1932.

TABLE II.

Cu II, $3d^9(^2D)4s$

	^3D Term values		Separations		
J	obs.	3V calc.	obs.	3V calc.	R–S
3	21925.0	21935.1	− 918.5	− 908.4	−1241.7
2	22843.5	*22843.5	−1151.2	−1160.5	− 827.8
1	23994.7	24004.4			
	^1D				
2	26260.7	*26260.7			

Cu I, $3d^9(^2D)4s5s$

	$(^3D)5s\ ^4D$ Term values			Separations			
J	obs.	4V calc.	3V′ calc.	obs.	4V calc.	3V′ calc.	R–S
3½	− 95.2	*− 95.2	+ 152.0	−545.0	−542.7	− 792.2	− 966
2½	− 640.2	− 637.9	*− 640.2	−636.2	−632.8	− 782.9	− 690
1½	−1276.4	−1270.7	−1423.1	−887.8	−893.8	− 494.2	− 414
½	−2164.2	−2164.5	−1917.3				
	$(^3D)5s\ ^2D$						
2½	−2349.5	−2353.5	*−2349.5	−602.2	−606.8	−1286.4	−1379.5
1½	−2951.7	−2960.3	−3635.9				
	$(^1D)5s\ ^2D$						
2½	−4834.3	−4832.4		−829.6	−829.7		
1½	−5663.9	−5662.1					

§7. COMMENTS UPON TABLES I–VI

Configurations of the type d^9 msns and d msns are represented by four secular determinants, two of order three and two of order one. The multiplets will be two doublets and a quartet. These should be amenable to the four vector problem as the d^k core is equivalent to a single electron. Thus the d^k core will of necessity conform to Russell-Saunder's coupling by virtue of the configuration. Examples of configurations of this type are to be found in Tables I and II. The parent ion d^k ms conforms to the three vector problem very well; and it follows that the multiplets arising from the addition of another s electron to this ion core should be amenable to the four vector problem. This is actually the case. In Y I, Table I, the "3V′ calc." procedure has been applied twice: The levels with the classification in Bacher and Goudsmit's book[10] are used in one case ("3V′ calc.*") and the levels with the classification indicated by the four vector problem calculations are used in the other case ("3V′ calc."). According to these calculations, the doublet classified in Bacher and Goudsmit as $(^3D)6s\ ^2D$ is more related to (^1D) than to (^3D). In any case the multiplet splitting in $(^1D)6s\ ^2D$ doesn't exist as far as a three vector or a Russell-Saunder's coupling approximation is concerned. The negative term values in Cu I, Table II, indicate that the energy values are higher than the first ionization potential.

Configurations of the type $d^8(^3F)$msns or $d^2(^3F)$msns treated as four vector problems are represented by five secular determinants, two of order one, two of order three, and one of order four. The multiplets are one quintet, two triplets, and one singlet. The parent ions d^8 ms and d^2 ms are not amenable to a three vector problem as the separations indicated in Tables III and IV illustrate. However, there is qualitative agreement between the "4V calc." and "observed" values for the d^k msns multiplets.

TABLE III.

Zr II, $4d^2(^3F)5s$

	^4F Term values		Separations		
J	obs.	3V calc.	obs.	3V calc.	R–S
$1\frac{1}{2}$	0.0	* 0.0			
$2\frac{1}{2}$	314.7	300.1	−314.7	−300.1	−315
$3\frac{1}{2}$	763.4	737.5	−448.7	−437.5	−441
$4\frac{1}{2}$	1322.9	*1323.0	−558.5	−585.5	−567
	^2F				
$2\frac{1}{2}$	5752.9	5646.9	−714.7	−885.0	−882
$3\frac{1}{2}$	6467.6	6532.5			

Zr I, $4d^2(^3F)5s6s$

	$(^4F)6s\ ^5F$ Term values			Separations			
J	obs.	4V calc.	3V′ calc.	obs.	4V calc.	3V′ calc.	R–S
1	35046.9	35042.1	35031.9				
2	35210.3	35212.1	*35210.3	163.4	170.0	178.4	189
3	35476.1	35479.2	35486.1	265.8	267.4	275.8	284
4	35860.8	35858.3	35865.8	384.7	378.8	379.7	378
5	36360.2	36365.1	36354.9	499.4	506.8	489.1	472
	$(^4F)6s\ ^3F$						
2	37459.6	37457.9	*37459.6				
3	37701.1	37919.1	37939.8	241.5	461.2	480.2	472
4	38101.1	38558.9	38568.1	400.0	639.8	628.3	629
	$(^2F)6s\ ^3F$						
2		40610.8					
3		40849.9			239.1		
4		41509.6			659.7		
	$(^2F)6s\ ^1F$						
3		42302.3					

The $(^2F)5s$ multiplets in Ni I, $3d^8(^3F)4s5s$ are especially interesting. To give the right separation with the "3V′ calc." between the singlet and triplet multiplets, the separation ϵ would have to be imaginary! This difficulty is avoided in the four vector problem where the calculated values agree very well with those observed. The ion for zirconium is very irregular with reference to Russell-Saunder's coupling, i.e., does not obey the Landé interval rule, and hence only approximate results could be expected for the four vector calculations. The ^3F terms for this configuration, Zr I, $4d^2(^3F)5s6s$, are decidedly irregular. The predicted term values for the $4d^25s(^2F)6s$ multiplets of Zr I fall in a region in which are to be found the multiplets $4d^25s(^4F)5d\ ^5G$, $4d^25s(^4F)5d\ ^5H$, and an unclassified ^5F multiplet.

In Table V there is a d^7 core and in Table VI a d^6 core. These cores certainly do not obey Landé's interval rule and hence the most one can expect of the "4V calc." is a qualitative agreement. Indeed the "3V′ calc." for the d^64s core in iron give better agreement than the "4V calc." For certain single separations the "4V calc." is very much better; e.g., $J=1$ to $J=0$ in the $(^4D)5s\ ^5D$ state of Fe I, Table VI. The term values of the multiplet pair $(^4D)5s\ ^3D$ and ^5D of Fe I are surrounded and intermingled with other levels in the same region. Indeed the multiplets $3d^7(^4F)5s$ (see Table XI) which fall

TABLE IV.

Ni II, $3d^8(^3F)4s$

	^4F Term values		Separations		
J	obs.	3V calc.	obs.	3V calc.	R–S
4½	8392.9	8433.4			
3½	9329.3	9329.4	− 936.4	− 896.0	− 972.9
2½	10114.7	*10114.7	− 785.4	− 785.3	− 756.7
1½	10663.0	10703.5	− 548.3	− 588.8	− 540.5
	^2F				
3½	13549.1	13509.4			
2½	14994.4	*14994.4	−1445.3	−1485.0	−1513.4

Ni I, $3d^8(^3F)4s5s$

	$(^4F)5s\,^5F$ Term values			Separations			
J	obs.	4V calc.	3V′ calc.	obs.	4V calc.	3V calc.	R–S
5	48466.5	48470.5	48443.1				
4	49085.9	49084.0	49120.5	− 619.4	− 613.5	− 677.4	− 810.8
3	49777.5	49736.8	49807.1	− 691.4	− 652.8	− 686.7	− 648.6
2	50346.4	50321.7	*50346.4	− 568.9	− 584.9	− 539.3	− 486.5
1	50744.6	50740.5	50713.2	− 398.2	− 418.8	− 366.8	− 324.3
	$(^4F)5s\,^3F$						
4	50466.1	50413.0	50239.6				
3	51306.0	51250.6	51282.5	− 839.9	− 837.6	−1042.9	−1081.0
2	52040.5	51997.7	*52040.5	− 734.4	− 747.1	− 758.0	− 810.8
	$(^2F)5s\,^3F$						
4	54237.1	54258.8					
3	54251.2	54294.1		− 14.1	− 35.3		− 825.9
2	55873.7	55977.6		−1622.5	−1683.5		− 619.4
	$(^2F)5s\,^1F$						
3	55576.8	55628.7					

in the energy region between the $3d^64s(^6D)5s$ and the $3d^64s(^4D)5s$ multiplet pairs of Fe I will probably have some perturbing effect upon the $3d^84s5s$ multiplets. The $3d^74s(^5F)5s\,^6F$ state of Co I has energy states which intermingle with those of the $3d^8(^3F)4s$ multiplets of Co I.[11] The predicted levels in Co I, more especially $(^3F)5s\,^2F$, fall in a region for which Bacher and Goudsmit[10] list several unclassified levels. However, none of the unclassified levels listed there seem to fit the calculated term values.

The fact that in many cases the d^k $msns$ levels are near other levels which probably have some perturbing effect may account for the fact that the agreement of the calculated levels with the experimental levels is not better than it is.[12] Of course the presence of the other near configurations indicates that the d^k core cannot conform to a case of Russell-Saunder's coupling. However, it is very remarkable that the agreement in most cases is as good as it is, especially in Ni I where the $3d^84s(^3F)5s\,^3F$ state falls in a region contaminated by the $3d^95d$ configuration and is surrounded by other near configurations.

[11] In Table X the multiplets $3d^8(^3F)4s$ of Co I are considered as a three vector problem.

[12] I wish to thank Dr. R. F. Bacher for stressing this fact in a recent conversation.

TABLE V.

Co II, $3d^7(^4F)4s$

	^5F Term values		Separations		
J	obs.	3V calc.	obs.	3V calc.	R-S
5	3350.5	3368.2			
			−678.4	−646.9	−662.1
4	4028.9	4015.1			
			−531.9	−530.6	−529.7
3	4560.8	4545.7			
			−389.2	−404.3	−397.2
2	4950.0	*4950.0			
			−254.5	−272.2	−264.8
1	5204.5	5222.2			
	^3F				
4	9812.7	9784.4			
			−895.4	−882.0	−882.8
3	10708.1	10666.4			
			−613.4	−655.1	−662.1
2	11321.5	*11321.5			

Co I, $3d^7(^4F)4s5s$

	$(^5F)5s\ ^6F$ Term values			Separations			
J	obs.	4V calc.	3V′ calc.	obs.	4V calc.	3V′ calc.	R-S
$5\frac{1}{2}$	45675.9	*45675.9	45679.3				
				−547.0	−524.1	−543.4	− 582.5
$4\frac{1}{2}$	46222.9	46200.0	46222.7				
				−483.8	−474.7	−478.8	− 476.5
$3\frac{1}{2}$	46706.7	46674.7	46701.5				
				−383.8	−390.6	−384.2	− 370.5
$2\frac{1}{2}$	47090.5	47065.3	47085.7				
				−274.0	−288.3	−278.8	− 264.8
$1\frac{1}{2}$	47364.5	47353.6	*47364.5				
				−163.8	−176.3	−168.8	− 158.9
$\frac{1}{2}$	47528.3	47529.9	47533.3				
	$(^5F)5s\ ^4F$						
$4\frac{1}{2}$	47524.4	47512.7	47439.1				
				−677.2	−661.0	−713.1	− 715
$3\frac{1}{2}$	48201.6	48173.7	48152.2				
				−516.9	−522.1	−542.9	− 556
$2\frac{1}{2}$	48718.5	48695.8	48695.1				
				−359.8	−375.9	−383.2	− 397
$1\frac{1}{2}$	49078.3	49071.7	*49078.3				
	$(^3F)5s\ ^2F$						
$3\frac{1}{2}$		52648.6					
					−956.7		−1030
$2\frac{1}{2}$		53605.3					
	$(^3F)5s\ ^4F$						
$4\frac{1}{2}$		52769.5					
					−828.7		− 662.1
$3\frac{1}{2}$		53598.2					
					−602.6		− 515.0
$2\frac{1}{2}$		54200.8					
					−182.1		− 367.9
$1\frac{1}{2}$		54382.9					

§8. COMPARISON OF THE VALUES OF THE PARAMETERS; d^k msns

The manner in which the values of the parameters have been chosen has already been discussed in §6. It should be particularly noted that the rigorous four vector problem embodies no more arbitrary parameters than does Russell-Saunder's coupling or the three vector problem. As the Russell-Saunder's coupling or the three vector problems are considered in this paper six parameters are needed to completely determine the term values for all the multiplets (four) belonging to a configuration of the type d^k msns. In the Russell-Saunder's coupling case for each multiplet pair (there are two multiplets for each d^k ms multiplet) there will be three parameters: the Landé interval constant A_s, and two origin values to fix the term values of the multiplets with reference to the normal state. Likewise in the three vector problem there will be the three

TABLE VI.

Fe II, $3d^6(^5D)4s$

	^6D Term values		Separations		
J	obs.	3V calc.	obs.	3V calc.	R-S
$4\frac{1}{2}$	0.0	*0.4			
			−384.8	−364.4	−366.4
$3\frac{1}{2}$	384.8	364.8			
			−282.9	−284.9	−284.9
$2\frac{1}{2}$	667.7	649.7			
			−194.9	−204.4	−203.5
$1\frac{1}{2}$	862.6	854.1			
			−114.3	−122.5	−122.1
$\frac{1}{2}$	976.9	*976.6			
	^4D				
$3\frac{1}{2}$	7955.2	7932.5			
			−436.7	−427.4	−427.4
$2\frac{1}{2}$	8391.9	8359.9			
			−288.5	−304.4	−305.3
$1\frac{1}{2}$	8680.4	8664.3			
			−166.3	−182.4	−183.2
$\frac{1}{2}$	8846.7	*8846.7			

Fe I, $3d^6(^5D)4s5s$

	$(^6D)5s\ ^7D$ Term values			Separations			
J	obs.	4V calc.	3V calc.	obs.	4V calc.	3V′ calc.	R-S
5	42815.9	*42815.9	42830.2				
				−347.5	−331.6	−333.1	−339.2
4	43163.4	43147.5	43163.3				
				−271.3	−269.6	−271.3	−271.4
3	43434.7	43417.1	*43434.6				
				−198.9	−206.9	−205.8	−203.5
2	43633.6	43624.0	43640.4				
				−130.4	−139.4	−138.1	−135.7
1	43764.0	43763.4	43778.5				
	$(^6D)5s\ ^5D$						
4	44677.0	44695.6	44681.4				
				−384.4	−367.9	−379.9	−379.9
3	45061.4	45063.5	*45061.4				
				−272.5	−276.4	−282.8	−284.9
2	45333.9	45339.9	45344.1				
				−175.3	−184.1	−187.5	−190.0
1	45509.2	45524.0	45531.6				
				− 85.9	− 92.6	− 93.5	− 95.0
0	45595.1	45616.6	45625.1				
	$(^4D)5s\ ^5D$						
3	51294.3	51283.7	*51294.3				
				−445.7	−442.4	−436.0	−457.9
2	51740.0	51726.1	51730.3				
				−300.0	−314.4	−315.4	−305.3
1	52040.0	52040.5	52045.7				
	$(^4D)5s\ ^5D$						
4	51350.5	*51350.5	51351.5				
				−420.1	−415.0	−419.1	−366.3
3	51770.6	51765.5	*51770.6				
				−279.3	−295.5	−296.6	−274.8
2	52049.9	52061.0	52067.2				
				−164.5	−176.1	−173.0	−183.2
1	52214.4	52237.1	52240.2				
				− 43.0	− 48.7	− 27.1	− 91.6
0	52257.4	52285.8	52267.3				

parameters for each multiplet pair: The Landé interval constant A_c, the separation ϵ_+ (or ϵ_-) between the two spin multiplets, and E', the origin of term values. In the four vector problem there are only five parameters, E, A, B, C and D. Since, however, the A (or A_c) Landé interval constant is usually taken from the parent ion actually only four parameters are needed for each problem to completely calculate all the term values belonging to the d^k msns configuration.

The parameters used in the calculations are grouped together in Table VII. The coefficients of the interaction energies are twice the negative values of the respective exchange integrals. One notes that the exchange integrals connecting d^k

TABLE VII. *Values of the parameters; d^k msns configurations.*

Table No.	Configuration	A	$B_d=\frac{-\epsilon}{S_d+\frac{1}{2}}$	B_e for $S_d+\frac{1}{2}$	B	C	D
I	Y I, $4d(^2D)5s6s$	+243.88	−2048.5	−1208.0	−2292.5	−1100.1	−1305.7
III	Zr I, $4d^2(^3F)5s6s$	+189.00	−3648.0	−1145.5	−3137.5	−1087.5	−1250.0
II	Cu I, $3d^9(^2D)4s5s$	−827.70	−3164.6	− 971.0	−3096.5	− 327.5	−2045.0
IV	Ni I, $3d^8(^3F)4s5s$	−324.30	−3116.7	− 750.5	−3102.7	− 309.7	−1924.4
V	Co I, $3d^7(^4F)4s5s$	−176.57	−3134.2	− 656.4	−3050.0	− 315.0	−1930.0
VI	Fe I, $3d^6(^5D)4s5s$	−101.76	−3155.8	− 606.0[a]	−3040.3	− 321.2	−1932.6

[a] B_e for $S_d-\frac{1}{2}=+32.72$.

and ms are very nearly the same for the neutral atom d^k msns and the parent ion d^k ms; i.e., in Table VII, $-\frac{1}{2}B_d=\epsilon/(2S_d+1)$ is very nearly the same as $-\frac{1}{2}B$. Furthermore, these exchange integrals change only slightly with similar configurations as we go from one atom to the next; which shows that the addition of the s electron distorts the radial wave functions of the interior of the atom but little. The column headed "B_e for $S_d+\frac{1}{2}$" refers to the coefficient of interaction energy of the d^k ms core with the ns electron for the higher order multiplet ($^{2S_d+2}L$) of d^k ms.

Reasonable results are obtained for the relative magnitudes of the exchange integrals. The exchange integrals $-\frac{1}{2}B$ connecting the d^k core with 4s in d^k4s5s configurations are almost the same as those connecting the d^k core with 5s in d^k5s6s configurations. The coefficient C is smaller than B, since the d^k core is shielded by the ms electron. That C is larger for d^k5s6s than for d^k4s5s is to be expected since a 5s electron would not shield the d^k core as well as does a 4s electron. Indeed the exchange integrals connecting 5s with the d^k core are about ten times larger than when the d^k core is shielded by a 4s electron (compare the first two values under the "B" heading with the last four under the "C" heading). The exchange integrals between the extra-core electrons are smaller, of the order of 650 cm^{-1}, for 5$s6s$ than for 4$s5s$, where they are of the order of 970 cm^{-1}.

If the values of C and D from Table VII are substituted into the relation (6) for B_e in terms of these coefficients we find the respective values −1203, −1142, −1186, −845, −720, −643, and +1 as compared to B_e choosen on the basis of the three vector problem to fit the experimental data, −1208, −1145, −971, −750, −656, −606 and +32, respectively. It is not to be expected that the latter set should agree very well with the former set since the three vector problem is not a good approximation; but the values are reasonably consistent.

§9. Ti I, $3d^24s(^4F)5s$ AS A THREE VECTOR PROBLEM

In Table VIII we have a very good example of a configuration, Ti I, $3d^24s(^4F)6s$, which may be treated by the three vector approximation. Indeed this is to be expected since Ti II, $3d^24s\ ^4F$ varies little from Landé's interval rule, and the overall multiplet width is almost the same for the atom (^5F multiplet width is 393.05 cm^{-1}) as for the parent ion (^4F multiplet width is

TABLE VIII.

Ti II, $3d^2(^3F)4s\ ^4F$ Separations:

obs.	R–S
93.94	93.62
131.53	131.07
167.75	168.53

$A_e=+37.45$

Ti I, $3d^24s(^4F)6s$ $\quad\epsilon=395.16\quad B_e=-197.58$

^5F Term values			Separations		
J	obs.	3V′ calc.	obs.	3V′ calc.	R–S
1	45764.71	45762.50			
2	45813.01	45813.17	48.30	50.67	56.18
3	45893.26	45894.00	80.25	80.83	84.26
4	46007.62	*46007.62	114.36	113.62	112.35
5	46157.76	46155.73	150.14	148.11	140.44
	^3F Term values				
2		46200.61			
3		46344.48		143.87	140.44
4	46530.45	*46530.45		185.97	187.25

TABLE IX.

1. Ti II, $3d^2(^3F)5s$

Ti III, $3d^2\,^3F$ Separations:

obs.	R–S
183.7	180.8
238.2	241.0

$A = 60.27$

Ti II, $3d^2(^3F)5s$ $\epsilon = 898.9$

J	^4F Term values		Separations		
	obs.	3V calc.	obs.	3V calc.	R–S
$1\frac{1}{2}$	62180.02	62179.89			
$2\frac{1}{2}$	62271.25	*62271.25	91.23	91.36	100.45
$3\frac{1}{2}$	62409.58	62410.40	138.33	139.15	140.63
$4\frac{1}{2}$	62594.27	62601.78	184.69	191.38	180.81
	^2F				
$2\frac{1}{2}$	63168.23	*63168.23	276.53	282.75	281.26
$3\frac{1}{2}$	63444.76	63450.98			

393.22 cm^{-1}).[13] Hence there would be little, if any, advantage in treating this example as a four vector problem.

§10. ADDITIONAL d^k ms CONFIGURATIONS

Tables IX–XI include calculations for the three vector problem applied to configurations d^k ms other than the parent ions already treated

TABLE X.

1. Ni II, $3d^9(^2F)5s$

$A = -324.3$ $\epsilon = 1122.6$

J	^4F Term values		Separations		
	obs.	3V calc.	obs.	3V calc.	R–S
$4\frac{1}{2}$	91797.3	91863.5	− 525.4	− 489.7	− 972.9
$3\frac{1}{2}$	92322.7	92353.2	−1064.1	−1033.6	− 756.9
$2\frac{1}{2}$	93386.8	*93386.8	− 677.1	− 746.8	− 540.5
$1\frac{1}{2}$	94063.9	94133.6			
	^2F				
$3\frac{1}{2}$	93525.1	93489.4	−1200.8	−1236.5	−1513.4
$2\frac{1}{2}$	94725.9	*94725.9			

[13] The multiplet width for the higher order multiplet will necessarily be the same for the parent ion and for the final configuration in all the vector problems for which $L \geq S_d+1$. In the parent ion d^k this multiplet ($^{2S_d+1}L$) width equals $AS_d(2L+1)$. In the three vector problem we obtain this same width on taking the difference of the energy values for maximum J and minimum J, since in Eq. (2) we have $W_{J=L+S_d+\frac{1}{2}} - W_{J=L-S_d-\frac{1}{2}} = AS_d(2L+1)$. In the four vector problem the difference in energy values for the two single rank matrices, i.e., the matrices for $J=L+S_d+1$ and $J=L-S_d-1$ in §4, equals this same value $AS_d(2L+1)$.

2. Co I, $3d^8(^3F)4s$ and Co I $3d^8(^3F)5s$

Co II, $3d^8\,^3F$ Separations:

obs.	R–S
−950.3	−912.7
−646.9	−684.5

$A = -228.17$

Co I, $3d^8(^3F)4s$ $\epsilon = 3632.7$

J	^4F Term values		Separations		
	obs.	3V calc.	obs.	3V calc.	R–S
$4\frac{1}{2}$	3482.8	3504.1			
$3\frac{1}{2}$	4142.6	4140.2	− 659.8	− 636.1	− 684.5
$2\frac{1}{2}$	4690.1	*4690.1	− 547.5	− 549.9	− 532.4
$1\frac{1}{2}$	5075.8	5101.3	− 385.7	− 411.2	− 380.3
	^2F				
$3\frac{1}{2}$	7442.4	7413.5	−1018.4	−1047.3	−1064.8
$2\frac{1}{2}$	8460.8	*8460.8			

Co I, $3d^8(^3F)5s$ $\epsilon = 465.35$

J	^4F Term values		Separations		
	obs.	3V calc.	obs.	3V calc.	R–S
$4\frac{1}{2}$	44781.9	44823.5			
$3\frac{1}{2}$	45105.4	45117.3	−323.5	−293.8	− 684.5
$2\frac{1}{2}$	45876.4	*45876.4	−771.0	−759.1	− 532.4
$1\frac{1}{2}$	46375.0	46420.7	−498.6	−544.3	− 380.3
	^2F				
$3\frac{1}{2}$	45924.8	45907.7	−821.0	−838.1	−1064.8
$2\frac{1}{2}$	46745.8	*46745.8			

3. Pd II, $4d^9(^2F)6s$

$A = -684.2$ $\epsilon = 1468$

J	^4F Term values		Separations		
	obs.	3V calc.	obs.	calc.	R–S
$4\frac{1}{2}$	104616.0	104541	− 692.2	− 916	−2052.6
$3\frac{1}{2}$	105308.2	105457	−2838.8	−2254	−1596.5
$2\frac{1}{2}$	108147.0	107711	−1183.0	−1619	−1140.4
$1\frac{1}{2}$	109330.0	*109330			
	^2F				
$3\frac{1}{2}$	108146.0	107829	−1782.5	−2535	−3193.0
$2\frac{1}{2}$	109928.5	110364			

and the singlet-triplet case of Houston's where $k=1$ or $k=9$. Only those configurations are included for which the three vector problem is applicable. The interval, ϵ, between the $S_d+\frac{1}{2}$ and the $S_d-\frac{1}{2}$ multiplets has been chosen so that the term values preceded by an asterisk are the same for the calculated as for the observed values. The parameters used in the calculations

TABLE XI.

1. Fe I, $3d^7(^4F)5s$

Fe II, $3d^7\ ^4F$ Separations:

obs.	R–S
−557.6	−533.5
−407.8	−414.9
−279.6	−296.4

$A = -118.56$

Fe I, $3d^7(^4F)5s$ $\epsilon = 782.0$

	^5F Term values		Separations		
J	obs.	3V calc.	obs.	3V calc.	R–S
5	47005.5	47011.7			
			−372.5	−366.3	−444.6
4	47378.0	*47378.0			
			−377.6	−379.0	−355.7
3	47755.6	47757.0			
			−281.1	−297.4	−266.8
2	48036.7	48054.4			
			−184.7	−202.2	−177.8
1	48221.4	48256.6			
	^3F				
4	47961.0	*47961.0			
			−570.9	−569.5	−592.8
3	48531.9	48530.5			
			−396.5	−413.9	−444.6
2	48928.4	48944.4			

2. Co II, $3d^7(^4F)5s$

$A = -177.31$ $\epsilon = 1200$

	^5F Term values		Separations		
J	obs.	3V calc.	obs.	3V calc.	R–S
5	84012.3	84033.2			
			−572.5	−551.6	−664.9
4	84584.8	*84584.8			
			−580.5	−564.9	−531.9
3	85165.3	85149.7			
			−482.6	−443.6	−398.9
2	85593.9	85593.3			
			−280.2	−301.6	−266.0
1	85874.1	85894.9			
	^3F				
4	85479.2	*85479.2			
			−864.6	−853.5	−886.6
3	86343.8	86332.7			
			−593.9	−620.4	−664.9
2	86937.7	86953.1			

are tabulated in Table XII. The values of A have been chosen from the d^k multiplet except for those cases with special footnotes. The experimental term values have again been taken from Bacher and Goudsmit's book.[10]

§11. COMMENTS ON TABLES IX–XII

In general, configurations of the type $nd^k(n+1)s$ conform more nearly to Russell-Saunder's coupling than do configurations of the type $nd^k(n+2)s$. Indeed, the separation between the multiplets of the former configuration are usually several times larger than those for the latter. Thus there is generally less interaction between the two spin states for $nd^k(n+1)s$ than for $nd^k(n+2)s$ and the corrections to Russell-Saunder's coupling are smaller. In fact, in some examples the separations adjusted to fit Russell-Saunder's coupling agree better with experiment for $nd^k(n+1)s$ than do the same separations calculated on the basis of the three vector problem. However, in most of the configurations of the type $nd^k(n+2)s$ the three vector problem is very much better than that which one gets with the approximation of Russell-Saunder's coupling. As an illustration of this distinction compare $3d^7(^4F)5s$ of Co II, in Table XI, with $3d^7(^4F)4s$ of Co II, in Table V. As another example, $3d^7(^5D)5s$ of Fe I, in Table XI, is approximated much better with the substitution of the three vector problem for that of Russell-Saunder's coupling, while the agreement is not improved with this substitution in $3d^7(^5D)4s$ of Fe I, which responds to the calculations in the same way that $3d^6(^5D)4s$ of Fe II, Table VI, does. However, the substitution of this three vector problem for Russell-Saunder's even in configurations of the form $nd^k(n+1)s$ may sometimes result in a big improvement; as for example in Ni II, $3d^8(^3F)4s$ in Table IV.

§12. APPLICATION OF THE THREE VECTOR PROBLEM TO OTHER CONFIGURATIONS

When the three vector consideration is applied to P configurations such as Co I, $3d^8(^3P)4s$ or Pd II, $4d^8(^3P)5s$ with multiplet separations which are very much different than those calculated for a case of Russell-Saunder's coupling, only slightly better results are obtained than those given by Russell-Saunder's coupling. Configurations of the type $p^k\,ms$ have also been examined as a three vector problem, under the assumption that the p^k core is such that it may be considered as obeying Russell-Saunder's coupling. In a few instances, as Br I, $4p^4(^3P)5s$; O II, $2p^2(^3P)4s$ and $5s$; N I, $2p^2(^3P)5s$ and Ne II, $2p^4(^3P)4s$, there is fair agreement; but these are less interesting as confirmation of the theory and no doubt other perturbing effects than that treated will have to be considered.

Besides those configurations mentioned already, it is found that a three vector problem applied to the following $d^k\,ms$ configurations give separations which deviate more from the observed separations than do the separations

TABLE XII. *Values of the parameters; d^k ms configurations.*

Table No.	Configuration	Overall multiplet width[13]		A	B	ϵ
		ion	d^k ms $^{2S_d+2}L$			
IX	Ti II, $3d^2(^3F)5s$	421.90	414.25	+ 60.27	− 599.3	898.9
X	Ni II, $3d^8(^3F)5s$		2266.6	−324.3[a]	− 748.4	1122.6
	Co I, $3d^8(^3F)4s$	1597.19	1593.06	−228.17	−2421.8	3632.7
	Co I, $3d^8(^3F)5s$	1597.19	1593.99	−228.17	− 310.2	465.4
	Pd II, $4d^8(^3F)6s$		4714.0	−684.2[b]	− 978.7	1468.0
XI	Fe I, $3d^7(^4F)5s$	1244.93	1215.81	−118.56	− 391.0	782.0
	Co II, $3d^7(^4F)5s$		1661.8	−117.31[c]	− 600.0	1200.0

[a] Chosen from Ni II, $3d^8(^3F)4s\ ^4F$.
[b] Chosen from the average of the overall multiplet widths of $5s\ ^4F$ and $6s\ ^4F$.
[c] Chosen from the $S_d+\frac{1}{2}$ multiplet.

calculated on the basis of Russell-Saunder's coupling: Ru I, $4d^7(^4F)5s$; Co II, $3d^7(^4F)4s$; Cu III, $3d^8(^3F)4s$;[14] Mn V, $3d^2(^3F)4s$; Y I, $4d^2(^3F)5s$; Rh I, $4d^8(^3F)5s$;[15] Ru II, $3d^6(^5D)5s$; Rh II, $3d^7(^4F)5s$; Zr II, $4d^2(^3F)6s$. The presence of other near configurations probably accounts for considerable perturbation of the levels belonging to these configurations. That they do not conform to the three vector problem can also be blamed on the fact that the d^k configuration does not obey Russell-Saunder's coupling, and so it is not permissible to assume that the L and S_d of the core have a meaning.

Some of the calculations were made by Earl Senkbeil in connection with a student FERA grant. The writer wishes to acknowledge his indebtedness and express his appreciation to Dr. R. Serber, who originally considered the three vector problem applied to d^k ms and who made many valuable suggestions and assisted considerably throughout the entire work. It is with the greatest pleasure that I thank Professor J. H. Van Vleck who suggested the four vector problem and who has assisted me in the preparation of this paper.

[14] Term value data on Cu III were taken from a paper by Raghavendra Rao, Zeits. f. Physik **88**, 135 (1934).

[15] Applying the three vector problem to the companion $6s$ configuration, Rh I, $4d^8(^3F)6s$, we find that the term values for the ^4F multiplet occur in the order of J values, $4\frac{1}{2}$, $3\frac{1}{2}$, $1\frac{1}{2}$ and $2\frac{1}{2}$, respectively. This is contrary to the experimental data where the term values have been classified in the order of J values, $4\frac{1}{2}$, $3\frac{1}{2}$, $2\frac{1}{2}$ and $1\frac{1}{2}$, respectively. Save for the separation between $J=2\frac{1}{2}$ and $J=1\frac{1}{2}$ however, the three vector problem yields separations which agree much better with experiment than those calculated for a case of Russell-Saunder's coupling.

Averages Over Portions of Configuration Space

GABRIEL HELLER AND LLOYD MOTZ, *Columbia University*

(Received July 12, 1934)

The integral $\int_\gamma^\delta R_{nl}^2\rho^{\sigma+2}d\rho$ is evaluated where R_{nl} is the radial hydrogen eigenfunction. The results are applied to the calculation of term shifts when the Born-Infeld potential function replaces the Coulomb potential function in the one-electron Schroedinger problem.

INTRODUCTION

IN the treatment of certain quantum-mechanical problems it is found necessary to evaluate integrals of functions of r (representable by Laurent series) over finite portions of configuration space. In problems involving screening effects, as for example in many electron problems, and also in collision problems such integrals arise. Again, the calculation of isotope shifts involve averaging processes which lead to similar integrals. And in general in problems where the fitting together of potential functions becomes necessary one meets with integrals of this type. In this paper we shall give a general method of evaluating these integrals for the Schroedinger hydrogenic eigenfunction.[1] As an illustration we shall calculate the term shifts arising from the replacement of the Coulomb potential by the Born-Infeld potential.

THEORY

The average of r^s over the interval γ to δ in atomic units[2] (A.U.) is

$$\overset{\gamma\text{---}\delta}{r_{nl}{}^s}=\int_\gamma^\delta \Re_{nl}{}^2 r^s r^2 dr=\frac{(n-l-1)\,!}{(n+l)\,!2n}\left(\frac{n}{2Z}\right)^s \times\left[I^{s+1}_{n+l,\ 2l+1}(\gamma)-I^{s+1}_{n+l,\ 2l+1}(\delta)\right], \quad (1)$$

where $\Re_{nl}=NR_{nl}$ is the normalized radial hydrogen eigenfunction for the state (n, l), and

$$I_{\lambda\mu}{}^\sigma(\gamma)=(\lambda\,!)^{-2}\int_\gamma^\infty e^{-\rho}\rho^{\mu+\sigma}(L_\lambda{}^\mu(\rho))^2 d\rho$$

$$=\text{coefficient of } (ut)^\lambda \text{ in } \frac{(ut)^\mu}{[(1-t)(1-u)]^{\mu+1}} \times\int_\gamma^\infty \rho^{\mu+\sigma}\exp\left[-\frac{\rho(1-ut)}{(1-t)(1-u)}\right]d\rho. \quad (2)$$

The last line is obtained in the familiar way[3] by expressing the associated Laguerre polynomials in terms of their generating functions.

We now note the formulas[4]

$$\int_\gamma^\infty e^{-\alpha\rho}\rho^m d\rho=\sum_{k=0}^\infty \gamma^k\alpha^{k-m-1}\cdot\frac{(-1)^{k+m}}{(k-1-m)\,!k} \qquad (m=\mu+\sigma>-1), \quad (3a)$$

[1] The results are also applicable to the Dirac eigenfunctions. Furthermore, it will be seen that the method is not restricted to Laguerre polynomials but is of a more general nature, and can be applied to other types of polynomials possessing generating functions.

[2] i.e., in multiples of $a_H=0.5281\times10^{-8}$ cm. For atomic units see, e.g., Bethe, Handb. d. Physik **24**, 1, 273 (1933). Unless otherwise stated our quantities will always be expressed in atomic units.

[3] Waller, Zeits. f. Physik **38**, 635 (1926). He evaluated integral (2) for $\gamma=0$. See also Bethe, reference 2, p. 283.

[4] From the familiar definition of negative factorials (Gauss) one obtains

$$\left[\frac{1}{(k-n)\,!k}\right]_{k=0}=(-1)^{n-1}(n-1)!;\ \binom{-s-1+i}{i}=(-1)^i\binom{s}{i}.$$

We also point out the identities

$$\sum_{j=0}^m(-1)^j\binom{k}{j}=(-1)^m\binom{k-1}{m};$$

$$\frac{1}{k!}\left[\frac{1}{k+1}\sum_{j=0}^{i}\frac{1}{\binom{k+j+1}{j}}-\frac{1}{k}\right]=\frac{-(i+1)!}{(k+i+1)\,!k}$$

which are made use of in summing the coefficients of like powers of γ. Finally, we remark that $\sum'_{k=-M+1}^{+\infty}$ means that the $k=0$ term is to be omitted, and that we define $\sum_{j=0}^{-1}=0$.

$$\int_\gamma^\infty \frac{e^{-\alpha\rho}}{\rho^M}d\rho = \sum_{k=-M+1}^{+\infty}{}' \gamma^k \alpha^{k+M-1}\cdot\frac{(-1)^{k-M}}{(k-1+M)\,!k} + \frac{(-\alpha)^{M-1}}{(M-1)\,!}\left(\sum_{i=0}^{M-2}\frac{1}{1+j} - 0.5773 + \log\frac{1}{\alpha\gamma}\right)$$

$$(-M=\mu+\sigma\leqslant -1). \quad (3b)^5$$

By expanding one obtains for the coefficient of $(ut)^{\lambda-\mu}$ in

$$\frac{1}{[(1-t)(1-u)]^{\mu+1}}\alpha^\nu = (1-ut)^\nu\cdot[(1-t)(1-u)]^s,$$

$$M_{\lambda\mu}{}^s = \sum_{i=0}^{\lambda-\mu}\binom{\mu+s+i}{i}\cdot\binom{s}{\lambda-\mu-i}^2$$

$$= \sum_{i=0}^{\lambda-\mu}\binom{s+\lambda-i}{\lambda-\mu-i}\cdot\binom{-s-1+i}{i}^2$$

$$= \sum_{i=0}^{\lambda-\mu}(-1)^{\lambda-\mu-i}\binom{-s-\mu-1}{\lambda-\mu-i}\cdot\binom{-s-1+i}{i}^2$$

$$(\nu=-s-\mu-1). \quad (4)$$

For $s\geq 0$, $0>s>-\mu-1$, $-\mu-1\geq s$ the first, second, and third expressions, respectively, are the most convenient.[6] For the coefficient of $(ut)^{\lambda-\mu}$ in $(\alpha^\nu\log\alpha)/[(1-t)(1-u)]^{\mu+1}$ one obtains

$N_{\lambda\mu}{}^\nu$ = coeff. of $(ut)^{\lambda-\mu}$ in

$$\frac{1}{[(1-t)(1-u)]^{(-s)}}\frac{d}{d\nu}(1-ut)^\nu + (1-ut)^\nu\frac{d}{d(-s)}\frac{1}{[(1-t)(1-u)]^{(-s)}}$$

$$= \sum_{j=0}^{\lambda-\mu}(-1)^j\binom{\nu}{j}\binom{-s+\lambda-\mu-j-1}{\lambda-\mu-j}^2 \times\left[\sum_{i=0}^{j-1}\frac{1}{\nu-i}+2\sum_{i=0}^{\lambda-\mu-j-1}\frac{1}{-s+i}\right]$$

$$(\nu=-s-\mu-1). \quad (5)$$

[5] $-0.5773=\int_1^\infty\frac{e^{-u}}{u}du+\int_1^0\frac{(-1)^j}{j!j}$.

[6] In the cases $\sigma>-\mu-1$ the $M_{\lambda\mu}{}^\sigma$ have simple physical meaning: $(\mu+\sigma)!M_{\lambda\mu}{}^\sigma=\rho_{\lambda\mu}{}^\sigma$ ($\bar\rho$ is defined by Eq. (8)).

We are thus led to a power series

$$I_{\lambda\mu}{}^\sigma(\gamma)=\sum_0^{+\infty}A_k\gamma^k \qquad (\sigma+\mu>-1) \quad (6a)$$

or to a Laurent series with an additional logarithmic term

$$I_{\lambda\mu}{}^\sigma(\gamma)=\sum_{\mu+\sigma+1}^{+\infty}B_k\gamma^k+B\log\gamma \quad (\sigma+\mu\leqslant -1) \quad (6b)$$

as the expressions for I.

The coefficients are given by the formulae

$$A_k(\sigma,\lambda,\mu)=\frac{(-1)^{k+\mu+\sigma}M_{\lambda\mu}{}^{\sigma-k}}{(k-1-\mu-\sigma)\,!k} \qquad (\sigma+\mu>-1\,;\,k\geqslant 0), \quad (7a)$$

$$B_{k\neq 0}(\sigma,\lambda,\mu)=\frac{(-1)^{k+\mu+\sigma}M_{\lambda\mu}{}^{\sigma-k}}{(k-1-\mu-\sigma)\,!k} \qquad (\sigma+\mu\leqslant -1\,;\,0\neq k\geqslant\sigma+\mu+1), \quad (7b)$$

$$B_0(\sigma,\lambda,\mu)=\left(\sum_{j=0}^{-\mu-\sigma-2}\frac{1}{1+j}-0.5773\right) \times\frac{(-1)^{-\mu-\sigma-1}}{(-\mu-\sigma-1)\,!}M_{\lambda\mu}{}^\sigma-\frac{(-1)^{-\mu-\sigma-1}}{(-\mu-\sigma-1)\,!}N_{\lambda\mu}{}^\sigma, \quad (7c)$$

$$B(\sigma,\lambda,\mu)=-(-1)^{-\mu-\sigma-1}M_{\lambda\mu}{}^\sigma/(-\mu-\sigma-1)\,!. \quad (7d)$$

One notices that the A_k coefficients vanish for $0<k<\mu+\sigma+1$.

The special case $\gamma\ll 1$ is of primary interest. Eqs. (6) then reduce to

$$I_{\lambda\mu}{}^\sigma=A_0=\sum_{i=0}^{\lambda-\mu}\frac{(\lambda+\sigma-i)\,!}{(\lambda-\mu-i)\,!}\binom{\sigma}{i}^2 \qquad (\sigma+\mu>-1), \quad (6^*a)$$

$$I_{\lambda\mu}{}^\sigma=B_{\mu+\sigma+1}\gamma^{\mu+\sigma+1} =\binom{\lambda}{\lambda-\mu}^2\gamma^{\mu+\sigma-1}/(-\mu-\sigma-1) \qquad (\sigma+\mu<-1), \quad (6^*b)$$

$$I_{\lambda\mu}{}^\sigma=B_0+B\log\gamma =\binom{\lambda}{\lambda-\mu}^2\left[\log\frac{1}{\gamma}-0.5773-2\sum_0^{\lambda-\mu-1}\frac{1}{\mu+1+i}\right] +\sum_1^{\lambda-\mu}\frac{1}{i}\binom{\lambda-i}{\lambda-\mu-i}^2 \qquad (\sigma+\mu=-1). \quad (6^*c)$$

TABLE I. $M_{\lambda\mu}{}^{s}$ $(M_{\lambda\mu}{}^{|s|}=M_{\lambda\mu}{}^{-|s|-1})$

s \ n,l	1,0	2,0	2,1	3,0	3,1	3,2	4,0	4,1	4,2	4,3
	$M_{11}{}^{s}$	$M_{21}{}^{s}$	$M_{22}{}^{s}$	$M_{31}{}^{s}$	$M_{32}{}^{s}$	$M_{33}{}^{s}$	$M_{41}{}^{s}$	$M_{42}{}^{s}$	$M_{43}{}^{s}$	$M_{44}{}^{s}$
1	1	4	1	9	6	1	16	20	8	1
0	1	2	1	3	4	1	4	10	6	1
−1	1	2	1	3	4	1	4	10	6	1
−2	1	4	1	9	6	1	16	20	8	1
−3	1	8	1	27	10	1	64	46	12	1
−4	1	14	1	69	16	1	216	98	18	1
−5	1	22	1	153	24	1	624	200	26	1
−6	1	32	1	303	34	1	1584	370	36	1
−7	1	44	1	549	46	1	3616	640	48	1
−8	1	58	1	927	60	1	7564	1046	62	1
−9	1	74	1	1479	76	1	14716	1630	78	1
−10	1	92	1	2253	94	1	26944	2440	96	1
−11	1	112	1	3303	114	1	46864	3530	116	1
−12	1	134	1	4689	136	1	78016	4960	138	1
−13	1	158	1	6477	160	1	125064	6796	162	1
−14	1	184	1	8739	186	1	194016	9110	188	1
−15	1	212	1	11553	214	1	292464	11980	216	1

TABLE II. $N_{\lambda\mu}{}^{s}$

s \ n,l	1,0	2,0	3,0	4,0	2,1	3,1	4,1
	$N_{11}{}^{s}$	$N_{21}{}^{s}$	$N_{31}{}^{s}$	$N_{41}{}^{s}$	$N_{33}{}^{s}$	$N_{43}{}^{s}$	$N_{53}{}^{s}$
−2	0	3	10½	23½			
−3	0	5	27½	83½			
−4	0	7	59½	245	0	7	73½

For the evaluation of coefficients A and B we need the values of the M's and N's. In Tables I and II sets of such values are given. They enable one to calculate the first few terms of $r_{nl}{}^{\kappa}$ for $|\kappa|<6$, $(n,l)=(1,0)$ to $(4,3)$.

We give below a few r averages as examples to illustrate the tendency of series (6) in their dependence upon the quantum numbers and the exponent of r. In general we can remark that for suitable γ's the series converge rapidly, because of their alternating nature and the appearance of factorials in the denominators of the coefficients. Denoting

$$\overline{r_{nl}{}^{\kappa}}=\frac{(n-l-1)!}{(n+l)!2n}\left(\frac{n}{2Z}\right)^{\kappa}\cdot\overline{\rho_{nl}{}^{\kappa}}, \tag{8}$$

we have

$$\gamma\overline{\rho_{10}{}^{2}}^{\infty}=4!-\frac{\gamma^5}{0!5}+\frac{\gamma^6}{1!6}-\frac{\gamma^7}{2!7}+\cdots,$$

$$\gamma\overline{\rho_{21}{}^{2}}^{\infty}=6!-\frac{\gamma^7}{0!7}+\frac{\gamma^8}{1!8}-\frac{\gamma^9}{2!9}+\cdots,$$

$$\gamma\overline{\rho_{20}{}^{2}}^{\infty}=4!-\frac{4\gamma^5}{0!5}+\frac{8\gamma^6}{1!6}-\frac{14\gamma^7}{2!7}+\cdots,$$

$$\gamma\overline{\rho_{20}{}^{-5}}^{\infty}=4\gamma^{-2}-\frac{8\gamma^{-1}}{1!1}+\frac{(3/2-0.5773)\times14-7}{2!}-\frac{14}{2!}\log\gamma+\frac{22}{3!1}\gamma-\frac{32}{4!2}\gamma^2+\cdots.$$

BORN-INFELD POTENTIAL

We shall now apply the foregoing results to the calculation of the Born-Infeld term-shifts. According to Born and Infeld,[7] an elementary charged particle (of charge e) gives rise to the potential

$$V_B(r)=\int_r^{\infty}e[r_0{}^4+R^4]^{-\frac{1}{4}}dR.$$

$$(r_0=2.28\times10^{-13}\text{ cm}=4.32\times10^{-5}a_H). \tag{9}$$

We shall consider the nucleus as an elementary particle of charge Ze giving rise to the B.I. potential, and proceed to calculate the term shifts in the one-electron Schroedinger problem using the difference between B.I. and Coulomb potentials as the perturbation.

By the usual perturbation method the energy shift (in A.U.'s) is given by

$$\Delta E=-Z\int_0^{\infty}\Re_{nl}{}^2(V_B-V_C)r^2dr$$

$$=-ZN_F{}^2r_0{}^2\int_0^1e^{-\gamma x}(\gamma x)^{2l}[F_{nl}(\gamma x)]^2\times\left[a-\sum_0^{\infty}\frac{(-1)^k(2k-1)!!}{(2k)!!(4k+1)}x^{4k+1}-\frac{1}{x}\right]x^2dx$$

$$-ZN_L{}^2r_0{}^2\int_1^{\infty}e^{-\gamma x}(\gamma x)^{2l}[L_{n+l}^{2l+1}(\gamma x)]^2\times\left[\sum_0^{\infty}\frac{(-1)^k(2k-1)!!}{(2k)!!(4k+1)}\cdot\frac{1}{x^{4k+1}}-\frac{1}{x}\right]x^2dx$$

$$=\int_0^1\text{I}+\int_1^{\infty}\text{II}, \tag{10}$$

where $\gamma=2Zr_0/n$,

$$(2n-1)!!=(2n-1)\cdot(2n-3)\cdot\ldots\cdot3\cdot1$$

$$x=r/r_0, \qquad (2n)!!=(2n)(2n-2)\cdot\ldots\cdot4\cdot2$$

$$(e/r_0)\cdot a=V_B(0)=1.854e/r_0. \qquad 0!!=(-1)!!=1$$

[7] M. Born and L. Infeld, Proc. Roy. Soc. London **A144**, 425 (1934).

We observe that $\gamma \ll 1$. Hence in $\int$I we replace the hypergeometric function, F_{nl}, and the exponential by 1. $\int$II can be written as

$$\Delta E_{nl}^{\mathrm{II}} = \left(\sum_{k>(l+1)/2}^{\infty} + \sum_{k=(l+1)/2} + \sum_{k=1}^{k<(l+1)/2} \right) \times H(k)\gamma^{4k-2} I^{-4k}_{n+l,\, 2l+1}(\gamma)$$

($k=(l+1)/2$ term does not appear for l even) where

$$H(k) = -ZN_L{}^2 r_0{}^2 \frac{(-1)^k(2k-1)!!}{(2k)!!(4k+1)} \cdot [(n+l)!]^2.$$

In $\Delta E_{nl}{}^{\mathrm{II}}$ only the lowest power of r_0* contributes in our approximation. For $l=0$ we therefore need keep only the first summation, for $l=1$ only the first two summations, and for $l \geq 2$ only the $k=1$ term of the third summation.

For the total shift we have then

$$\Delta E_{nl} = \Delta E_{nl}{}^{\mathrm{I}} + \Delta E_{nl}{}^{\mathrm{II}},$$

$$\Delta E_{n0} = (0.494+0.172)(Z^4 r_0{}^2/n^3)\text{A.U.} = 2.72\times 10^{-4}(Z^4/n^3)\ \mathrm{cm}^{-1}, \quad (11a)$$

$$\Delta E_{n1} \lesssim 10^{-19} Z^6\ \mathrm{cm}^{-1}, \quad (11b)$$

$$\Delta E_{n,\, l\geq 2} < \Delta E_{n1}. \quad (11c)$$

Recent experiments[8] on the fine structure of the Balmer series show a disagreement between calculated and observed term values. Though expressions (11) give corrections in the right direction they are barely observable even in the most favorable cases of highly penetrating orbits and hence cannot account for the discrepancies.

We have also applied these formulas to x-ray levels and found that the results were negligible.

One might conjecture that a rigorous treatment using Dirac eigenfunctions would noticeably affect the results. But a simple examination shows that for light atoms the increase in shift is extremely small, and even for the heaviest atoms it is only a fraction of (11).

We wish to thank Professor I. I. Rabi for his interest and help.

* $r_0{}^2$ for $l=0$, $r_0{}^4$ for $l>0$.

[8] E.g., Houston and Sheih, Bull. Am. Phys. Soc. **8**, No. 5 (1933).

Observations on Hilbert's Independence Theorem and Born's Quantization of Field Equations

HERMANN WEYL, *Institute for Advanced Study, Princeton, New Jersey*

(Received July 6, 1934)

Born recently proposed a quantization of the field equations which is based upon Hilbert's independence theorem of the calculus of variations.[1] My intention here is to give, in the first purely mathematical Part A, a formulation as simple and explicit as possible of the independence theorem. The agreement between the principle of variation and the independence theorem, complete in the case of one independent variable and one unknown function, fails in two respects in the case of several variables and functions; the independence theorem specializes the extremal vector field on the one hand and it discards the assumption of integrability on the other hand.[2] In Part B, I first suggest a modification of Born's scheme without which it would be in disagreement with ordinary quantum mechanics even in the one-dimensional case. After the modification, a comparison with Heisenberg-Pauli's quantization becomes possible under the simplest circumstances. Born's scheme proves to be too narrow. Finally I raise the principal objection that the quantum-mechanical equation should not be of the form: four-dimensional divergence of ψ equals $H\psi$ with a scalar operator of action H but that it should rather consist of four components stating that differentiation of ψ with respect to the four space-time coordinates is performed by means of the operators: energy and momentum.*

[1] Proc. Roy. Soc. **A143**, 410 (1934).

[2] These are known facts. Born himself refers to: Prange, Thesis, Göttingen, 1915. But the theory was developed before Prange and in a more general and suitable form by Volterra (1890), Fréchet (1905) and de Donder. Cf. de Donder, Mém. Acad. Roy. de Belgique, ser. 2, III (1911); *Théorie invariantive du calcul des variations*, Paris, 1930, Chaps. VII and VIII.

* The abstract will also serve as a summary and introduction to the paper.—EDITOR.

A. Hilbert's Independence Theorem for Several Arguments

§1. The problem of variation

The problem of the calculus of variation in r independent variables $t^1 \cdots t^r$ consists in determining ν functions or a "surface"

$$z^\alpha = z^\alpha(t^1 \cdots t^r), \qquad (\alpha = 1, 2 \cdots \nu) \tag{1}$$

such that the variation

$$\delta \int L(t^i, z^\alpha, z_i^\alpha) dt^1 \cdots dt^r = 0 \tag{2}$$

for arbitrary variations $\delta z^\alpha(t)$ which vanish at the border of the domain of integration. L is here a given function of the arguments t^i, z^α, z_i^α; one has to substitute the functions (1) for z^α and the derivatives dz^α/dt^i for z_i^α.

§2. Surface field and vector field

A family of ∞^ν surfaces $z^\alpha = z^\alpha(t^1 \cdots t^r)$ simply covering a piece Ω of the $(r+\nu)$, dimensional space of coordinates (t^i, z^α) may be called a *surface field* in Ω. At every point (t, z) of Ω we have the "gradient vector"

$$dz^\alpha/dt^i = z_i^\alpha(t, z) \tag{3}$$

of the surface passing through (t, z). Conversely, if one is given the *vector field* $z_i^\alpha(t, z)$ arbitrarily, one can find a corresponding field of surfaces provided Eqs. (3) are completely integrable. As one readily sees, the necessary and sufficient conditions of integrability are the relations

$$\left(\frac{\partial z_k^\alpha}{\partial t^i} - \frac{\partial z_i^\alpha}{\partial t^k}\right) + \left(\frac{\partial z_k^\alpha}{\partial z^\beta} z_i^\beta - \frac{\partial z_i^\alpha}{\partial z^\beta} z_k^\beta\right) = 0. \tag{4}$$

(Always sum over two-fold occurring indices!) A vector field satisfying these equations may be called *integrable*.

§3. Three stages of independent variables

We distinguish three standpoints: (1) t^i, z^α, z_i^α are taken as independent variables, as for instance in the function L. The derivatives with respect to these variables are distinguished by an attached index. (2) By using a given vector field, the z_i^α are replaced by functions of the t^i and z^α. The partial derivatives with respect to the arguments t^i and z^α are then denoted by $\partial/\partial t^i$, $\partial/\partial z^\alpha$. (3) The substitution

$$z^\alpha = z^\alpha(t^1 \cdots t^r) \quad \{z_i^\alpha = dz^\alpha/dt^i\}$$

changes functions which appeared in the second (or the first) standpoint, into functions of the t alone. The derivatives with respect to the t's are denoted by d/dt^i.

We have already complied with these conventions in paragraphs 1 and 2.

§4. Extremal vector field

The Lagrangian equations of the problem of variation (2) are (standpoint 3)

$$dL_{z_i^\alpha}/dt^i = L_{z^\alpha}. \tag{5}$$

A solution of these equations may be designated as an *extremal surface*. We start with a *field of extremal surfaces*. Such a field is, according to (5), characterized by the equations (standpoint 2):

$$\frac{\partial L_{z_i^\alpha}}{\partial t^i} + \frac{\partial L_{z_i^\alpha}}{\partial z^\beta} z_i^\beta = L_{z^\alpha}. \tag{6}$$

A vector field $z_i^\alpha(t, z)$ satisfying (6) is called an *extremal vector field* whether it is integrable or not.

§5. Legendre transformation

We introduce (standpoint 1) the momenta

$$p_\alpha{}^i = L_{z_i^\alpha} \tag{7}$$

and

$$p = L - p_\alpha{}^i z_i^\alpha. \tag{8}$$

From the total differential

$$\delta L = L_{t^i} \delta t^i + L_{z^\alpha} \delta z^\alpha + L_{z_i^\alpha} \delta z_i^\alpha,$$

there follows

$$\delta p = L_{t^i} \delta t^i + L_{z^\alpha} \delta z^\alpha - z_i^\alpha \delta p_\alpha{}^i.$$

It is therefore natural to assume that p is given as function of t^i, z^α, $p_\alpha{}^i$,

$$p = H(t^i, z^\alpha, p_\alpha{}^i).$$

We then have $z_i^\alpha = -H_{p_\alpha{}^i}$ as the converse of the relation (7).

We now should write (standpoint 2) $p_\alpha{}^i$ instead of $L_{z_i^\alpha}$ on the left side of (6). In order to determine the right side, one has to differentiate the Eq. (8) or

$$p = L - p_\beta{}^i z_i^\beta$$

with respect to z^α:

$$\frac{\partial p}{\partial z^\alpha} = L_{z^\alpha} + L_{z_i^\beta} \frac{\partial z_i^\beta}{\partial z^\alpha} - p_\beta{}^i \frac{\partial z_i^\beta}{\partial z^\alpha} - \frac{\partial p_\beta{}^i}{\partial z^\alpha} z_i^\beta.$$

Here the second and third terms cancel each other, and consequently the equations characteristic of an extremal vector field read as follows:

$$\frac{\partial p_\alpha{}^i}{\partial t^i}+\left(\frac{\partial p_\alpha{}^i}{\partial z^\beta}-\frac{\partial p_\beta{}^i}{\partial z^\alpha}\right)z_i{}^\beta=\frac{\partial p}{\partial z^\alpha}; \tag{9}$$

$$p=H(t^i, z^\alpha, p_\alpha{}^i), \quad z_i{}^\alpha=-H_{p_\alpha{}^i}. \tag{10}$$

§6. Special extremal vector field and Jacobi-Hamilton equation

Eq. (9) is satisfied in particular if

$$\frac{\partial p_\alpha{}^i}{\partial z^\beta}-\frac{\partial p_\beta{}^i}{\partial z^\alpha}=0, \quad \frac{\partial p_\alpha{}^i}{\partial t^i}=\frac{\partial p}{\partial z^\alpha}. \tag{11}$$

We then speak of a *special extremal vector field.* One makes good these equations by putting

$$p_\alpha{}^i=\partial s^i/\partial z^\alpha$$

and by assuming that the new unknown quantities s^i fulfil the equation

$$\partial s^i/\partial t^i=p.$$

In this way determination of a special extremal vector field is reduced to the integration of the *Jacobi-Hamilton equation*

$$(\text{div } s=)\,\partial s^i/\partial t^i=H(t^i, z^\alpha, \partial s^i/\partial z^\alpha). \tag{12}$$

If one wants the vector field $z_i{}^\alpha=-H_{p_\alpha{}^i}$ to be integrable one has to satisfy further Eqs. (4).

§7. Invariance. Flux

The t^i as well as the z^α may be subjected to an arbitrary transformation among themselves. Let us treat $z_i{}^\alpha$ as a vector contravariant in the Greek, covariant in the Latin, indices; L as a scalar density with respect to the t^i and as a scalar in z_α; $p_\alpha{}^i$ as a contravariant vector density in i, as a covariant vector in α; s^i as a contravariant vector density with respect to the t^i (as a scalar with respect to z^α). Under such circumstances all our equations remain unaltered by the transformation. Hence the *flux* of s^i through an arbitrary $(r-1)$-dimensional "cross section" Λ of the r-dimensional t-space:

$$S=\int_\Lambda \begin{vmatrix} s^1 & \cdots & s^r \\ dt^1 & \cdots & dt^r \\ \cdot & \cdots & \cdot \\ \delta t^1 & \cdots & \delta t^r \end{vmatrix} \tag{13}$$

has an invariant significance. In forming (13) we operate on a surface Σ: $z^\alpha=z^\alpha(t^1\cdots t^r)$ (standpoint 3), and Λ is to be considered as an $(r-1)$-dimensional "line" on the surface Σ.

§8. The independent integral

Following Gauss' theorem, one can change the flux (13) through a *closed* Λ into an integral extending over the piece of Σ bounded by Λ; its integrand

$$\frac{ds^i}{dt^i}=\frac{\partial s^i}{\partial t^i}+\frac{\partial s^i}{\partial z^\alpha}\frac{dz^\alpha}{dt^i}=p+p_\alpha{}^i\frac{dz^\alpha}{dt^i}$$

contains only the original quantities $p_\alpha{}^i$ and p instead of the s. This is Hilbert's "*independent integral*," for it does not change its value if one changes in an arbitrary manner the piece of surface Σ bounded by Λ in the $(r+\nu)$-dimensional (t^i, z^α)-space, provided the boundary line Λ is preserved.

§9. Case of no forces

If L depends only on the third group of variables $z_i{}^\alpha$ and if H consequently depends only on the $p_\alpha{}^i$ then

$$p_\alpha{}^i=\text{const.}, \qquad p=H(p_\alpha{}^i)=\text{const.}$$

yields a special integrable extremal vector field. The corresponding s^i is:

$$s^i=p_\alpha{}^i z^\alpha+(1/r)pt^i. \tag{14}$$

This particular solution is of course not endowed any longer with the general invariance as described in section 7.

B. Critical Remarks Concerning Born's Proposal of a Quantization of Electromagnetic Field Equations

§10. Born's procedure

Professor Born propounds the following procedure for the transition to quantum physics. One first forms the flux S, (13) of the vector density (14) through an arbitrary closed line Λ and takes $\psi=e^{iS}$ ("plane wave"); one then builds up wave packets or a general ψ by forming linear superpositions of plane waves that correspond to several values of the constants $p_\alpha{}^i$. Each such ψ is a function of the following arguments:

$$V=\int_{\Sigma} dt^1\cdots dt^r; \quad \int_{\Sigma}\frac{dz^\alpha}{dt^i}dt^1\cdots dt^r. \qquad (15)$$

Here Σ denotes the domain in our r-dimensional t-space surrounded by the line Λ. $|\psi|^2$ should be interpreted as the probability that the integrals (15) assume given values in a domain Σ of given volume V. All domains of the t-space here, be it noticed, if they only have the same volume, are thrown into the same pot without regard to their shape and situation! This sounds queer enough and, as a matter of fact, Born's interpretation does not coincide with the usual well-proved interpretation of quantum mechanics even in the one-dimensional case where t=time is the only variable. For there $|\psi|^2$ is the probability that the quantities z^α assume given values at the instant t, whereas Born is urged to look upon it as a probability of transition, namely, the probability that the quantities z^α experience given changes $\Delta z^\alpha=\int(dz^\alpha/dt)dt$ in a time interval of given length Δt—irrespective of the temporal localization of the interval Δt. One obviously has to tear asunder the closed "null-dimensional line," which bounds the one-dimensional time interval and consists of two time points, into its initial and end point. We are able to imitate this procedure in r dimensions by determining the flux S through a *cross section* Λ of the t-space instead of a *closed* Λ. Let us think of the whole t-space as dissolved into a simply infinite sequence of such cross sections. In the physical applications r is equal to 4, and $t^1, t^2, t^3; t^0=t$ are the 4 space and time coordinates. *After choosing the planes of simultaneity* t=const. as our cross sections Λ, Born's procedure becomes somewhat comparable to the Heisenberg-Pauli quantization.

§11. Comparison of the Born and the Heisenberg-Pauli process in the simplest case

The comparison can actually be carried out for the particular case of an L depending only on the temporal derivatives $z_\alpha{}^\alpha=dz^\alpha/dt$. In this case the fundamental ψ, the plane wave, becomes, according to Born,

$$\exp\left[i\int\int\int\{\tfrac{1}{4}tH(p_\alpha{}^0)+p_\alpha{}^0z^\alpha\}dt^1dt^2dt^3\right].$$

Here the $p_\alpha{}^0$ are constants; the z^α are arbitrary functions of t^1, t^2, t^3. The Heisenberg-Pauli procedure yields the same result, with the difference however that this time the $p_\alpha{}^0$ are arbitrary functions of the space coordinates t^1, t^2, t^3: the probability refers to the question as to which values the physical quantities z^α assume *at all possible space points*. This more general formulation, obviously required by the nature of the problem, is not entirely beyond the scope of Born's quantization. For in the present circumstances the following p's:

$$p_\alpha{}^0=\text{arbitrary functions of } t^1, t^2, t^3, \qquad [p_\alpha{}^i=0\ (i=1, 2, 3)]$$

furnish a special extremal vector field. But it is not integrable! Thus one is led to *renounce the assumption of integrability*.

§12. Objections and hopes

Nevertheless I am unable to see how, by means of an analogous extension of Born's scheme, the general case could be brought into agreement with fundamental physical experience. For the characteristic commutation rules of coordinates and corresponding momenta, q and p, are missing in Born's theory, owing to the fact that he subsumes the field equations under the mechanical "problem without forces"; but these commutation rules seem to be essential for the possibility of considering the electromagnetic ether as a superposition of oscillators (photons). On the other hand, I am fairly sure that the scheme of quantum physics should not be obtained from the one equation (12) in the form div$=H$ by means of Schrödinger's quantum-mechanical transmutation, but that it should consist rather of four equations

$$d/dt^i=T_i$$

in which the four operators T_i represent the energy and the three components of momentum. The recipe for forming the T_i is rather complicated in the Heisenberg-Pauli theory and the fact that they form a covariant 4-vector in the sense of relativity theory needs a special proof. One may perhaps expect that a way similar to that followed by Born will lead to an essentially simpler formulation and perhaps a modification of this prescription so as to put the relativistic invariance in evidence from the beginning.

On the Constitution of Metallic Sodium. II

E. WIGNER AND F. SEITZ, *Palmer Physical Laboratory, Princeton University*

(Received June 18, 1934)

The present work represents an extension to a previous development by the same authors, on the theory of metallic sodium. In the first part of this paper a completely self-consistent solution of Fock's equations for the sodium lattice is carried through indirectly, this being the approximation in which one-electron functions are employed. The question of the correlations between electrons with parallel spin is investigated quantitatively and the Fermi "zero-point energy" is calculated using the proper effective field. The results show that the electrons behave almost exactly as if they were entirely free, the binding energy being 9 kg cal and the lattice constant 4.86A, as compared with the observed values 26.9 kg cal and 4.23A. To complete the picture, the correlations between electrons with anti-parallel spins are investigated in the latter part, since these are not included in the Fock picture. A general discussion of this question is presented and a quantitative treatment of its effect is made which yields a new binding energy of 23.2 kg cal and a lattice constant of 4.75A. The source of the remaining discrepancy is discussed.

I. THE POTENTIAL INSIDE THE LATTICE

1.

In a previous paper by the same authors a method of calculating the binding properties of metals was developed[1] and applied to sodium. The procedure employed was essentially one of solving the Fock system of equations[2] for the valence electrons (i.e., the system of equations to which the Schrödinger equation reduces when one electron functions are assumed). This solution did not proceed from a formal investigation of Fock's differential equations, but was developed indirectly under the guiding principles of the picture afforded by the free electron theory.

To begin with, the lattice was subdivided into polyhedrons of equal size and form, which we shall call *s*-polyhedrons, each of which surrounds one ion lying in its center, and is bounded by the planes which bisect, perpendicularly, the lines connecting the corresponding ion with its 14 neighbors (the alkali metals form body centered lattices). Since these polyhedrons closely resemble spheres, they may be replaced by spheres of equal volume for many purposes and these we shall designate as *s*-spheres, their radius being $r_s = (3v_0/4\pi)^{\frac{1}{3}}$, where v_0 is the atomic volume.

Concerning the nature of the electronic states of the lattice, we know that there will be bands of allowed levels, no more than two electrons occupying each level because of the restrictions imposed by the Pauli principle, and that the lowest state in the lowest band will possess the symmetry of the lattice. From this it follows that its normal derivative will vanish on the boundaries of the *s*-polyhedrons and to obtain its wave function, it is only necessary to solve the Schrödinger equation within one polyhedron, by using a suitable effective field and this boundary condition. Approximate wave functions of other electrons may be obtained from this by multiplying it with factors of the form

$$e^{2\pi i(\nu_1 x+\nu_2 y+\nu_3 z)/L}, \qquad (1)$$

where ν_1, ν_2, ν_3 are positive or negative integers and L is the length of the crystal-edge, corresponding to free electrons with nonvanishing eigenvalues of momentum.

In order to find the effective potential field inside of an *s*-polyhedron, we first replace them by *s*-spheres, correcting later for the small error arising from this. For an electron at a given point the field consists of three parts: first, the potential arising from the ion at the center of the *s*-sphere, second, the potential of the other ions; and third, the potential arising from the other free electrons. Instead of making a direct calculation of each of these in the order given it is found far more advantageous to begin with an investigation of the third for it happens that simplifying assumptions concerning the nature of this interaction may be fully justified at a later stage and allow a simple treatment of the first two.

[1] E. Wigner and F. Seitz, Phys. Rev. **43**, 804 (1933).
[2] J. C. Slater, Phys. Rev. **35**, 210 (1930); V. Fock, Zeits. f. Physik **61**, 126 (1930).

The potential of the electron under consideration arising from the other electrons is equal to that arising from a continuous electron fluid of density which is e times the probability of having an electron at the corresponding point of the lattice. If we assume that all wave functions arise from one by multiplication with a factor of the form (1), the probability distribution will be the same for each. Moreover, since it will be spherically symmetric within each sphere the effective field of each ion will be neutralized outside of the sphere in which it is contained, and the only field which remains to be taken into account for our chosen electron is that arising from the charge within the s-sphere which contains it. Since this will give rise to a spherically symmetric field and a spherically-symmetric wave function, the assumption of spherical symmetry is completely self-consistent. The error introduced by replacing the s-polyhedrons by spheres is calculated in appendices 1 and 2 and turns out to be negligibly small.

In the previous work only the field arising from the ion in each s-sphere was taken into account and it was assumed that correlations were such that other electrons did not penetrate the given sphere. Under this assumption, the wave function turned out to be practically constant for more than 90 percent of the volume of the sphere (cf. Fig. 1), a fact which allows us to take the other electrons into account very simply and correct for the inaccuracies involved. For if we now introduce the assumption that all of the electrons have the distribution given by ψ_{000} of Fig. 1 (with factors (1)), it is found that this set of one-electron functions forms a practically self-consistent solution of Fock's equations for the lattice.

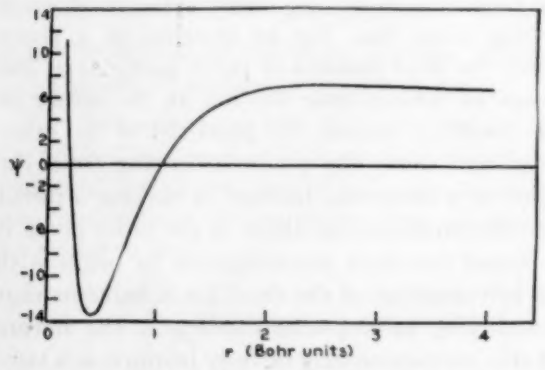

FIG. 1. Metallic wave function for lowest electronic state. The corresponding energy is -0.6 Rydberg units and the proper boundary condition is satisfied at 4.04 Bohr units.

The potential $V(x, y, z)$ which enters into the wave equation of an electron in Fock's system is not the ordinary average of the potentials of the other particles for all configurations, but the average of the potentials with each configuration taken with the weight it has under the assumption that the considered electron is in the point x, y, z. We have seen Eq. (6) that there is a hole in the otherwise uniform electron fluid around every electron because the probability of two electrons having parallel spin being very near is very small. We shall call this the Fermi hole. Its effect is such as to make the potential more negative than it would otherwise be. Since its shape is practically independent of the position of the electron, the change of the potential arising from it is constant and it alters the energy but not the wave function. The previous work merely gave an estimate of this change and we shall give a more accurate calculation here.

Because the wave functions of electrons of higher energy are given by multiplying ψ_{000} by (1) only in the case of free electrons (i.e., when ψ_{000} is constant), we have investigated this very important point in more detail (cf. Section II), and have found that the energy differences between the different states is the same as that obtained when the electrons are free. The wave functions are not simply ψ_{000} multiplied by (1), however, but each is multiplied in addition by a factor which is nearly constant within a sphere one Bohr unit in radius but becomes exponential outside.

In all of the work sketched in the previous paragraphs we have been able to restrict ourselves to the one electron picture, that is, the wave function for all of the electrons may be assumed to be a determinant of single electron functions. This leads to correlations between electrons of parallel spin of the type expressed by the Fermi holes and to none whatever between electrons of antiparallel spin. There are such correlations, however, arising from the mutual repulsion terms, but they lie beyond the scope of Fock's equations. We shall call these holes "correlation holes" and the corresponding

energy "correlation energy," and shall attempt to handle them in Section III.

2.

Under the assumption of a uniform charge distribution the potential within the s-sphere at the distance r from the ion is

$$V(r)+(3e^2/2r_s)-(e^2r^2/2r_s^3), \qquad (2)$$

where the first term arises from the ion, and the other two from the electron fluid inside the s-polyhedron. In reference 1 the wave equation for the potential $V(r)$ alone—which was taken from Prokofjew's work[3]—was solved and the corresponding characteristic value determined. The correction for the fact that this is not exactly the energy of the corresponding wave function is taken care of in Appendix 1. The second term in (2) is independent of r, leaving the wave function unchanged, and gives a positive contribution

$$E_{11}=3e^2/4r_s \qquad (3)$$

to the energy. A factor $\frac{1}{2}$ enters, since the interactions between electrons have to be counted only once.

In order to take into account the last term, the Schrödinger perturbation theory may be applied and this yields

$$E_{12}=\tfrac{1}{2}\left(-\frac{e^2}{2r_s^3}\int\psi^2r^2dv+\frac{e^4}{4r_s^6}\sum_k{}'\frac{(\int\psi\psi_k r^2dv)^2}{E-E_k}\right) \qquad (4)$$

up to the second approximation where ψ and E are the solutions of the wave equation with the potential $V(r)$ alone, which we know from reference 1. The factor $\frac{1}{2}$ arises for the same reason given before. To determine the first part of (4) we have numerically evaluated the integral over ψ^2r^2 for three different values of the lattice constant, i.e., r_s and the corresponding energy. The results are tabulated in Table I, the energy being given in Rydberg units, r_s in Bohr units, and the integral in squares of Bohr units. For the actual lattice constant $r_s=4$, the integral has the same value that it would have if ψ were a constant. The last column gives the ratio f of the numerically calculated integral to that calculated with a constant ψ for the other cases.

TABLE I.

E	r_s	$\int\psi^2r^2dv$	f
−0.60	4.05	9.90	0.994
−0.55	4.74	12.95	0.962
−0.50	5.48	16.50	0.916

[3] W. Prokofjew, Zeits. f. Physik **58**, 255 (1929).

In the second part of (4) the denominator may be replaced by a mean value $E-E_k$ and the summation in the numerator gives $\int\psi^2r^4dv-(\int\psi^2r^2dv)^2$ in the usual way.[4] By taking ψ to be constant for this small term one obtains

$$-\frac{1}{E_k-E}\cdot(e^4/r_s^2)\cdot\left(\frac{3}{56}-\frac{9}{200}\right)=-0.005e^2/r_s. \qquad (5)$$

The mean value of E_k has been estimated to be +0.3 Rydberg units. The effect of the perturbing terms in (2) on the wave functions can safely be said to be extremely small because of the smallness of (5), and their total contribution to the energy is

$$E_{12}=(-0.15f-0.005)e^2/r_s. \qquad (6)$$

The fact that we must deal with the s-polyhedron instead of s-sphere is taken into account in Appendix 2.

3.

In the preceding section we have calculated using the ordinary average potential. We know, however, that in order to calculate the potential of an electron at a certain point we should average over the configuration of the other electrons with the weights which they would have if the electron under consideration were at the given point. It was shown in reference 1 that if there is an electron at a given point the probability of another electron being at a distance r from it is

$$\tfrac{1}{2}\frac{e}{v_0}\left[1-9\left(\frac{\sin(r/d')-(r/d')\cos(r/d')}{(r/d')^3}\right)^2\right]. \qquad (7)$$

The factor $\frac{1}{2}$ expresses the fact that only the distribution of charge with parallel spin is affected, v_0 is the atomic volume and $d'=(v_0/3\pi^2)^{\frac{1}{3}}$. (7) was derived under the assumption that ψ_{000} is constant and that the higher ones are obtained from it by multiplication with (1). Both assumptions will be shown to be practically correct

[4] A. Unsöld, Zeits. f. Physik **43**, 563 (1927).

insofar as energies are concerned. The total amount of charge removed because of the hole expressed by (7) is exactly e and may be viewed as being concentrated in the electron at the center of the hole. To this approximation it has been assumed that all of this hole is in the parallel charge distribution—an assumption not exactly correct, however.

The decrease in the potential energy of the electron at the center of the hole is

$$\frac{9}{2}\frac{e^2}{v_0}\int_0^\infty \frac{1}{r}\left(\frac{\sin(r/d')-(r/d')\cos(r/d')}{(r/d')^3}\right)^2 4\pi r^2 dr = \frac{3^{4/3}e^2}{2\pi^{1/3}v_0^{1/3}} = \frac{3^{5/3}}{2^{5/3}\pi^{2/3}}\frac{e^2}{r_s} = 0.916\frac{e^2}{r_s}. \tag{8}$$

Since this energy[5] does not depend on the position of the electron, it is to be carried forward at once as an energy with a factor $\frac{1}{2}$, in order that the interactions between pairs of electrons is taken into account only once. We have, therefore,

$$E_2 = -0.458e^2/r_s. \tag{9}$$

If the wave function were not entirely flat in the lowest state, (7) should be more rigorously multiplied by $v_0\psi_{000}$. The integral (8) will hardly be affected by this, however, because the regions in which ψ_{000} changes appreciably are small compared to the distance in which (7) has appreciable variation and the mean value of (8) for different positions of the electron will differ from the calculated value by even a smaller percentage.

The sum $E_{11}+E_{12}+E_2$ from the viewpoint of Fock's equation, gives the effect arising from the fact that the potential at any point is not exactly $V(r)$ (where r is the distance from the nearest ion), as it would be if the hole in the electron fluid of the other electrons extended exactly over the s-sphere. It really surrounds (cf. Fig. 2) the electron under consideration spherically in such a way that part (A) of the s-sphere is left uncovered. On the other hand, it extends over regions (C) outside the s-sphere. Now E_2 represents the effect of the entire hole $(B+C)$, while $E_{11}+E_{12}$ represents the effect of the lack of hole in the regions A and B. The fact that we made all calculations under the assumption that the electron density is constant, will not greatly affect our final result, since in the largest region, B, it does not matter which density we use, as long as we use the same density in both cases.

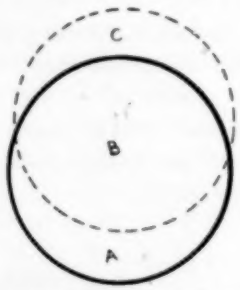

FIG. 2. Schematic diagram of prominent regions in the unit cell.

An error will be introduced only by using an improper density in A and C—but here ψ_{000} is very nearly constant.

II. THE FERMI ENERGY

4.

Our next task is the calculation of the zero-point energy of the free electrons. First of all, an error in reference 1 should be corrected, for it was stated there that the zero-point energy is actually smaller than it would be for free electrons. It was observed that $\psi^0_{\nu_1\nu_2\nu_3} = \psi_{000}\exp[2\pi i(\nu_1 x+\nu_2 y+\nu_3 z)/L]$ possessed the proper transformation properties for a state with the quantum numbers ν_1, ν_2, ν_3 (the "components of momentum" being[6] $2\pi\hbar\nu_1/L$, $2\pi\hbar\nu_2/L$, $2\pi\hbar\nu_3/L$). Moreover its mean energy was higher than that of ψ_{000} by the amount $2\pi^2\hbar^2(\nu_1^2+\nu_2^2+\nu_3^2)$ which is just the Fermi cor-

[5] This formula was first found by F. Bloch, Zeits. f. Physik **57**, 545 (1929).

[6] $\hbar$ in this paper is Dirac's h, namely, Planck's constant divided by 2π. We would like to correct another error of reference 1 here. The subtraction of 2500 cal. from the binding energy at the end of Section IV is incorrect. The fact that the binding energy of the inner shells decreases with increasing binding of the valence electrons does not appear in the Prokofjew picture because the potential energy of the valence electron is taken to be ρV instead of $\frac{1}{2}\rho V$, so that it is not necessary to consider the change of the potential acting on the other particles.

rection for an entirely free electron. As the real $\psi_{\nu_1\nu_2\nu_3}$ is the solution of a minimum problem, it was concluded that its energy is even lower than that of $\psi^0_{\nu_1\nu_2\nu_3}$.

This argument is not correct, however, since $\psi_{\nu_1\nu_2\nu_3}$ has the lowest energy of only those states which are orthogonal to the states of the K and L shells. This is correct for ψ_{000} but not for $\psi^0_{\nu_1\nu_2\nu_3}$ and the real $\psi_{\nu_1\nu_2\nu_3}$ should be calculated just as ψ_{000} was—by solving a differential equation.

At any rate, it can be assumed from the transformation property of $\psi_{\nu_1\nu_2\nu_3}$ that it has the form

$$\psi_{\nu_1\nu_2\nu_3} = \chi_{\nu_1\nu_2\nu_3} \exp\left[2\pi i(\nu_1 x + \nu_2 y + \nu_3 z)/L\right], \tag{10}$$

where $\chi_{\nu_1\nu_2\nu_3}$ has the translational periods of the lattice. By inserting (10) into the Schrödinger equation, one obtains

$$\begin{gathered} H\chi_{\nu_1\nu_2\nu_3} + \frac{2\pi i\hbar^2}{mL}\left(\nu_1\frac{\partial}{\partial x} + \nu_2\frac{\partial}{\partial y} + \nu_3\frac{\partial}{\partial z}\right)\chi_{\nu_1\nu_2\nu_3} = F_{\nu_1\nu_2\nu_3}\chi_{\nu_1\nu_2\nu_3}, \\ E_{\nu_1\nu_2\nu_3} = F_{\nu_1\nu_2\nu_3} + (2\pi^2\hbar^2/mL^2)(\nu_1^2+\nu_2^2+\nu_3^2). \end{gathered} \tag{11}$$

If we neglect the second term on the left side to begin with, the equation is identical with the equation for ψ_{000}, which we shall denote by ψ_0 in this section, the other solutions of (11) with $\nu_1=\nu_2=\nu_3=0$ being designated by ψ_κ. To this approximation $E_{\nu_1\nu_2\nu_3} = E_{000} + 2\pi^2\hbar^2/mL^2(\nu_1^2+\nu_2^2+\nu_3^2)$ which is just the result of reference 1.

We shall take into account the second term of (11) by the Rayleigh-Schrödinger perturbation method. The first approximation gives zero, since $\int\psi_0\partial\psi_0/\partial x$ vanishes, and the second approximation will be proportional to the ν's. From considerations of the s-polyhedron, the boundary conditions were found to be such that the value and derivative of the wave functions should be equal in the two points at which a line perpendicular to the boundary plane cuts the boundary. We know furthermore from group theory that all solutions ψ_κ of the unperturbed problem are either even or odd functions of x, y, z. Now if we calculate the second approximation for the energy, we need integrals of the type $\int\psi_0\partial\psi_\kappa/\partial x$, and since ψ_0 is an even function of the coordinates, ψ_κ must be even in y, z and odd in x, or the integral vanishes. Therefore, all three perturbing terms in (11) will give non-vanishing matrix elements only with different ψ_κ. The second approximation for the energy is, therefore

$$F_{\nu_1\nu_2\nu_3} = \frac{4\pi^2\hbar^4}{m^2L^2}(\nu_1^2+\nu_2^2+\nu_3^2)\sum_\kappa{}' \frac{|\int\psi_\kappa\,\partial\psi_0/\partial x|^2}{E_0-E_\kappa}, \tag{12}$$

since the integral with the y and z-derivatives can be replaced by integrals with x derivatives, E_κ is the energy of the state ψ_κ. The sum in (12) contains one positive term (arising from the $2p$ level) and all other terms are negative. Since the value of the positive term is very sensitive to the actual shape of the wave function ψ_0, we tried to transform (12) in a form more suitable for the calculation in the following way.

If ψ_0 and ψ_κ were the characteristic functions of an atom, (12) could be evaluated by the Thomas-Kuhn sum rule and would give just the negative Fermi correction, so that the sum of the first and second approximation would be zero. In the present case of periodic boundary conditions, however, the partial integrations cannot be performed in the same way. We obtain from the Schrödinger equation for ψ_κ by multiplication with $x\psi_0$ and subtracting the corresponding equation for ψ_0 multiplied by $x\psi_\kappa$

$$(E_\kappa - E_0)\int x\psi_0\psi_\kappa = -\frac{\hbar^2}{2m}\int\left[x\psi_0\Delta\psi_\kappa - \psi_\kappa\Delta(x\psi_0)\right] - \frac{\hbar^2}{m}\int\psi_\kappa\frac{\partial\psi_0}{\partial x}. \tag{13}$$

The first term can be transformed by Green's theorem into a surface integral and we have

$$\int\psi_\kappa\frac{\partial\psi_0}{\partial x}dv = \frac{m(E_0-E_\kappa)}{\hbar^2}\int x\psi_\kappa\psi_0 dv - \tfrac{1}{2}\int\left(x\psi_0\frac{\partial\psi_\kappa}{\partial n} - \psi_\kappa\frac{\partial(x\psi_0)}{\partial n}\right)df, \tag{14}$$

where $\partial/\partial n$ denotes the normal derivative. For the usual boundary conditions, the last term in (14) would vanish. After replacing *one* of the integrals in (12) by the expression (14), the summation over κ can be carried out in the first term by the completeness-relation[7] and yields

$$(4\pi^2\hbar^2/mL^2)(\nu_1^2+\nu_2^2+\nu_3^2)\int x\psi_0(\partial\psi_0/\partial x)dv. \tag{15}$$

Since ψ_0 is a function of r alone, we have

$$\int x\psi_0\frac{\partial\psi_0}{\partial x}dv=\frac{2\pi}{3}\int_0^{r_s} r^3\frac{\partial\psi_0^2}{\partial r}dv=\tfrac{1}{2}v_0\psi_0(r_s)^2-\tfrac{1}{2}.$$

The $-\frac{1}{2}$ gives the negative Fermi correction and cancels the first approximation. The first term, however, gives an expression very similar to the Fermi correction, namely

$$\frac{2\pi^2\hbar^2}{mL^2}(\nu_1^2+\nu_2^2+\nu_3^2)v_0\psi_0(r_s)^2, \tag{16}$$

the difference being that the value of ψ_{000} at the boundary enters instead of the mean value.

The second term of (14), inserted into (12), gives

$$-\frac{2\pi^2\hbar^4}{m^3L^2}(\nu_1^2+\nu_2^2+\nu_3^2)\sum_\kappa{}'\frac{\int(\psi_\kappa\,\partial\psi_0/\partial x)dv}{E_0-E_\kappa}\int x\psi_0\frac{\partial\psi_\kappa}{\partial n}df, \tag{17}$$

since all odd ψ_κ vanish at the boundary. To this sum the $2p$ state does not contribute anything more, because its wave function is practically zero outside $r=3$. Similarly we found upon direct computation, that the integral $\int\psi_\kappa\partial\psi_0/\partial x d\vartheta$ vanishes "accidentally" for $r_s=4$ for the next higher odd state. The energy of the next is of the order of magnitude $+5$ Rydberg units and we have replaced E_κ in the denominators of (17) by a mean value E_κ of this magnitude. Now $\int\psi_\kappa\partial\psi_0/\partial x d\vartheta$ is the expansion coefficient of ψ_κ in the series for $\partial\psi_0/\partial x$ so that the summation can be carried out in the numerator and gives $\int x\psi_0(\partial/\partial n)(\partial\psi_0/\partial x)df$. Since ψ_0 is a function of r alone, (17) can further be transformed into

$$-\frac{2\pi^2\hbar^4}{m^2L^2}(\nu_1^2+\nu_2^2+\nu_3^2)\frac{4\pi}{3}r_s^3\psi_0(r_s)\frac{\partial^2\psi_0(r_s)}{\partial r^2}. \tag{18}$$

Here $\partial^2\psi_0/\partial r^2$ can be calculated from Schrödinger's equation and we obtain for the entire zero-point energy the sum of (16) and (18)

$$E_{\nu_1\nu_2\nu_3}-E_{000}=(2\pi^2\hbar^2/mL^2)(\nu_1^2+\nu_2^2+\nu_3^2)v_0\psi_0(r_s)^2[1+2(E_0-V(r_s)/(E_0-\bar{E}_k)]. \tag{19}$$

This equation shows that the ratio of the actual zero-point energy of the electrons to the zero point energy of free electrons is

$$v_0\psi_0(r_s)^2[1+2(E_0-V(r_s)/(E_0-\bar{E}_k)] \tag{19a}$$

can be larger than 1. It approaches zero for very large r_s but increases greatly with decreasing r_s when the pressing of the valence electrons into the inner shells becomes appreciable. The second term of (19) is negligible, and several values of the first are given in the table below:

r_s	3.67	4.05	4.74	5.48
$v_0\psi_0(r_s)^2$	1.08	0.99	0.89	0.76

Once again, it is found that ψ_{000} behaves at $r=4$ as if it were constant. Moreover it is remarkable that the second term in (19a) increases the Fermi energy over the classical value by a very small amount, if the potential is taken as arising entirely from the ion, and it decreases it somewhat below that value if ψ_0 is supposed to be

[7] This is exactly London's reasoning (Zeits. f. Physik 39, 322 (1926)) with the only difference that the partial integration must be carried through more carefully than in his case.

the solution of a Schrödinger equation with the potential (2).

5.

If one plots the Fermi energy against $(\nu_1^2+\nu_2^2+\nu_3^2)^{\frac{1}{2}}$ Eq. (19) should give the curvature of the plot at the zero point. It would not be right, however, to assume that it is correct for all ν. As a matter of fact we know from the work of F. Bloch[8] that for higher ν it may depend upon the ratios $\nu_1 : \nu_2 : \nu_3$ and from the work of P. M. Morse, R. Peierls[9] and especially L. Brillouin[10] that it is not a continuous function of the ν's everywhere but has discontinuities corresponding to wave-lengths for which the Bragg-Laue conditions of x-ray reflections are fulfilled.

According to Brillouin this discontinuity in the space of the ν's is on the rhombdodecahedron $\nu_1 \pm \nu_2 = \pm L/d$, $\nu_1 \pm \nu_3 = \pm L/d$, $\nu_2 \pm \nu_3 = \pm L/d$ where d is the lattice constant in the space of the ν's. In order to obtain an idea of the size of these discontinuities, we have taken three points of this rhombdodecahedron, corresponding to the three directions (100), (110), (111) and tried to obtain the two energy values for each of them, the transformation properties of the corresponding waves being determined for the symmetry elements of the space group.

It was an easy matter to find a function which had the proper transformation properties within the s-polyhedron but it seemed difficult for us to satisfy the continuity conditions at the boundary. The procedure finally adopted possesses no rigorous justification, but it was decided most reasonable to select wave functions which were continuous only at the midpoint of the fourteen boundary planes, with linear combinations of s, p, d, f and g functions. For the point $\nu_1 = \nu_2 = L/2d$, $\nu_3 = 0$ ((110) direction) it was sufficient to take a linear combination of the s, d and g functions for the lowest function at the discontinuity and a p function for the upper. For the (111) direction the lower was represented by a linear combination of p and d functions and the upper by a combination of s, f and g while for the (100) direction the lower part was a linear combination of p and d functions and the upper was a d function. The results for the observed lattice constants are shown in Fig. 3 in which the abscissa is $(\nu_1^2+\nu_2^2+\nu_3^2)^{\frac{1}{2}}d/L$ and the energy is in Rydberg units. The parabola corresponds to free electrons; the heavy section representing the extent to which electrons would occupy the levels, and the other three curves correspond to the designated direction $\nu_1 : \nu_2 : \nu_3$. In accord with the remarks in previous paragraphs that the electrons behave almost as if free, the discontinuities are not very pronounced. The calculations leading to Fig. 3 do not justify an accuracy greater than 0.05 Rydberg units for absolute values of energy, although the energy differences at the discontinuities are probably more accurate.

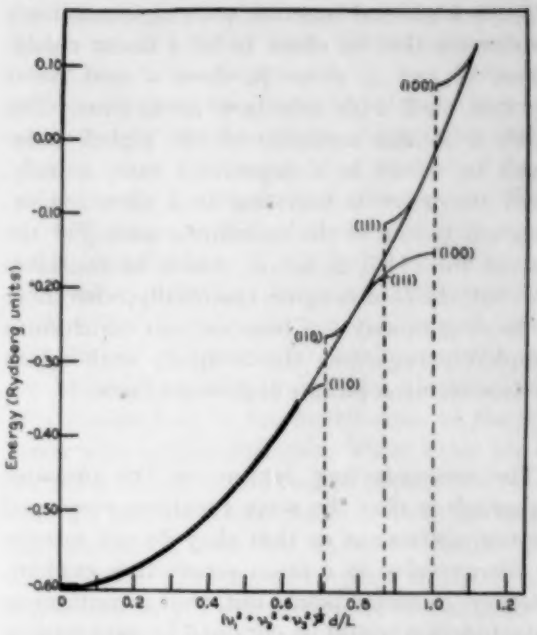

FIG. 3. Graph showing the energy as a function of $(\nu_1^2+\nu_2^2+\nu_3^2)^{\frac{1}{2}}d/L$ for wave functions of electrons 'moving' in three prominent crystallographic directions.

In a recent paper which has appeared while this manuscript was in preparation, Slater[11] has investigated this phase of the problem from a viewpoint similar to that presented here. He has made a formal solution satisfying the proper boundary conditions at the centers of the eight hexagonal faces of the s-polyhedron, which

[8] F. Bloch, Zeits. f. Physik **52**, 555 (1928).
[9] P. M. Morse, Phys. Rev. **35**, 1310 (1930); R. Peierls, Ann. d. Physik **4**, 121 (1930).
[10] L. Brillouin, Die Quantenstatistik, Berlin 1931, p. 281–316.
[11] J. C. Slater, Phys. Rev. **45**, 794 (1934). Cf. also H. Jones, N. F. Mott, H. W. B. Skinner, Phys. Rev. **45**, 379 (1934).

requires a general function with eight arbitrary parameters that he chose to be a linear combination of one s, three p, three d and one f function each with arbitrary coefficients. This yields a secular equation of the eighth order which he solves in a degenerate case, namely, when the wave is traveling in a direction orthogonal to one of the coordinate axes. For the case of the (110) direction, which he considers in detail, the results agree, essentially, with those we have obtained and bear out our conclusions completely regarding the accuracy with which the free electron picture represents facts.

6.

The unsatisfactory feature of the previous paragraph is that the wave functions employed are not continuous so that they do not possess an energy-value in a strict sense. It is evident, however, as Slater points out, that a continuous wave function would be obtained by superposing an infinite number of wave functions with different angular factors, which is also possible in the case of a constant potential, though it would be a rather awkward procedure, since we know the wave functions accurately. This would correspond to a development of $e^{2\pi i\nu z/L}$ into a series

$$e^{2\pi i\nu z/L}=f_0(r)+P_1(\theta,\varphi)f_1(r)+P_2(\theta,\varphi)f_2(r), \quad (20)$$

where the P_l are the spherical harmonics and the f_l depend only on the distance from the center of the s-polyhedron and are essentially Bessel-functions. If we determine (20) in each s-polyhedron, the resulting functions will join each other continuously, since they all represent the same function $e^{2\pi i\nu z/L}$. For the energy value of 0.15 Rydberg units which in the case of free electrons corresponds to $\nu d/L=\frac{1}{2}$, the quantities rf_l'/f_l are given at the surface of the s-sphere in the first line of the table below:

l	s 0	p 1	d 2	f 3
Free electron	−0.9666	0.049	1.647	2.7
Electron in lattice	−1.00	0.044	1.674	2.8

The last line gives the same quantities for the Prokofjew-field of Na for the distance $r_s=4$ and the energy value −0.45 Rydberg units, which lies 0.15 above the energy value −0.60 of the electron with the lowest energy. The first two numbers were obtained by graphical integration, and the others are those for a simple Coulomb field, since the field of the Na ion does not give different values from those of a simple Coulomb field for d, f and higher terms. It is seen that the deviation of the two sets of numbers in the table are very small. Hence, if one adds the s, p, d, etc., solutions of the Prokofjew field with such coefficients that the value of each function at $r=r_s$ is equal to the value of the corresponding function f_l in (20) for the same radius, one obtains a function within the s-polyhedron which will join similar functions in the other s-polyhedra continuously and even with practically continuous first derivatives. This shows that the energy of the waves for $(\nu_1^2+\nu_2^2+\nu_3^2)^{\frac{1}{2}}d/L=\frac{1}{2}$ is higher than that of the wave $\nu_1=\nu_2=\nu_3=0$ by the same amount (0.15 Rydberg units) in both cases. The same is true for all ν's which characterize states occupied by electrons.

If the numbers of the first line were smaller than those of the second, the Fermi energy would be smaller for free electrons than in the actual lattice. A more detailed numerical consideration shows that this is actually the case, though only to a very small extent. The situation seems to be opposite, however, if one takes into account the perturbation given in (3). The difference does not amount to more than 1 or 2 percent in either case, however, and we shall employ the numbers corresponding to free electrons in the following.

Of course the coincidence of the two sets of numbers arises simply from the fact that the electrons in our picture behave very nearly like free electrons. We know that the optical properties of metals can also be explained very well on this assumption,[12] so it possesses additional backing.

When all the energy terms calculated in section 1 are added, one obtains the lower curve of Fig. 4 for the energy of the bottom of the Fermi distribution as a function of the lattice constant, which is represented by the radius of the s-sphere. The upper curve contains the Fermi energy and gives the total energy of the electrons in the Fock picture. It yields a lattice constant of 4.76A and a binding energy of 9.0 cal.

[12] C. Zener, Nature **137**, 968 (1933); R. de L. Kronig, Nature **133**, 211 (1934).

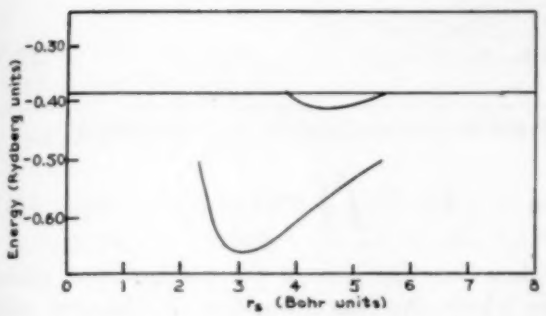

FIG. 4. Energies as functions of r_s. The lower curve is the energy of the lowest electronic state while the upper curve represents the energy of the entire lattice computed on the basis of the one-electron picture.

III. CORRELATIONS BETWEEN ELECTRONS WITH ANTIPARALLEL SPIN

7.

In proceeding with a generalization of the foregoing sections to include electron correlations more general than those allowed by the one electron picture, we no longer have at hand guiding principles that are as definite as those which we had there. Since the energy is to be minimized, the extensions to be made rest principally upon the possibility of forming a hole around every electron in the charge distribution of the other electrons. This possibility is, of course, given by the multi-dimensionality of the wave function, which allows a different probability distribution of the other electrons for different positions of the one considered. Since such a hole is already present in the charge distribution of the electrons with parallel spin, we have principally to consider the possibility of a similar hole in the distribution of the electrons with antiparallel spin. These holes are not included in the one electron picture (cf. reference 3), but we know them to exist in atomic eigenfunctions from the works of Bethe[13] and Hylleraas.[14] They seem to play an even more important rôle in metals than in free atoms.[15]

The wave function employed in the previous sections for $2n$ electrons, may be written under neglect of the spin part, as[16]

$$\Psi(x_1 \cdots x_n, y_1 \cdots y_n) = (1/n!) \begin{vmatrix} \psi_1(x_1) & \cdots & \psi_1(x_n) \\ \cdot & & \cdot \\ \cdot & & \cdot \\ \psi_n(x_1) & \cdots & \psi_n(x_n) \end{vmatrix} \cdot \begin{vmatrix} \psi_1(y_1) & \cdots & \psi_1(y_n) \\ \cdot & & \cdot \\ \cdot & & \cdot \\ \psi_n(y_1) & \cdots & \psi_n(y_n) \end{vmatrix}. \tag{21}$$

Here x_k represents the three Cartesian coordinates of the kth electron with upward spin and the y refer in a similar way to the electrons with downward spin. The functions $\psi_1, \cdots, \psi_n$, previously designated by $\psi_{r_1 r_2 r_3}$ are the n lowest energy wave functions for an electron in the field of all the ions and the other electrons, regarded as a charge distribution. The task of the previous section, which we believe to be solved to a sufficient degree of accuracy, was to calculate the functions ψ and the energy of the total Ψ of (21) as functions of the lattice constant.

A natural suggestion for the generalization of (21) is to include the coordinates of all electrons of antiparallel spin in $\psi_r(x_k)$ as parameters. This function will then be a different function of x_k for different values of $y_1, \cdots, y_n$, and will have a minimum around every value of the set. We shall consider the effect on the function ψ_r and the energies if we replace the continuous charge distribution of the electrons by point charges at $y_1 \cdots y_n$. This replacement will alter the field acting on the electron x and we shall use a perturbation method to calculate its consequences.

We shall set

$$\Psi(x_1, \cdots, x_n; y_1, \cdots, y_n) = (1/n!) \begin{vmatrix} \psi_1(y_1, \cdots, y_n; x_1) & \cdots & \psi_1(y_1, \cdots, y_n; x_n) \\ \cdot & & \cdot \\ \cdot & & \cdot \\ \psi_n(y_1, \cdots, y_n; x_n) & \cdots & \psi_n(y_1, \cdots, y_n; x_n) \end{vmatrix} \cdot \begin{vmatrix} \psi_1(y_1) & \cdots & \psi_1(y_n) \\ \cdot & & \cdot \\ \cdot & & \cdot \\ \psi_n(y_1) & \cdots & \psi_n(y_n) \end{vmatrix} \tag{22}$$

[13] H. Bethe, Zeits. f. Physik **57**, 815 (1929).
[14] E. A. Hylleraas, Zeits. f. Physik **48**, 469 (1928).
[15] We are much indebted to Professor Slater for the remark that possibly the disagreement between experiment and his theory for the order and distance of atomic terms due to the same configuration, also arises from the fact that the correlation energy is greater for singlets than for higher multiplets.
[16] M. Delbrück, Proc. Roy. Soc. (London) **A129**, 686 (1930).

and denote by

$$\Psi_0(x_1, \cdots, x_n; y_1, \cdots, y_n) = \psi_1(y_1, \cdots, y_n; x_1) \cdots \psi_n(y_1, \cdots, y_n; x_n) \cdot |y|, \tag{22a}$$

the part of (22) which is not yet antisymmetrized in the x's, where $|y|$ is the second determinant in (22). When no ambiguity arises, we shall designate $\psi_\nu(y_1 \cdots y_n, x)$ by $\psi_\nu(x)$, in which it is to be understood that both x and ν correspond to sets of three numbers. In addition, it will be assumed that both $\psi_\nu(y_1 \cdots y_n, x)$ and its complex conjugate appear in the first determinant of (22) when this function is not real, that the same is true regarding $\psi_\nu(y)$ in $|y|$, and that the $\psi_\nu(y_1 \cdots y_n, x)$ as functions of x are solutions of a characteristic value problem so that

$$\int \psi_\nu(y_1, \cdots, y_n; x)^* \psi_{\nu'}(y_1, \cdots, y_n; x) dx = \delta_{\nu\nu'} \tag{23}$$

for all values of y.

It is well known that the total energy of Ψ can be written in the form [17]

$$\int\int \Psi^*(K_x + K_y + V_0 + V)\Psi_0 dxdy,$$

where K_x and K_y are the operators for the kinetic energy of the electrons of upward and downward spin respectively, V_0 is the old potential function calculated from the viewpoint in which the electrons are regarded as smeared out over the entire crystal, and V is the potential function required to account for the change incurred by viewing the y-electrons to be point charges with regard to their interaction with the x-electrons. The first three terms are those dealt with in the previous work and yield the wave function (21), while the last is a perturbing term and will yield a perturbation energy. If we retain the old wave functions in the neighborhood of the ions and replace them by a more general solution of (22) in regions where they behave like $e^{2\pi i \nu z/L}$, the expectation value of V_0 will be left unchanged since the electron density is changed nowhere, and in addition, it may be seen that (7) remains essentially true. The sum of the energy correction E and the Fermi energy F will be given, therefore, by the integral

$$E + F = \int\int \Psi^*(K_x + K_y + V)\Psi_0 \tag{24}$$

taken over the part of the configuration space in which the wave function is changed and which we shall assume to be the entire space.[18] It is to be noted that for an entirely flat wave function the expectation value of V, namely

$$\int\int V|y|^2 dxdy \tag{25}$$

is zero. We shall proceed with a calculation of the energy correction E.

8.

To begin with, we shall transform the three terms of (24) to a more suitable form. In calculating the expectation value of $\hbar^2/2m \cdot \Delta_x$, we can use (23) to carry out the integration over all of the remaining x's and obtain

$$\int\int \Psi^* K_x \Psi_0 dxdy = -\frac{\hbar^2}{2m}\frac{1}{n!}\sum_\nu \int\int \psi^* \times \Delta_x \psi_0 |y|^2 dxdy. \tag{26}$$

If the same is done for $-\hbar^2/2m \cdot \Delta_y$, the terms arising from the second derivative of the determinant are

$$(4\pi^2\hbar^2/2m)\sum \nu^2. \tag{27a}$$

Those terms containing the derivatives of the $\psi_\nu(y_1 \cdots y_n, x_\nu)$ and of the determinant may be integrated over all of the x's except x_ν and lead to expressions of the form

$$\int\int y_\nu(x_\nu)^* |y| \frac{\partial \psi_\nu(x_\nu)}{\partial y_\kappa} \frac{\partial}{\partial y_\kappa} |y| dx_\nu dy.$$

If this is added to the similar term containing the derivative of ψ_ν^* it follows from (23) that the sum will vanish upon integration over x_ν. Finally, those terms which contain the second derivative of Ψ_0 are of two types, namely,

[17] Cf. e.g. E. Wigner, Gruppentheorie und ihre Anwendung. Braunschweig 1931. p. 323.

[18] The difference of the two volumes is negligible.

$$-(\hbar^2/2m)(1/n!)\sum_\nu \int\int \psi_\nu(x_\nu)^* \Delta y_\nu \psi_\nu(x_\nu)\,|y|^2 dx_\nu dy \tag{27b}$$

and

$$-(\hbar^2/2m)(1/n!)\sum_{\nu\neq\mu}\int\int [\psi_\nu(x_\nu)^*\psi_\mu(x_\mu)^* - \psi_\nu(x_\mu)^*\psi_\mu(x_\nu)^*]\cdot \operatorname{grad}_{y_k}\psi_\nu(x_\nu)\operatorname{grad}_{y_k}\psi_\mu(x_\mu)\,|y|^2 dx_\nu dx_\mu dy.$$

If $\psi_\nu \neq \psi_\mu^*$ we can add to the latter the term in which ψ_ν^* replaces ψ_ν and the sum will vanish upon integration over x. Hence the only terms resulting from the first term in the bracket are

$$-\hbar(^2/2m)(1/n!)\sum_\nu \int \left|\int \psi_\nu(x_\nu)^* \operatorname{grad}_{y_k}\psi_\nu(x_\nu)dx_\nu\right|^2 |y|^2 dy \tag{27c}$$

and those from the second are such as to yield

$$-(\hbar^2/2m)(1/n!)\sum_{\mu\neq\nu}\int\left|\int \psi_\mu(x)^* \operatorname{grad}_{y_k}\psi_\nu(x)dx\right|^2 |y|^2 dy. \tag{27d}$$

If $\mu=\nu$ in (27d), we obtain (27c), so that the sum of (26), (27a, b, c, d) and

$$(1/n!)\sum_\nu \int\int |\psi_\nu(y_1,\cdots,y_n;x)|^2 V(y_1,\cdots,y_n;x)dx\,|y|^2 dy$$

leads to

$$\frac{1}{n!}\sum\int\int \psi_\nu(x)^*\left[V(y_1,\cdots,y_n;x) - \frac{\hbar^2}{2m}\left(\Delta_x+\Delta_{y_1}+\cdots+\Delta_{y_n}+\frac{4\pi^2\nu^2}{L^2}\right)\right]\cdot\psi_\nu(x)dx\,|y|^2 dy$$

$$-(\hbar^2/2m)(1/n!)\sum_k\sum_{\mu,\nu}\int\left|\int \psi_\nu(x)\operatorname{grad}_{y_k}\psi_\nu^*(x)dx\right|^2 |y|^2 dx = E \tag{28}$$

for the change in energy since

$$F=(\hbar^2/2m)2\sum_\nu(4\pi^2\nu^2/L^2)$$

is the Fermi energy. The summations over μ and ν are to be extended over all occupied states. In the following it will appear from the form given $\psi_\nu(y_1\cdots y_n, x)$ (i.e., see (29)) that the last expression in (28), which could only lower the energy, vanishes.

We shall proceed under the assumption that $\psi_\nu(y_1\cdots y_n, x)$ has the form

$$\psi_\nu(y_1,\cdots,y_n;x)=e^{2\pi i\nu\cdot x/L}\chi_\nu(x-y_1,\cdots,x-y_n), \tag{29}$$

in which χ_ν to the approximation considered here, is a constant plus a sum of functions, each of which depends on one argument $x-y_k$. When substituted in (28) this yields

$$E=\sum_\nu\int\int \chi_\nu^*[V(y_1,\cdots,y_n;x)-(\hbar^2/2m)(2\Delta_x+(4\pi i/L)\nu\cdot\operatorname{grad}_x)]\psi_\nu\cdot|y|^2 dxdy. \tag{30}$$

In order to minimize this χ_ν must satisfy the equation

$$-(\hbar^2/2m)\Delta\chi_\nu-(2\pi i\hbar^2/mL)\nu\cdot\operatorname{grad}\chi_\nu+V(y_1,\cdots,y_n;x)\chi_\nu=\epsilon_\nu\chi_0(y_1,\cdots y_n;x). \tag{31}$$

Eq. (31) is much the same as (11), the principal difference being that the relative mass $\frac{1}{2}m$ appears instead of m.

9.

The characteristic values ϵ_ν of (31) will depend on the position $y_1 \cdots y_n$ of the electrons with downward spin, and we must average this characteristic value using $|y|^2$ as a weight-function to obtain a final value. It is possible to perform this general calculation to a sufficient degree of accuracy using a modification of the usual Rayleigh-Schrödinger perturbation process, since it does not converge in its usual form, but this involves a rather lengthy computation, so we shall content ourselves here with an estimate of the solution to (31) and present the more general solution at a later time.

It is evident that if the y's are to be most favorable for a large negative value of the correction energy we shall want the regions in which no y occurs to be as large as possible. In these regions $\chi_\nu(y_1 \cdots y_n, x)$ will have large maxima and the electron x will have the greatest probability of being as far as possible from the electrons of opposite spin. A secondary effect resulting from this will be an alteration of the original Fermi distribution $|y|^2$, and, as a consequence, (8), but we shall not take this into account in the present calculation.[19]

The most disadvantageous configurations for the y's, that is those giving the smallest $-\epsilon_\nu(y \cdots y_n)$, are the close-packed lattices, while the most advantageous is one in which all of the y electrons are at one corner-point of the lattice. This latter is practically impossible for the Fermi distribution, however, while the former possess the greatest probability. A graphical integration of (8), however, shows that the mean distance of the nearest electron with parallel spin to a given electron is $1.1r_s$ in contrast with the nearest distance of $2.3r_s$ for close-packed configurations. For this reason it seems reasonable to us, as far as energy is concerned, to make use of a "mean configuration" of the electrons with downward spin in which pairs of electrons form a body-centered lattice. In this the nearest electron will be much closer than it should be but there are no clusters of more than two electrons present, which compensates the fact that the pairs are at the most disadvantageous position.

The energy $\epsilon_\nu(y_1 \cdots y_n)$ of this mean configuration can be calculated very simply by the method employed in reference 1; the radius of the sphere surrounding every electron is $(4)^{\frac{1}{3}}r_s$ and the potential energy within the sphere is

$$V = 2e^2/r + e^2r^2/r_1^3 - 3.6e^2/r_1, \qquad (32)$$

in which the last term has been introduced in order to satisfy (25). We shall designate $\chi_\nu(y_1, \cdots, y_n, x)$ by $\chi_\nu(x, y, z)$ when the configuration of the $y_1, \cdots, y_n$ introduced here is implied.

In order to determine the χ_0 associated with the lowest energy, we shall regard V in (31) as a perturbation, for which the unperturbed problem is

$$-(\hbar^2/m)\Delta\xi(x, y, z) = \eta\xi(x, y, z). \qquad (33)$$

Each of the solutions of this possess an "azimuthal quantum number" l, these for $l=0$ and $l=1$ being of the form $r\xi_{0\kappa} = \int m\omega_\kappa r$, and $r\xi_{1\kappa} = \partial/\partial x \sin \omega_\kappa r$, etc., where the ω_κ are to be determined from the relation $\tan \omega_\kappa r_1 = \omega_\kappa r_1$ arising from the boundary conditions. The normalized solutions for $l=0$, are, to a sufficient degree of accuracy

$$\xi_{00} = (3/4\pi r_1^3)^{\frac{1}{2}}; \quad \xi_{01} = \frac{1.024}{(2\pi r_1)^{\frac{1}{2}}} \frac{\sin 1.43\pi r/r_1}{r} \qquad (34)$$

$$\xi_{0\kappa} = (1/2\pi r_1)^{\frac{1}{2}} \frac{\sin (2\kappa+1)\pi r/2r_1}{r} = (1/2\pi r_1)^{\frac{1}{2}} \frac{\sin \omega_1 r}{r}$$

for which the corresponding unperturbed energies are

$$\eta_{00} = 0, \qquad \eta_{0\kappa} = \hbar^2\omega_\kappa^2/m. \qquad (34a)$$

The matrix elements $V_{0\kappa}$ of V may be obtained as follows. We have

$$V_{0\kappa} = \int \xi_{00} V \xi_{0\kappa} dV$$

$$= -(3/4\pi r_1^3)^{\frac{1}{2}}(1/\omega_1^2) \int V \Delta\xi_{0\kappa} dV, \qquad (35)$$

in which the Laplacian may be made to operate on the V by use of partial integration. From Poisson's equation ΔV is $-8\pi e^2(\delta(r) - \frac{3}{4}\pi r_1^3)$ in which the last term gives rise to a vanishing contribution since it, like ξ_{00}, is constant and the

[19] It cannot be taken into account without also replacing the effect of electrons with parallel spin on each other by point charges in a similar way to that carried through here for the electrons with antiparallel spin. If this is not done, the two kinds of electrons will push each other into different parts of the crystal, thus invalidating the assumption under which we have calculated their mean effect.

integral over it vanishes in (35). The first term yields

$$V_{0\kappa}=(24)^{\frac{1}{2}}e^2/\omega_\kappa r_1^2 \tag{36}$$

so that the solution of (31) for $\nu=0$ is

$$\chi_{00}=(3/4\pi r_1^3)^{\frac{1}{2}}-\sum_\kappa{}' \frac{V_{0\kappa}}{\hbar^2\omega_\kappa^2/m+V_{\kappa\kappa}}\xi_{0\kappa} \tag{37}$$

and the corresponding energy is[20]

$$1/(16.2+3.07r_s)+0.005. \tag{38}$$

Although this is given in atomic units, the correction is true for only half of the electrons and must be taken in Rydberg units. The solution (37) has also been obtained by use of numerical integration and is illustrated in Fig. 5.

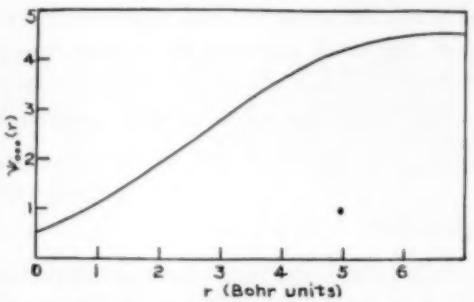

FIG. 5. Wave function corresponding to a solution of (30) with $\nu=0$ and $r_s=4$.

The wave function of an electron has only about 30 percent of its mean value in the region where two other electrons are situated and only 50 percent in the region where there is an electron with antiparallel spin.

For ν other than 0, we shall have greater energy gains because the Fermi distribution will be narrower as a result of the presence of the field arising from the $y_1\cdots y_n$ electrons than it would be without this field. In this case we can take the second term of (35) into account as a perturbation, the calculation being very similar to that employed in Section 4. The first approximation is zero, while the second, namely

$$(4\pi^2\hbar^4/m^2L^2)\nu^2\sum|\int(\partial\Psi_{00}/\partial x)\chi_\kappa|^2/-E_\kappa \tag{39}$$

is evidently negative, and would vanish if χ_{00} were entirely flat. Because of the selection rules, it is sufficient to take wave functions with $l=1$ for χ_κ, which are simply derivatives of the functions (34) to a first approximation, while χ_{00} must be taken from (37). The sum (39) may be conveniently compared with the Fermi energy of free electrons and a simple calculation shows that it is 4 percent of this quantity.

If this result and (38) are subtracted from the upper curve in Fig. 4, one obtains Fig. 6 which

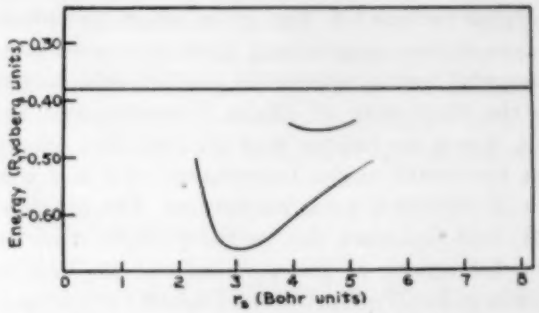

FIG. 6. The upper curve replaces that of Fig. 4 and contains the results arising from the correction to the one-electron picture.

yields $r_s=4.40$ or a lattice constant of 4.75A, and a heat of sublimation of 23.2 kg. cal. The experimental values are 4.23A and 26.9 kg. cal., respectively. For the observed lattice constant the calculated energy is 18.6 cal. It may be mentioned at this point that the preceding calculation of the correlation energy is valid only in the neighborhood of $r_s=4$.

It is to be noted that the actual χ_ν will not have, in general, forms such as those we have calculated here. For irregular configurations of the electrons with downward spin they will be rather complicated linear combinations of these functions, possessing energies that are nearly the same, however. Each function ψ_ν going with an energy ϵ_ν will have a maximum in that region in which the potential has a trough allowing such a characteristic value and will be small everywhere else as a result of interference of the superposed waves.[21] This does not affect the actual wave function (22), for all of the electrons, however, since this is a determinant of the ψ_ν and does not change upon taking such a linear combination.

[20] The V_{kk} must be calculated graphically. We obtained $V_{11}=2.4\,e^2/r_1$.

[21] Cf. the discussion of a very similar problem by F. Hund, Zeits. f. Physik **40**, 742 (1927).

10.

It is hardly necessary to mention that the calculation of the last section must be regarded only as an attempt to find the correct wave function for the electrons in the metal, and we are well aware that we could guess its form only roughly. We should like to mention that the deviation of the wave function from the determinantal form (21) using plane de Broglie waves is much more pronounced here than in the one electron picture (cf. Fig. 5) in which the plane waves were a surprisingly good representation. They still form a reasonably good approximation to the true state of affairs, however, and for this reason we believe that the fact that (22) is not symmetric under interchange of x and y is not of extremely great importance. The function (22) still possesses this property if we consider the differences of the ψ_r from the de Broglie waves as small quantities and neglect the second order terms.

The remaining discrepancy of 3.7 kg. cal. we believe to arise from two sources. First it is not evident that the Prokofjew field is completely suitable for calculations of this kind and, in fact, it is surprising that the atomic levels are as good as we have found them to be. Rigorously the exchange terms between the valence electrons and the closed shells cannot be transformed into the form of potentials because they are represented by more general operators, and there is a possibility that the effect of these is not described accurately enough for the states occurring in the crystal by an effective potential field. This important point is being more accurately investigated in connection with a treatment of Li to appear shortly and it is hoped that more light may be thrown upon it.

On the other hand, it is also possible that the actual wave function is not represented to a sufficient degree of accuracy by a wave function of the form (2). It does not seem to be easy to use wave functions of a greater generality, however.

Appendix 1

It is possible to continue the wave function with the same spherically symmetric potential over the whole volume of the s-polyhedron. If one assumes this ψ to be valid in all the s-polyhedrons of the lattice, the resulting wave function will be continuous everywhere, but the derivatives will be discontinuous at the boundary planes. The energy, therefore, is not the characteristic value of the differential equation, but must be calculated as the sum of kinetic and potential energy. The correction for the potential energy will be given in Appendix 2, while the correction for the kinetic energy is

$$(\hbar^2/2m)\left\{\int_{V_1}(\text{grad }\psi)^2 d\vartheta - \int_{V_2}(\text{grad }\psi)^2 d\vartheta\right\}, \tag{1}$$

where V_1 is the region of the s-sphere outside of the s-polyhedron and V_2 is the equally large volume of the s-polyhedron outside of the s-sphere. In the neighborhood of the s-sphere, we can set

$$\frac{\hbar^2}{2m}\text{grad }\psi = \frac{\hbar^2}{2m}\frac{d^2\psi(r_s)}{dr^2}(r-r_s) = (V(r_s)-E)\psi(r_s)(r-r_s), \tag{2}$$

so that (1) becomes

$$(2m/\hbar^2)(V(r_s)-E)^2\psi(r_s)^2\left\{\int_{V_1}(r-r_s)^2 dv - \int_{V_2}(r-r_s)^2 dv\right\}. \tag{3}$$

Now the mean value of $r-r_0$ is certainly smaller than $r_0/20$, V_1 is smaller than $v_0/10$, and $\psi(r_s)^2 v_0 \sim 1$, so that the first part of (3) is

$$(2mr_s^2/\hbar^2)(V(r_s)-E)^2/4000 = 0.0004 \text{ Rydberg units.}$$

In addition to this, the second term of (3) essentially cancels the first, so that the total correction really is negligible.

Appendix 2

It is necessary to calculate the potential energy of a body-centered lattice of positive point charges in a fluid of negative charge of density $\rho = \psi^2$ and then to compare this energy with the electrostatic energy of the s-sphere.

To begin with, we can draw s'-spheres around each positive charge which are smaller than the s-spheres and just touch one another. Outside of these s'-spheres we may assume the density to be uniform and of magnitude ρ. Relative to the regions of space outside of the lattice, the energy of the s'-spheres is as large as if the negative charge had a constant density within the sphere. This is because the potential outside a sphere arising from a spherically symmetric charge distribution is independent of the radial distribution inside of the sphere.

The total electrostatic energy of the lattice may now be divided into two parts: first, the energy E_1 of a body-centered lattice of positive charges $v_s\rho = e$ with a uniform negative charge-density and second the difference, E_2, of the inner energy of an s'-sphere with the actual s'-sphere on the one hand and an s'-sphere with uniform charge distribution on the other. Since the density is actually ρ outside of the s'-sphere, the second energy is equal to the difference in energy of the actual s-sphere and one with constant negative distribution ρ. This second part is

$$E_2 = E_t - (3^{5/3}\pi^{1/3}/5)(\rho^2 v_0^2/d) = E_t - 3.6557\rho^2 v_0^2/2d,$$

where E_t is the energy of the actual s-sphere, that is, the energy employed in the text, and $-3.6557\rho^2 v_0^2/2d$ is the energy of an s-sphere with uniform charge distribution.

If E_1 were $-3.6557\rho^2 v_0^2/4d$ our calculation would be exactly correct. Since it is actually $-3.6391\rho^2 v_0^2/4d$, as will be shown at once, the total energy is smaller than that used in the text by the amount

$$0.0166\rho^2 v_0^2/2d = 0.004e^2/r_s,$$

which for $r_s = 4$ is only 0.62 kg. cal.

The calculation of E_1 is a problem of electrostatics, we have used essentially the procedure of Appell-Madelung. Since the proper energy of the positive point charge, which must be obtained, is infinite, we must assume positive charges of finite size concentrated into small cubes with edges 2δ.

The Fourier expansion of the density is, then,

$$\sum_{\kappa,\lambda,\mu=-\infty}^{\infty} a_{\kappa\lambda\mu} \exp\left[2\pi i(\kappa x + \lambda y + \mu z)/d\right]$$

with

$$a_{\kappa\lambda\mu}\begin{cases} 2\rho v_0 \sin\alpha\kappa \sin\alpha\lambda \sin\alpha\mu/d^3\alpha^3\kappa\lambda\mu, \\ 0 \end{cases}$$

where $\alpha = 2\pi\delta/d$ and the first line is valid for $\kappa+\lambda+\mu$ even and the second for this odd in addition to the case $\kappa = \lambda = \mu = 0$.

The total energy per atom of the lattice is

$$E_{11} = \sum d^5 |a_{\kappa\lambda\mu}|^2/4\pi(\kappa^2+\lambda^2+\mu^2).$$

The density distribution of the positively charged cube may be written in the form of the Fourier integral

$$\int\int\int_{-\infty}^{\infty} a(\kappa\lambda\mu) \exp\left[2\pi i(\kappa x + \lambda y + \mu z)/d\right] d\kappa d\lambda d\mu$$

with

$$a(\kappa\lambda\mu) = \rho v_s \sin\alpha\kappa \sin\alpha\lambda \sin\alpha\mu/d^3\alpha^3\kappa\lambda\mu$$

and the corresponding energy is

$$E_{12}=(d^3/2\pi)\int\int\int_{-\infty}^{\infty}|a(\kappa\lambda\mu)|^2/(\kappa^2+\lambda^2+\mu^2)d\kappa d\lambda d\mu.$$

The energy E_1 is now simply $E_{11}-E_{12}$. If we put $\delta=0$ both E_{11} and E_{12} diverge, but if we take the difference before passing to the limit and then set $\delta=0$, we obtain

$$E_1=\lim_{N\to\infty}\lim_{\delta\to 0}\sum_{\kappa,\lambda,\mu=-N}^{N}\frac{d^3}{4\pi}\frac{|a_{\kappa\lambda}|^2}{\kappa^2+\lambda^2+\mu^2}-\frac{d^3}{2\pi}\int\int\int_{(-N-\frac{1}{2})}^{(N+\frac{1}{2})}\frac{|a(\kappa\lambda\mu)|^2}{\kappa^2+\lambda^2+\mu^2}d\kappa d\lambda d\mu$$

$$=\lim_{N\to\infty}\frac{\rho^2v_0^2}{\pi d}\left\{\sum_{-N}^{N}\frac{1}{\kappa^2+\lambda^2+\mu^2}-\tfrac{1}{2}\int\int\int_{(-N-\frac{1}{2})}^{(N+\frac{1}{2})}\frac{d\kappa d\lambda d\mu}{\kappa^2+\lambda^2+\mu^2}\right\}.$$

In $\sum'$, the values for which $\kappa+\lambda+\mu$ is odd and the case $\kappa=\lambda=\mu=0$ are to be omitted.

The summation and integration over μ were carried out directly and yield

$$E_1=\frac{\rho^2v_0^2}{2d}\left\{\sum_{\kappa+\lambda\text{ odd}}\left(\frac{1}{\kappa^2+\lambda^2}\right)^{\frac{1}{2}}\operatorname{tgh}\frac{\pi}{2}(\kappa^2+\lambda^2)^{\frac{1}{2}}+\sum_{\kappa+\lambda\text{ even}}\left(\frac{1}{\kappa^2+\lambda^2}\right)^{\frac{1}{2}}\operatorname{ctgh}\frac{\pi}{2}(\kappa^2+\lambda^2)^{\frac{1}{2}}-\int\int\frac{d\kappa d\lambda}{(\kappa^2+\lambda^2)^{\frac{1}{2}}}\right\},$$

which was then calculated directly. The tgh and ctgh may be replaced by 1 when either κ or λ is greater than 3. For κ or λ greater than 9, the bracketed difference is $1/24(\kappa^2+\lambda^2)^{\frac{1}{2}}$ with sufficient accuracy, and the integration over κ and λ was carried out in this region. The terms for which $\kappa\leqq 3$, $\lambda\leqq 3$ yielded -3.57221, while the second sum gave

$$E_1=-3.6391\rho^2v_0^2/2d.$$

The van der Waals attraction of the ions is -0.12 cal. per mol.

Note added in proof. In Fig. 3 the upper point of the (110) discontinuity, given by a pure p function, lies at -0.33 Rydberg units in place of the value shown. The lower is at -0.34. Although the first lies below the parabola, this is undoubtedly of no real significance.

Errata:—Acoustic Resonator Interferometer

J. C. HUBBARD, *The Johns Hopkins University*

(Phys. Rev. **38**, 1011 (1931); **41**, 523 (1932))

MR. E. G. WITTING of this laboratory has kindly drawn my attention to the errors noted below leading to corrections in several equations. Fortunately, these corrections do not significantly change the values of velocity or of absorption coefficients deduced from experiment, but they do change the deduced values of reflection coefficients, the new values departing from unity by almost exactly twice as much as do the values deduced by means of the published equations.

In Part I, Eqs. (12) and (13) should read, respectively:

$$P_x=\frac{[e^{-ax}-\gamma^2e^{-a(4r-x)}]\cos\omega x/v+\gamma[e^{-a(2r-x)}-e^{-a(2r+x)}]\cos\omega(2r-x)/v}{1-2\gamma e^{-2ra}\cos 2r\omega/v+\gamma^2e^{-4ra}}, \quad (12)$$

$$Q_x=\frac{[e^{-ax}+\gamma^2e^{-a(4r-x)}]\sin\omega x/v+\gamma[e^{-a(2r-x)}+e^{-a(2r+x)}]\sin\omega(2r-x)/v}{1-2\gamma e^{-2ra}\cos 2r\omega/v+\gamma^2e^{-4ra}}. \quad (13)$$

These equations lead to obvious changes in Eqs. (19) and (20) of the same paper, and in Eqs. (3), (4), (14), (16), (17), (18), (20), and (21) of Part II. In particular, Eq. (14), Part II, becomes, $P_m=(1+\gamma e^{-2ra})/(1-\gamma e^{-2ra})$ and Eq. (16), $P_m=1/(r\alpha+\beta/2)$, approximately. For β should be substituted $\beta/2$ in Eq. (17), and Eq. (18) should read $S'=2S/\beta$. The values of P and Q used in Eq. (19) are obtained from (12) and (13) above, putting $x=$ zero.

With expectation that these corrections would be included in another paper of this series, they were privately circulated among interested correspondents. Further delay in their publication, however, seems undesirable.

LETTERS TO THE EDITOR

PROMPT publication of brief reports of important discoveries in physics may be secured by addressing them to this department. Closing dates for this department are, for the first issue of the month, the twentieth of the preceding month; for the second issue, the fifth of the month. The Board of Editors does not hold itself responsible for the opinions expressed by the correspondents.

To Contributors

It is now five years since the establishment of the Letters to the Editor section in the *Physical Review*. Its growth in that period, both in volume and in interest, has been gratifying, but there are two considerations which cause us some concern.

The more serious of these is the growing tendency among contributors to be satisfied with the hasty, incomplete, and often inadequate record of their investigations which the Letters to the Editor section provides. Few enjoy the labor of preparing a complete, critical and well considered report of their work, particularly when the primary urge to secure priority for it can be satisfied by dashing off a Letter to the Editor.

The less serious, but none the less troubling, consideration is the ever increasing cost of maintaining this section. In the past five years there has been a healthy growth in the number of Letters submitted, from 120 to about 220 per year. There has, however, been at the same time a not so healthy growth in the average length of these Letters from about 500 to 750 words.

These considerations make it necessary to use rather more Editorial supervision of the Letters submitted than in the past and the Editors would, therefore, like to formulate the policies which will govern that supervision.

The primary purpose for which the Letters to the Editor section was established was to provide prompt publication for new results in fields of general current interest or importance, or for the exchange of ideas about them. It was intended neither that it should be a place for the preliminary announcement of *all* work nor that, in the fields covered, it should replace more formal and critical articles. If the present tendency to record much of the important work in several laboratories by a series of Letters to the Editor of gradually increasing length is continued, the standard of scientific exposition in the *Physical Review* will be seriously lowered.

The Editors ask for your cooperation in the following particulars:

1. In cases where there may be doubt each contribution in the form of a Letter to the Editor should be accompanied by a letter stating the reasons this form of publication is desired.

2. Except under unusual circumstances no Letter to the Editor should be longer than 600 words.

THE BOARD OF EDITORS

Hysteresis Losses and the Area of the Hysteresis Loop

Emil Warburg[1] was the first to propose that the area of what later came to be called a hysteresis loop measures the energy losses during a slow traversal of the magnetic states represented by its consecutive points. He was careful to remark in his analysis that the magetic force was assumed to be homogeneous throughout the specimen. In the wires he used, also, the magnetic force H was parallel to the magnetization I. (We translate his terminology into more modern form.) Under these conditions his result may be stated as follows:

$$W_h = \oint H dI.$$

More generally, if $\mathbf{H}$ and $\mathbf{I}$ are vectors:

$$W_h = \oint \mathbf{H} \cdot d\mathbf{I}.$$

The assumption of homogeneous $\mathbf{H}$ in actual ferromagnetic specimens is no longer tenable, for it now appears that $\mathbf{I}$ is merely a space average over a multitude of small regions (domains) in each of which there is always approximate saturation, $I_i = I_\infty$, in some direction. Changes in $\mathbf{I}$ in the neighborhood of $I=0$ are principally due to reversals of magnetization in such domains. This involves extreme inhomogeneity in magnetic force, even if we consider only its average value in single domains, $\mathbf{H}_1, \mathbf{H}_2, \cdots, \mathbf{H}_i$. If as in actual specimens with residual strains, large numbers of domains reverse together, $\mathbf{H}$ may be still more variable. Now it is not generally true that the average scalar product of two vector point functions is equal to the scalar product of their averages. We conclude that the equations given above can only be approximately correct and may, for very small loops, be very far from adequate. It is also, we think, obvious that inhomogeneous $\mathbf{H}_i$ generally involve additional positive terms in W_h. As an extreme case we may suppose that a reversal occurs in a domain magnetized at right angles to the average magnetic field. This would contribute nothing to $\oint \mathbf{H} \cdot d\mathbf{I}$ but would still involve dissipation of energy. Even as regards the components of the $\mathbf{H}_i$ parallel to $\mathbf{H}$ it is reasonable to suppose that contributions to the space average $d\mathbf{I}$ are more probable where $\mathbf{H}_i$ has a larger component parallel to $d\mathbf{I}$ than has the space average $\mathbf{H}$. The values of $\mathbf{H}_i$ at places where changes occur will, on this view, be in advance of the value $\mathbf{H}$ in a cyclic process.

This argument offers a new approach to the problem of anomalous losses in alternating magnetization of small amplitude when total losses are of the order of 10^{-4} erg/cm³/cycle. The alternating-current bridge, which measures all energy losses, would be expected to include the effects of inhomogeneity which are missed by ballistic and magnetometric methods. It will then be unnecessary to suppose[2] that the quasi-static $I-H$ loop differs from the loop traversed at frequencies of a few cycles per second. The correction to Warburg's law will depend upon the distribution function for $\mathbf{H}_i$ and this may be expected to vary widely in different materials. Such variability is characteristic of the anomalous losses.

It may be well to consider how the extra energy gets into a specimen from a primary circuit, especially in the case of alternating magnetization. The energy represented by the ordinary hysteresis loop may be regarded as due to a net inward energy flux through the bounding surface depending on the mean vector product of the electric vector $\mathbf{E}$ and the magnetic vector $\mathbf{H}$ at all its points. The internal inhomogeneities must result in local variations of $\mathbf{E}$ and $\mathbf{H}$ from point to point on this boundary corresponding to an additional inward flux of energy. The importance of the dimensions of comagnetized regions is perhaps more readily appreciated from this point of view, which may be more natural to many. We are indebted to T. C. Fry for bringing this way of presenting the matter to our attention.

L. W. McKeehan
Sloane Physics Laboratory, New Haven
R. M. Bozorth
Bell Telephone Laboratories, New York

August 6, 1934.

[1] E. Warburg, Ann. d. Physik [3] **13**, 141–164 (1881).
[2] As, for example, has recently been done by E. A. Neumann, Zeits. f. Physik **89**, 309–318 (1934).

Electron Microscopy of Biological Objects

In a previous communication[1] we discussed the possibilities of electron-microscopy of biological objects and presented 4 methods to preserve the objects from destruction: (1) Intense cooling of the object (for example, by contact with an extremely thin metal foil); (2) Impregnating the object with a substance which makes the object less destructible; (3) Impregnating the object in such a way that a framework of the object is preserved although the object itself is destroyed; (4a) Combining methods (1) and (2) or (4b) Combining methods (1) and (3).

In the same communications we presented our first microphotographs obtained by the third method. This method presents the disadvantage that only coherent "frameworks" can be photographed. In the case of vegetal or animal tissues, for instance, they are only the cell-walls which are visible and the inner parts of the cells (protoplasm, nucleus) are failing in absence of any object-holder (Fig. 1).

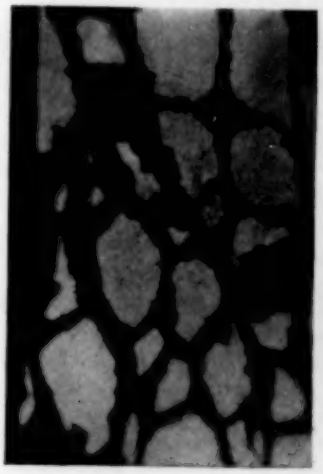

FIG. 1. Seaweed. ×1000.

To overcome this difficulty we applied method (4b) (Fig. 2). As object-holder we used a 0.5μ Al-foil. The

FIG. 2. Seaweed on Al-foil. × about 500.

osmium-impregnated tissue does not give in that case a picture of the same sharpness as Fig. 1, but we can distinguish the nucleus in some cells.

Besides the enumerated four methods to preserve cells from destruction there is a fifth: By diminishing the exposure there must be a limiting exposure-time, below which the cells are not destroyed. In other words, we might try to photograph the cells before their destruction.

We are constructing now a new microscope which will allow us to take instantaneous microphotographs (for instance: enlargement of 10,000 times in a 1/100 sec.).

L. MARTON

University of Brussels,
August 7, 1934.

[1] Martin, Nature **133**, 911 (1934); Bull. acad. Belgique **20**, 439 (1934).

Attempts to Detect the Emission of Deutons in Nuclear Transmutations

The impact of alpha-particles on nuclei is known to cause transmutations with emission of neutrons and protons. It has been suggested by F. Perrin[1] that emission of deutons is also likely, so this possibility must be considered in attempting to explain the various groups of emitted particles. The recent discovery of separate groups makes uncertain the conclusion reached by Rutherford[2] and Stetter[3] that all the heavy charged particles are protons, since they did not consider the properties of each group, but only those of the aggregate. We have, therefore, carried out magnetic deflection experiments on the disintegration products of boron and nitrogen to see whether the short range groups show any evidence for the presence of particles heavier than protons. At the same time we were able to verify directly that the particles produced by alpha-particles striking heavy hydrogen are deutons, as concluded by Rutherford and Kempton[4] from measurements of their range.

The experimental arrangement is a modification of Rutherford's original deflection apparatus. A lead block in an evacuated box prevents disintegration products moving in straight lines from entering half the window of a counting chamber. When the assembly is placed between the poles of an electromagnet, a field in one direction (designated as positive) bends paths around the block and into the counter. A field in the other direction (negative) bends paths away from the counter. A curve of numbers against the field was plotted for known protons (produced by bombardment of thin hydrogenous material by alpha-particles) and this was compared with corresponding curves for unknown particles. Account was taken of difference of initial velocity by selecting for counting (by stopping foils at the counter) particles having ranges between 3.0 cm and 9.0 cm after entering the magnetic field.

I. Projected particles from heavy hydrogen, in Ca $(OD)_2$

The results showed clearly that these particles were less easily deflected than those from hydrogen itself. Adjusting the ordinate scales to give the same maximum yield, the ratio of the experimentally found maximum slopes is 1.8 : 1 (protons to deutons) while the theoretically expected ratio is 1.7 : 1. The conclusion is that the particles from $Ca(OD)_2$ are deutons.

II. Particles from the disintegration of boron

The reaction

$$_5B^{10}+{}_2He^4={}_6C^{12}+{}_1D^2$$

seems to be most promising for deuton emission. Consideration of the mass defects shows that polonium alpha-particles could thus cause emission of a group of deutons of about 16 cm ranges. Bothe and Heidenreich found evidence of particles of about this range.

Deflection experiments were made on particles having between 8 cm and 14 cm total range. Natural protons from the source are present in this region, but the fact that the deflection proved to be as easy as for pure proton beams means there is no group of deutons comparable in number to the natural protons. The group found by Bothe and Heidenreich must therefore be protons.

III. Particles from the disintegration of nitrogen

Particular attention has been given to this by F. Perrin.[1] He suggests the reaction

$$_7N^{14}+{}_2He^4={}_8O^{16}+{}_1D^2$$

and predicts a deuton range of 7.2 cm for full range polonium alpha-particles. A repetition of his calculation with Bainbridge's value for the mass of the deuton shows this estimate to be rather high. Nevertheless, a careful preliminary search was made for a short range group besides the resonance group already known. Additional

evidence for a broad resonance level giving a group of yield approximately 0.4 that of the main group was found, but there was no sign of any second group of range greater than 4 cm produced by the full range alpha-particles.

In spite of this the magnetic deflection was tested. The minimum range entering the counter was reduced to 5 cm and a comparison made with protons from coal gas. The curves show a resonable agreement and the conclusion is that the short range products from nitrogen are principally protons.

Thus we have found no evidence of emission of deutons in polonium alpha-particle disintegrations of boron and nitrogen.

We wish to thank Professor A. F. Kovarik for his advice and help in discussion, Professor H. C. Urey for a gift of heavy water, and Dr. C. T. Lane for advice in running the magnet.

ERNEST POLLARD*
WILLIAM W. EATON

Sloane Physics Laboratory,
Yale University,
August 11, 1934.

[1] F. Perrin, C. R. **194**, 2211 (1932).
[2] Rutherford, Chadwick and Ellis, *Radiations from Radioactive Substances*, p. 290.
[3] G. Stetter, Zeits. f. Physik **34**, 158 (1925).
[4] Rutherford and Kempton, Proc. Roy. Soc. **A143**, 724 (1934).
* Sterling Fellow.

The Absorption Spectra of Formaldehyde and Hydrogen Cyanide in the Far Ultraviolet

We have recently found a new absorption spectrum of formaldehyde in the region 1750–1150A. The absorption is very strong and most of the bands appear at a pressure of 0.1 mm in the spectrograph, the light path being about 1.5 meters. They consist mainly of two electronic series going to the same limit. About seven members of each series were found. The lower members are accompanied by many vibrational transitions. The higher ones can be extrapolated in the form of a Rydberg series to an ionization potential of 10.9 volts. This agrees very well with the value 11.3 ± 0.5 volts found by Jewitt[1] employing the usual methods of electron impact.

In this connection it is interesting to note the agreement between the limits of the electronic series in acetylene and ethylene[2] with the values for their ionization potentials as given by Tate and Smith,[3] and Kallman and Dorsch.[4] The values we obtain are 11.4 and 10.4 volts, respectively, which are in good agreement with the values 11.6 ± 0.1 and $10.0\pm?$ volts determined by the methods of electron impact.

The bands of formaldehyde show very strong predissociation in the region 1740A. If it is assumed that this is due to interaction with the initial state the process being $H_2CO \rightarrow H_2C + O$ we find the strength of the C=O bond to be 164 cal./mol. in fairly good agreement with thermochemical data.

The general similarity between the ultraviolet absorption spectra of acetylene, ethylene and formaldehyde is quite striking. They all have spectra in the region 3000A to 1800A which come out at fairly high pressures. They also possess spectra of an apparently different type having much higher transition probabilities below 1800A. These latter consist of electronic series going to the ionization potentials of the molecules.

The investigations on HCN revealed bands extending from 1450A to well below 1000A. The bands in the region 1400A are single headed and are shaded towards the red. They are given very well by the following formula

$$\nu = 68{,}645 + 901(v+\tfrac{1}{2}) - 22(v+\tfrac{1}{2})^2. \qquad (1)$$

Slight predissociation sets in at the $v=4$ band. The same vibration pattern does not repeat itself in the bands at lower wave-length, the vibration frequencies being considerably larger. The latter bands are too diffuse to be analyzed thoroughly but it is probable that they form an electronic series going to the ionization potential of HCN at 14.8 volts. The bands given by (1) come out at somewhat higher pressures than those at lower wave-lengths. This indicates that here again we have the two types of absorption found in the previously mentioned molecules.

W. C. PRICE

Department of Physics,
The Johns Hopkins University,
August 11, 1934.

[1] Private communication from Professor R. G. J. Fraser.
[2] W. C. Price, Phys. Rev. **45**, 843 (1934).
[3] Tate and Smith, Phys. Rev. **39**, 270 (1932).
[4] Kallman and Dorsch, *Abhandlung aus der Kaiser Wilhelm Institut*, Vol. 12 (1929).

Surface Magnetization in Ferromagnetic Crystals. II

We reported in a recent Letter to the Editor[1] certain peculiarities of the surface magnetization of a single crystal of silicon iron, the polished face of which was not much inclined to a plane of form {100}. In order to explain the maze-like pattern of narrow lines formed by temporary condensation of a magnetic colloid close to this surface, and the enhancement of alternate lines of the maze by normal magnetic fields of the two possible signs, we had to suppose that the surface consisted of small blocks (possibly cubes) of square section, magnetized parallel to the surface along axes of form <100> and <110>, the former being preferred. These two directions are, respectively, directions for easiest magnetization and for next-to-easiest magnetization in single crystals of silicon iron.

It occurred to us that the patterns obtainable on a {100} plane in nickel should be different from those found in iron; for even if the surface still broke up into square blocks, all directions of easiest magnetization—here of form <111>—would now lie at 35° to the polished surface. After some optical difficulties occasioned by the smaller scale of the patterns developed on a suitable polished disk cut from a single nickel crystal,[2] we are able to show that conditions are, indeed, different from those in silicon iron. Fig. 1 gives two pictures of the same region with normal magnetic fields of opposite sign. The colloid particles collect in dots of various density which we find show best under slightly oblique illumination, so that each seems to cast a shadow.

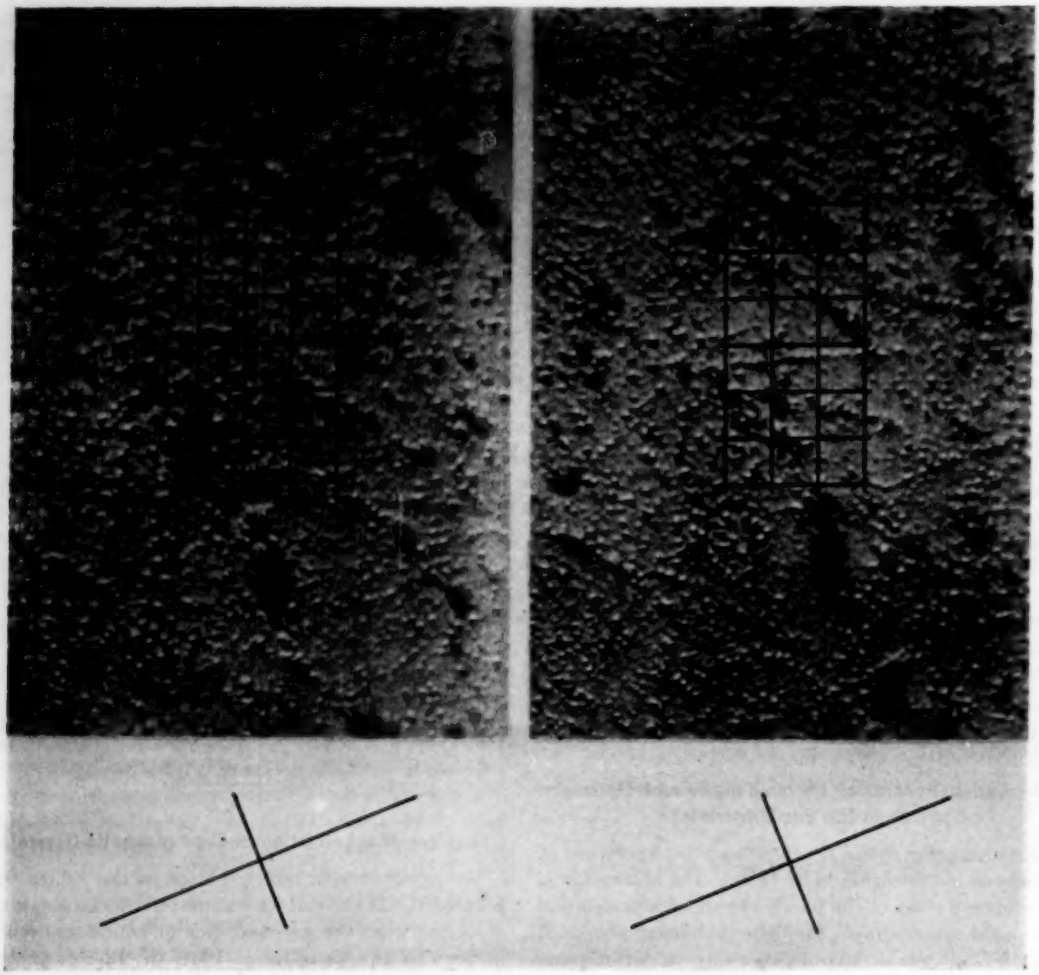

FIG. 1. Colloid patterns on nickel with **H** normal to the surface. The plane of the surface is 12° from a plane of form {100}, and the traces of the two other planes of this form have the directions shown beneath each photograph. The grille of 18 squares is $24\mu \times 12\mu$.

The minimum distances between well-defined dots is about 0.6μ.

Careful comparison of the two patterns here shown, and of others less clearly resolved, shows that associated pairs of patterns are reciprocal in a limited sense, conspicuous dots on one falling in nearly featureless regions on the other. Dots on a single pattern line up in several directions, but these directions are so numerous, and differ so much in nearby regions that we are as yet unable to say whether a structure of equal blocks exists or to specify the local directions of magnetization.

A possibility which we have particularly considered is that the surface is composed of cubes, each spontaneously magnetized along a direction of form <111>. If this is correct we should expect a normal field to increase the inclination of the local magnetization to the surface in about half of the blocks, decreasing this inclination in the rest of the blocks. Fig. 2 has been constructed to illustrate what might then be observed with normal fields in the two possible directions. A region containing $15 \times 22 = 330$ blocks of the size shown in one corner of each diagram has

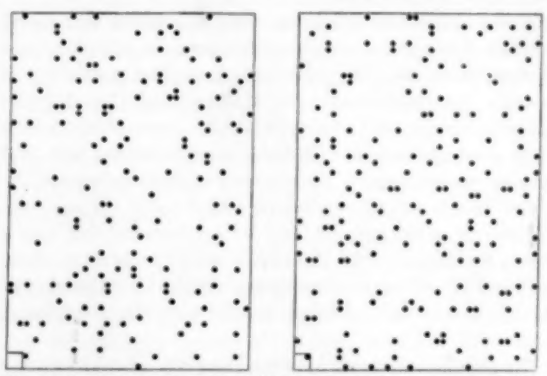

FIG. 2. Loci of strong stray fields in the surface of a layer of 330 equal cubes originally magnetized at random along body diagonals, for two directions of applied field normal to the paper. One cube is outlined in the corner of each drawing.

been represented. A direction of magnetization, of form <111>, has been assigned at random to each block. About half of them therefore have a component of I up from the paper. A black dot has been placed in the appropriate corner of each such square in the left-hand diagram. These dots would be enhanced by an applied field toward the observer. The rest of the squares have a component of I into the paper. A black dot has been placed in the appropriate corner of each such square in the right-hand diagram. These dots would be enhanced by an applied field away from the observer. The halves of Fig. 2 are reciprocal in the same sense as the halves of Fig. 1, but show even fewer collineations and other groups. If the suggested model is at all similar to the actual magnetic structure of a polished nickel surface it seems probable that the magnetization of adjacent blocks is not completely independent.

L. W. McKeehan
W. C. Elmore

Sloane Physics Laboratory,
Yale University,
August 14, 1934.

[1] L. W. McKeehan and W. C. Elmore, Phys. Rev. [2] **46**, 226 (1934).
[2] Grown by the method described by S. L. Quimby, Phys. Rev. [2] **39**, 345–353 (1932).

High Energy Gamma-Rays from Lithium and Fluorine Bombarded with Protons

We have shown that some of the light elements, when bombarded with protons or deutons emit γ-rays, and we have in several instances measured the absorption coefficient of the radiation in lead, and from this attempted to estimate the quantum energy. Recently Professor Oppenheimer has called our attention to the fact that, owing to the rapidly increasing probability of pair production with increasing quantum energy the quantum energy of a γ-ray is not always uniquely determined by the absorption coefficient in a single substance. This is seen from Fig. 1,

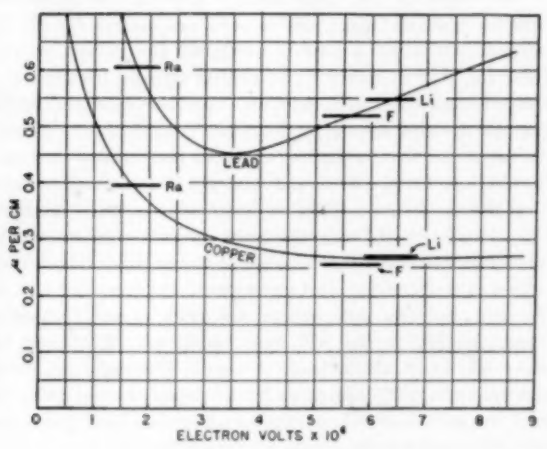

FIG. 1. Total absorption coefficient (Klein-Nishina + photoelectric + pair) of γ-rays in lead and in copper, as a function of their quantum energy.

which shows the total absorption coefficient for γ-rays in lead and in copper, as a function of quantum energy, plotted from theoretical figures kindly supplied us by Professor Oppenheimer.

In confirmation of this double valued absorption coefficient McMillan[1] has reported γ-rays from fluorine bombarded with protons and has shown, by measurements in various substances, that their absorption coefficients are correctly predicted by the theory if the quantum energy is about 5.5 m.e.v.

This consideration made it desirable to reinvestigate some of the γ-rays upon which we have previously reported, by making absorption measurements in at least one substance in addition to lead. This we have done in the case of the γ-rays emitted by lithium and by fluorine* bombarded with protons,[2] using lead and copper absorbers. The absorption coefficients found are indicated by horizontal lines intersecting the theoretical curves in Fig. 1. A correction for scattering has been applied to these values, and will be discussed below. Although the absorption coefficients in lead of these γ-rays are not very different from that of radium γ-rays, it is clear from the corresponding absorption coefficients in copper that their quantum energy is such as to place them on the high energy side of the minimum, at about 6.3 m.e.v. for lithium, and 5.6 m.e.v. for fluorine, rather than on the low energy side, as we previously supposed.

It is difficult to estimate the correction to be applied for scattering, over such a wide range of energy, especially where the mechanism of absorption is different at the high and the low energies. With the present experimental set-up we find an apparent absorption coefficient for radium γ-rays which is about 10 percent too low. However, while the attenuation of the radium γ-rays is due primarily to Klein-Nishina scattering, only about 40 percent of the attenuation of the 5.6 m.e.v. radiation from fluorine is due to Klein-Nishina scattering and the remaining 60 percent to pair formation. The 60 percent absorbed in pair formation contributes no scattered radiation directly, since the quantum is supposedly completely absorbed, but the resulting high velocity positive and negative electrons, in traversing the lead, give rise to some continuous x-radiation, in addition to the two 0.5 m.e.v. quanta resulting from the ultimate annihilation of the positron. Since in the high energy region this latter radiation tends to compensate for the smaller amount of scattered radiation, we have retained the 10 percent correction found for radium γ-rays, and have applied it uniformly to all our data.

In order to obtain the quantum energy of the above γ-rays in an independent way, and to check the theoretical absorption curves, we have undertaken to investigate by means of a cloud chamber the energy spectrum of negative and positive electrons ejected from a lead plate.

Fig. 2 shows the energy spectrum of the negative and positive electrons ejected from a 3 mm lead plate by the radiation from CaF_2 bombarded with 0.8 m.e.v. protons. The energies were determined by measuring the curvature in a magnetic field of 1200 gauss. A total of 641 measurable tracks above 0.5 m.e.v. were obtained; 434 negatives and 207 positives. From these curves we find, after applying

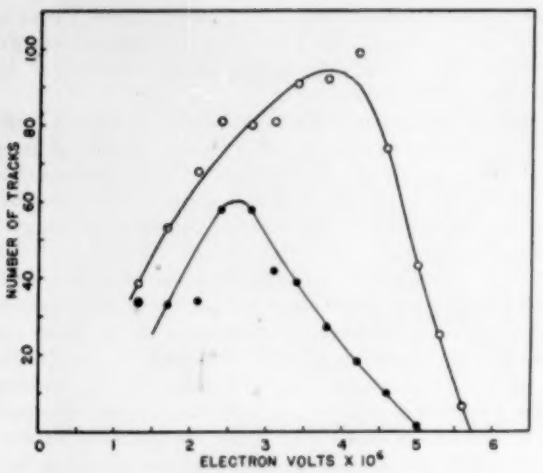

FIG. 2. Energy spectra of positive and negative electrons ejected from a thick lead plate by the radiation from fluorine bombarded with protons. Dots refer to positives, and circles to negatives, each representing the number of electrons in a 0.7 m.e.v. energy interval.

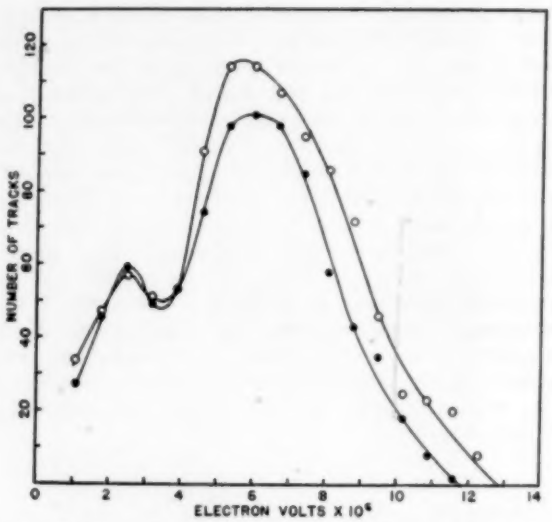

FIG. 3. Energy spectra of positive and negative electrons ejected from a thick lead plate by the radiation from lithium bombarded with protons. Dots refer to positives, and circles to negatives, each representing the number of electrons in a 1.4 m.e.v. energy interval.

appropriate corrections,[3] 5.4 m.e.v. as the quantum energy of the γ-ray. It is reasonably certain that no other γ-ray of comparable intensity is present above 2 m.e.v. No tracks below 1 m.e.v. were plotted, because of the larger errors which might be introduced. The value of the energy obtained is in agreement with the value obtained by absorption measurements, both by McMillan and by ourselves (see Fig. 1).

In Fig. 3 is shown the energy spectrum obtained under the same conditions with LiCl bombarded with protons. In this case 956 measurable tracks above 1.0 m.e.v. were obtained; 521 negatives and 435 positives. The distribution indicates with certainty a γ-radiation of approximately 12 m.e.v. and apparently a second component of about 4 m.e.v. In spite of the fact that the second component is much less conspicuous in the diagram, it must be of intensity comparable to that of the 12 m.e.v. component for several reasons: (1) Because of the shorter range of the electrons, a smaller effective thickness of lead is made use of. (2) A smaller number of electrons are produced in a given volume of lead because of the lower absorption coefficient. (3) The 4 m.e.v. component will be to some extent masked by the slower electrons and the softened radiation resulting from the 12 m.e.v. component.

The absorption coefficient for the radiation in lead (Fig. 1) corresponds to about 6.3 m.e.v., and this is not inconsistent with a composite radiation consisting of roughly equal intensities of 12 and 4 m.e.v. components, as suggested by the electron spectrum. No exact comparison is possible, since the relative intensities are not accurately known.

It is seen in Figs. 2 and 3 that the high energy limit of the negative electrons is roughly 1 m.e.v. higher than that of the positive electrons,† and this is consistent with the theory of pair formation. On the assumption that the number of negatives belonging to pairs is equal to the number of positives, and that the positives and negatives resulting from pairs have essentially the same initial energy spectrum, we can subtract the number of positives from the total number of negatives to find the number of negatives which do not belong to pairs. Further, since the average energy of a member of a pair is somewhat less than half that of a photoelectron or a forwardly directed Compton recoil electron, the effective thickness of lead contributing members of pairs is less than half that contributing single negatives. Therefore to find the number of pairs formed per unit volume relative to the number of single negatives, we must multiply the number of positives observed by a factor of approximately 2. This gives, for the 5.4 m.e.v. radiation, 1.8 pairs per single negative, and for the 12 m.e.v. radiation, 10 pairs per single negative, and this is in good agreement with Oppenheimer's theoretical calculations.

The shape of the high energy side of the observed positive electron spectrum is well accounted for if we assume that when a pair is produced the energy of the quantum is most likely to be shared equally between the positive and negative electron, and the probability of unequal division of energy decreases roughly linearly with the departure from equality, until the probability that one member receives all of the energy is practically zero. That the curve drops off on the low energy side is due to the fact that many of the electrons originating below the surface fail to come out because of the high probability of large angle scattering and consequent large energy loss in the lead. For the same reason we must expect that only comparatively rarely will both members of a pair be observed when thick lead is used. Although we have observed relatively few pairs in our experiments with thick lead, in preliminary observations using thin lead, pairs are relatively much more frequently observed.

We wish to express our appreciation to Professor J. R. Oppenheimer and to Professor R. C. Tolman for many

helpful discussions in connection with this work, and to the Seeley W. Mudd Fund financial support.

H. R. CRANE
L. A. DELSASSO
W. A. FOWLER
C. C. LAURITSEN

Kellogg Radiation Laboratory,
California Institute of Technology,
August 16, 1934.

[1] McMillan, Am. Phys. Soc. Meeting, Berkeley, June 18–23, 1934.
[2] Targets of LiCl and CaF_2 were used, and $CaCl_2$ was bombarded to make sure that neither Ca nor Cl gave an appreciable effect.
[3] Presented at the Berkeley meeting of the Am. Phys. Soc., June 18–23, 1934.
[4] Chadwick, Blackett and Occhialinni, Proc. Roy. Soc. **A144**, 235 (1934).
† If no photoelectrons are observed, as may be the case at these high energies, the difference between the maximum energies of the positive and negative will be only 0.78 m.e.v., due to the fact that the energy of the fastest Compton recoil must be 0.24 m.e.v. less than the quantum energy of the γ-ray.

Zeeman Effect in Neon

A measurement of the Zeeman splitting of two neon lines has been carried out with two purposes in view. One was to obtain a value of e/m; and the other was to investigate with high precision the validity of the g-sum rule in a particular case. The apparatus and method are essentially the same as previously described for the determination of e/m from measurements of the Zeeman effect in Zn and Cd.[1] A determination from neon lines was desirable since no theoretical correction factor needs to be applied, and since neon's spectral type is different from that of zinc and cadmium.

The g-sum rule states that the sum of the Landé g-values for all the levels in one electronic configuration which have the same J-value is the same for all types of coupling and for all magnetic field strengths. The neon lines λ5852 and λ6074 were found to be sufficient to make a precise check of this rule. Table I contains information regarding these

TABLE I.

λ5852		λ6074	
$2p^5\,3s\,{}^1P_1 - 2p^5\,3p\,(2p_1)$		$2p^5\,3s\,{}^3P_1 - 2p^5\,3p\,(2p_2)$	
$g=1.000$	$g=0/0$	$g=1.500$	$g=0/0$
$J=1$	$J=0$	$J=1$	$J=0$

lines. The g-values given are those calculated from Russell-Saunders coupling. As may be noticed in any table of spectroscopic levels[2] these levels are the only ones in their electronic configurations with the respective given J-values. Consequently, the g-sum rule may be applied.

By assuming that no splitting takes place in a magnetic field for the levels with $J=0$, the values of g for the levels with $J=1$ were found to be

Line	No. Plates Meas.	g
5852	13	1.0350 ± 7
6074	15	1.4667 ± 9

In order to compute these values of g, the value of $e/m = 1.7570$ was used. The sum of these values is then 2.5017 ± 0.0016 which agrees with 2.5000 to within the experimental error. Therefore it seems that in this case the g-sum rule is valid to better than 0.1 percent.

If instead of assuming a value of e/m, one assumes the validity of the g-sum rule, the value of e/m is found to be $e/m = 1.7580\pm0.0014\times10^7$ e.m.u./g. This value is in satisfactory agreement with other values obtained from the Zeeman effect.

L. E. KINSLER

Norman Bridge Laboratory of Physics,
California Institute of Technology,
August 20, 1934.

[1] L. E. Kinsler and W. V. Houston, Phys. Rev. **45**, 104 (1934).
[2] Bacher and Goudsmit, *Atomic Energy States*.

Zeeman Effect in Helium

Since publishing an abstract[1] regarding an anomalous Zeeman splitting of three helium singlet lines, λ6678, λ5015 and λ4921, the cause of this anomaly has been found to be experimental. Photographs of the helium line interference patterns were taken with the same apparatus and in much the same manner as has been described for Zn and Cd.[2] The constriction in the discharge tube from which the spectrum originated was cooled by a surrounding jacket into which liquid air was blown. This reduced the line widths by some 40 percent. However, it was necessary to make microphotometer records of the original plates in order to adequately measure the separation of the two displaced σ components.

The error in the previous results was caused by the presence of the undisplaced π component at 30 times the intensity expected from the angle subtended at the source by the condensing lens. This increased intensity has subsequently been shown to be caused by scattered and reflected light. Presence of a weak π fringe between every pair of σ fringes in the interference pattern caused the maxima of the latter to be displaced and led to the published erroneous results. Such a difficulty arises only for broad lines such as those of the light elements since for heavy elements this component is resolved.

It was found possible to eliminate this component by placing a 1 mm×4 mm slit at the re-entrant window of the discharge tube and painting the remainder of the tube black. Consequently, no scattered or reflected light could reach the slit of the spectrograph. In the results that follow six or more plates at different magnetic field strengths were measured for each line.

Line	Value of e/m
6678	$1.7570\pm0.0007\times10^7$
5015	$1.7552\pm0.0010\times10^7$
4921	$1.7568\pm0.0011\times10^7$

By giving the result for λ6678 double weight the average value of e/m is $1.7564\pm0.0009\times10^7$. λ6678 was given greater weight because the interferometer spacing was three times that for the other lines which resulted in greater resolution and since the π component had been more completely eliminated. The deviation of λ5015 is in such a direction as to be explained by the possible presence of the π component.

The values of e/m obtained with this apparatus from four elements by measurement of the Zeeman splitting of their

singlet lines are

Element	Value of e/m
Zinc	$1.7570 \pm 0.0009 \times 10^7$
Cadmium	$1.7570 \pm 0.0008 \times 10^7$
Helium	$1.7564 \pm 0.0009 \times 10^7$
Neon	$1.7580 \pm 0.0014 \times 10^7$

By weighting the values according to their individual errors the average value of the specific charge of the electron is found to be $e/m = 1.7570 \pm 0.0007 \times 10^7$ e.m.u./g.

L. E. KINSLER
W. V. HOUSTON

Norman Bridge Laboratory of Physics,
California Institute of Technology,
August 20, 1934.

[1] L. E. Kinsler and W. V. Houston, Phys. Rev. **45**, 134 (1934).
[2] L. E. Kinsler and W. V. Houston, Phys. Rev. **45**, 104 (1934).

New Band Systems in Nitrogen

A new band system belonging to nitrogen has been discovered in the same tube that I have described on several occasions recently.[1] These bands degrade to the violet and consist of only one progression. They have been photographed on a small quartz Hilger spectrograph, and the wave-lengths of the band heads are approximately 2153, 2225, 2301 and 2381. The frequency differences between the lower vibrational levels correspond very closely to the frequency differences between the lower vibrational levels of the band system recently discovered by van der Ziel.[2] It is suggested therefore that the two band systems have a common lower electronic state. If we assume that these new bands originate on the $v' = 0$ level of a new electronic state, and then calculate the difference between this new state and the initial state of the van der Ziel system, this difference corresponds very exactly with the difference between two of the new levels which form part of the Rydberg absorption series of N_2 discovered by Hopfield.[3, 4] These two levels correspond to the absorption bands 671.2 and 675.2, and the difference between them is 883 cm^{-1}, as compared with 881 cm^{-1} for the difference between the initial state of these new bands and the van der Ziel bands.

In addition to these bands there are present many other new bands. Of these the three bands 2740, 2635 and 2536 are similar in appearance, and probably form part of another system. Other fairly strong bands having wave-lengths 2359, 2397, 2421, 2452, 2459 are also present. A set of five bands between 2510 and 2530, and numerous new bands above 2600 are also present, but so far it has been impossible to arrange them into systems. It is suggested, however, that these bands originate on the other levels which were discovered by Hopfield. Further work is now in progress in an attempt to interpret these bands.

The new system recently reported by van der Ziel, two members of which were first observed by Appleyard, is very strongly excited in these experiments. It is of some interest to point out that the intensity distribution among these bands is not in agreement with the Franck-Condon principle. Thus, the band (1,1) is missing whereas the band (1,7) is very strong. Similar anomalies occur in the $v' = 0$ sequence. The present writer has often called attention to a similar phenomenon in the first-positive system of nitrogen. It is therefore of some interest to report a similar phenomenon in another system of nitrogen.

JOSEPH KAPLAN

University of California at Los Angeles,
August 20, 1934.

[1] Kaplan, Phys. Rev. **44**, 783 (1933).
[2] van der Ziel, Physica **1**, 513 (1934).
[3] Hopfield, Phys. Rev. **36**, 789A (1930).
[4] Mulliken, Phys. Rev. **46**, 144 (1934).

New Bands in Nitrogen

At the Berkeley meeting of the American Physical Society I reported the discovery of some new members of the second-positive positive band system. The five strongest of these new bands could be easily recognized as three-headed and degraded to the red. The short wave-length heads were 4732, 4435, 4174, 3010 and 2864A. The first three bands were observed only at pressures below 0.1 mm, while the other two were present at all pressures. At the time of their discovery it was recognized that the frequency differences between corresponding heads in general indicated that the lower level of these bands coincided with the $B^3\Pi$ initial state of the well-known first-positive system. They were identified as members of the second-positive system originating on high vibrational states, since the enhancement of high-vibrational states was a characteristic of the tube in which these bands were observed. The different behavior of the three visible bands as contrasted with the two ultraviolet bands suggests, however, that my first explanation is incorrect, and that these bands are members of two separate systems in nitrogen. The three visible bands are then readily identified as the (v',12), (v',11) and (v',10) bands of a new system, and the two ultraviolet bands as (0,1) and (0,0).

It was remarked earlier that the bands possess three heads. The two shortest wave-length heads are nearer to each other than the two longest wave-length heads. In the case of the first-positive bands the two longest wave-length heads are closer to each other than the two shortest wave-length heads. This fact is an argument in favor of my identification of the lower level of these bands, since the $B^3\Pi$ state is the initial level for the first-positive bands.

The enhancement of the visible bands as the pressure is lowered is of interest, since several other new band systems of nitrogen are enhanced at lower pressures, e.g., the Appleyard-van der Ziel bands, the ultraviolet system which was reported by me in a recent letter in the *Physical Review*, and one which was reported in a letter in *Nature*.

It is also significant that the three visible bands end on the $v'' = 12$, 11 and 10 levels of the $B^3\Pi$ state. These three are enhanced in the nitrogen afterglow, and this may have something to do with their excitation. Further investigation with regard to all these new bands is now under way.

JOSEPH KAPLAN

University of California at Los Angeles,
August 24, 1934.

The Acetylene Bond Frequency in Heavy Acetylene (C_2D_2)

Gaseous heavy acetylene (C_2D_2)[1] at two atmospheres pressure and at total volume of 33 cc was exposed in a Pyrex tube to a mercury discharge. The line 4358 Hg caused Raman scattering. One scattered frequency could be measured definitely on four different plates. It is 1761 cm^{-1} and is ascribed to the acetylene bond vibration. The former investigations of Raman scattering on ordinary acetylene (C_2H_2) are shown in Table I.

TABLE I.

C_2H_2 (gas)		C_2D_2 (gas)
Segré[2]	1979 ±5 cm^{-1}	—
Bhagavantam[3]	1974	—
Daure and Kastler[4]	1978 ±5	—
This investigation	1973.1	1761 cm^{-1}

Since only a small sample of C_2D_2 was available it was considered essential to run ordinary acetylene (C_2H_2) under the same circumstances with the result shown in Table I.

If one were to predict the acetylene bond vibration for C_2D_2 from the known value (1973.1 cm^{-1}) of ordinary acetylene (C_2H_2) by the use of the equation pertaining to a simple harmonic oscillator:[5]

$$\nu = (1/2\pi)(k/\mu)^{\frac{1}{2}} \tag{1}$$

or

$$\nu_0^2\mu_0 = \nu_h^2\mu_h \tag{2}$$

one would obtain

$$\nu_h = (\mu_0/\mu_h)^{\frac{1}{2}}\nu_0 = [(13/2)/(14/2)]^{\frac{1}{2}} \times 1973 \tag{3}$$

$$\nu_h = 1901 \text{ cm}^{-1}.$$

Either Eq. (1) does not apply or the substitution of deuterium has a remarkable influence on the force constant k between the carbon atoms. The latter alternative is difficult to believe and therefore it is clear that the oscillator producing the acetylene bond frequency is not as simple as is implied by Eq. (1).

A very faint line at 3425 cm^{-1} appears on some of the plates but it is located very near to a mercury line so that further work is necessary to establish its definite existence. We hope to find the lower frequencies of C_2D_2 by greatly prolonged exposure.

We are indebted to the Research Grant Committee of the Graduate School of the University of Minnesota for financial assistance which enabled us to carry out this investigation.

GEORGE GLOCKLER
H. M. DAVIS

Minneapolis, Minnesota,
August 20, 1934.

[1] We are greatly indebted to Professor H. S. Taylor for the loan of this sample which was prepared under his direction by Dr. J. C. Jungers; C. R. B. fellow from Louvain.
[2] Segré, Linc. rend. **12**, 226 (1930).
[3] Bhagavantam, Nature **127**, 817 (1931); J. Ind. Phys. **6**, 319 (1931).
[4] Daure and Kastler, Compt. rend. **192**, 1721 (1931).
[5] Mecke, Zeits. f. Physik **64**, 173 (1930).

The Azimuthal Asymmetry of Cosmic Radiation on Mount Evans, Colorado

Johnson[1] has shown that a knowledge of the variation of the east-west azimuthal asymmetry of cosmic radiation with altitude will be helpful in determining the nature of this radiation. Hence a measurement of this asymmetry at altitudes varying from 5000 to 14,000 ft. at the same geomagnetic latitude has been initiated. The following is a report of observations made on Mt. Evans, Colorado. The altitude and magnetic declination of the observation station were 14,085 ft. and 13.5°, respectively.

The apparatus consisted of a triple Geiger counter telescope which could be set at any zenith angle and rotated about a vertical axis. The copper cylinders of the counters were each 15 cm in length, 4 cm inside diameter and the distance between the centers of the outside counters was 14 cm. The axis of rotation was made vertical within 3 minutes by means of a sensitive level and this adjustment was checked several times daily during the period of observation.

Laboratory tests showed that the counting rate varied slightly with temperature. The temperature of the apparatus ranged from 4 to 19°C. The intensity of the radiation is a function of atmospheric pressure which varied from 18.30 to 18.55 inches of mercury. In an effort to compensate for these effects the counts were taken in the following order: E–W–E–W–E for approximately an hour in each direction. The ratios of each west to the average of the east readings immediately preceding and following this west were computed. A mean of these ratios was taken as the best value for the east-west asymmetry. The probable error, r, was computed from residuals, the theoretical probable error, R, was computed from the total number of counts and the total time in minutes.

The results are shown in Table I. Z is the zenith angle, C the total number of counts while W and E in this column stand for the magnetic west and east, respectively, T the total time in minutes, N the number of data and W/E the mean ratio of the west to east rates. In calculating W/E the accidental rate of 0.73 per minute was subtracted before the division was performed.

TABLE I.

Z	C	T	N	W/E	r	R
15°	West 19500	1200	15	1.016	0.0064	0.0067
	East 20313	1278				
30°	West 14831	1168	17	1.021	0.005	0.0077
	East 15837	1265				
45°	West 6424	718	10	1.019	0.010	0.019
	East 7402	886				

The agreement between r and R indicates that the apparatus was operating satisfactorily, and while the asymmetry is small the magnitude of the probable error, in addition to the finding of a greater westward intensity for each zenith angle, makes it highly probable that the observed asymmetry is real.

The equipment was built with funds provided by The

National Research Council and The Rumford Committee of the National Academy of Arts and Sciences.

The authors are particularly indebted to Mr. Carl Hedberg who constructed a great deal of the apparatus.

J. C. STEARNS,
University of Denver.
DAROL K. FROMAN,
Macdonald College, McGill University.

August 21, 1934.

[1] T. H. Johnson, Phys. Rev. **45**, 569 (1934).

Hyperfine Structure in Silver

Hyperfine structure has been found in the resonance lines of silver. An etalon of quartz plates with aluminum surfaces was used with a Zeiss spectrograph. The best results were obtained with a 23 mm spacer. The source was a water-cooled hollow cathode 8 cm long and 2 cm bore, with current supplied by a 2000-volt d.c. generator. Low current had to be used on account of self-reversals. The series of exposures described below was made with the 23 mm spacer as the current was changed by small steps from 0.7 ampere to 0.05 ampere. At 0.7 ampere both lines are much reversed and the wing of the reversal to the red is broader and more intense than the one to the violet for both lines. Only a few examples from the series will be described here.

At 0.34 ampere the reversal of λ3383 is much reduced and a hyperfine structure component begins to show on the red side. This reversal is shown by microphotometer trace I.

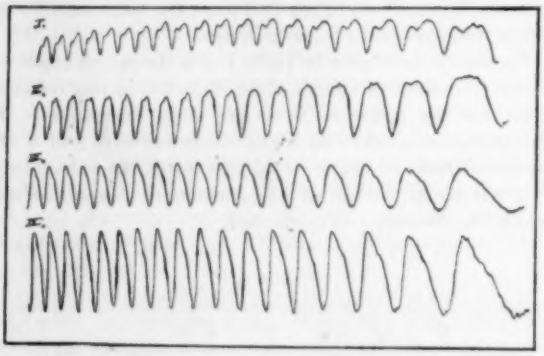

FIG. 1. Traces of fringe system of λ3383 showing reversal and h.f.s. I—0.34 ampere; II—0.17 ampere; III and IV—0.1 ampere.

Trace II shows that the reversal has practically disappeared at 0.17 ampere and the component on the red side is definitely visible on the original plate. Traces III and IV are made from two different exposures of λ3383 at 0.1 ampere. Here there is no sign of reversal although IV shows some broadening. The faint component is clearly visible on both traces and is unmistakable on original plates. At 0.08 ampere the intensity drops but there is not much change in the appearance of the ring system of the line. Measurements of plates exposed at 0.1, 0.08 and 0.05 ampere give an approximate separation of 0.06 cm^{-1}.

At 0.7 ampere the wings of the reversal of λ3281 are much farther apart than those of λ3383 at the same current, as might be explained by the larger J value of the P term of λ3281. The wing on the violet side in one order is very near the wing on the red side of the next lower order. At 0.34 ampere λ3281 has about the same appearance as λ3383 at 0.7 ampere. At 0.17 ampere it is about the same as λ3383 at 0.34 ampere. At 0.1 it is comparable to λ3383 at 0.17 ampere. The results for λ3281 are less easily reproduced than those for λ3383 and microphotometer traces are more difficult to obtain. At 0.05 ampere λ3281 shows its component in approximately the same manner as λ3383 does at 0.1 ampere but the intensity is naturally very much less. Measurements of plates exposed at 0.08 and 0.05 ampere give an approximate separation of 0.06 cm^{-1} also.

These results differ from those of Mohammad and Sharma[1] who, using high currents, found three components, two of about equal intensity, approximately 0.23 cm^{-1} apart and one faint component approximately 0.18 cm^{-1} to the violet of the middle component. Their results were not confirmed by Williams and Middleton[2] who, using a hollow cathode source and reflection echelon, found no structure. Williams' plates were examined by Tolansky[3] who concluded that any structure must be less than 0.05 cm^{-1} wide. Jackson[4] using a capillary tube as source and a reflection echelon concluded that 0.07 cm^{-1} was the upper limit for structure. It would seem, therefore, that the present results are not inconsistent with the conclusions of other recent observers.

HARRY HILL

Ryerson Physical Laboratory,
University of Chicago,
Chicago, Illinois,
August 22, 1934.

[1] Mohammad and Sharma, Ind. J. of Phys. **6**, 75 (1931 and 1932).
[2] Williams and Middleton, Nature **131**, 692 (1933).
[3] Tolansky, Proc. Phys. Soc. London **45**, 559 (1933).
[4] Jackson, Nature **131**, 691 (1933).

The Structure of the Hydrogen Sulfide Molecule from a New Vibration-Rotation Band at 10,100A

About one hundred lines in this band have been recorded photographically in the first order spectrum of a twenty-one foot grating. The absorption cell was seventy-one feet in length. Assignments have been made for the lines involving the energy levels up to $j=4$. From these the following molecular constants have been deduced:

	Normal state	*Excited state*
I_A	2.68×10^{-40} g cm^2	2.81×10^{-40} g cm^2
I_B	3.08	3.32
I_C	5.85	6.20
Bond angle	92° 20′	93°
H–S distance	1.35A	1.39A

This band is believed to be the $\nu_2+3\nu_3$ combination band, with ν_0 at about 9911 cm^{-1}. The electric moment oscillates along the axis of least inertia, perpendicular to the symmetry axis of the molecule. A very faint absorption region was detected at about 11,000 cm^{-1} which is probably due to the combination $3\nu_2+\nu_3$. These assignments are compatible with the vibrational interpretation given by Mecke[1] except that ν_2 should be at about 2630 cm^{-1}.[2] Since the absorption at 3790 cm^{-1} is probably due to the $\nu_2+\nu_3$

combination, ν_3 should be at about 1260 cm^{-1}, where absorption has been reported by Rollefson.[3]

The absorption is so weak that, with few exceptions, only the lines originating in antisymmetric states are observed. The inability to observe many of the lines involving the levels of low j values has made it impossible to construct the term values. Consequently it has been necessary to obtain the moments of inertia by successive approximations, employing easily identified transitions between levels of higher j values. This procedure has reached the stage where the identification of all the strong lines is possible, and the final approximation will be made by least squares. It is hoped to include an approximate correction for the distortion of the molecule by rotation. The final results will be used to calculate the entropy.

Details of the experimental results, procedure of analysis, and entropy calculation will be published in the near future.

PAUL C. CROSS

National Research Fellow in Chemistry,
California Institute of Technology,
Pasadena, California,
August 27, 1934.

[1] R. Mecke, Zeits. f. physik. Chemie **B16**, 431 (1932).
[2] A. D. Sprague and H. H. Nielsen, Phys. Rev. **43**, 375 (1933).
[3] A. H. Rollefson, Phys. Rev. **34**, 604 (1929).

Evidence of an Excited State in the Alpha-Particle

It has been shown[1] that lithium bombarded with protons gives rise to a gamma-ray of about 12 m.e.v. and probably a second gamma-ray of about 4 m.e.v. energy. The 12 m.e.v. component we ascribe to the process

$$_3Li^7 + {}_1H^1 \rightarrow 2\ {}_2He^4$$

because this appears to be the only reaction involving lithium and protons in which sufficient energy is released. This gamma-ray is particularly interesting, for presumably the only possible source of the radiation is the final product, He^4. That such strong radiation could be emitted in the impact of the protons on the lithium nuclei seems very improbable, both from theoretical considerations and from experimental data at present available, though a small probability for the emission of radiation during the impact cannot be excluded. Analogous cases are known which give strong support to the belief that a gamma-ray is in general to be associated with an excitation level in one of the final products of the reaction. These are the cases in which a given product can be produced by more than one combination of initial particles, for example,

$$_5B^{10} + {}_2He^4 \rightarrow {}_6C^{13} + {}_1H^1 + \gamma,$$
$$_6C^{12} + {}_1H^2 \rightarrow {}_6C^{13} + {}_1H^1 + \gamma.$$

The first of these was studied by Bothe and Becker[2] and the second by ourselves,[3] and in both instances the quantum energy of the gamma-rays was found to be a little over 3 m.e.v. Since only the products are common to the two reactions, it seems certain that the energy 3 m.e.v. represents a level in the C^{13} nucleus. Other equally good examples are B^{10} produced by Li^7 He^4 and by Be^9 H^2. Both of these have been studied[4, 5] and found to give gamma-rays which are of the same energy (0.6 to 0.7 m.e.v.) and therefore presumably characteristic of the final product, B^{10}.

It is more difficult to account for the 4 m.e.v. radiation arising from lithium bombarded with protons. We have not observed it in other reactions in which alpha-particles are given off with more than 4 m.e.v. and less than 12 m.e.v. energy, as in Be, B and F bombarded with protons. Two suggestions as to its origin can be made, which are in keeping with these data. It could be due to an excitation level in He^3, or it could be due to an additional level in the alpha-particle, lying above the 12 m.e.v. level already discussed.

Oliphant, Kinsey and Rutherford[6] have observed the production of He^3 in the reaction

$$_3Li^6 + {}_1H^1 \rightarrow {}_2He^4 + {}_2He^3$$

and have given as the ranges of the particles 7 and 12 mm, when the energy contributed by the bombarding protons was about 0.2 m.e.v. In our experiment sufficient energy is available to excite the He^3 to 4 m.e.v., but there would be very little energy left to appear in the form of kinetic energy of the two particles, and hence they would not be easy to observe. The only other reaction in which He^3 is known to be a product is

$$_1H^3 + {}_1H^2 \rightarrow {}_2He^3 + {}_0n^1,$$

but only about 2.5 m.e.v. of energy is available and we should therefore not expect to find the 4 m.e.v. gamma-rays unless deutons of very high energy are used.

If, on the other hand, we ascribe the 4 m.e.v. gamma-ray to a second level in the alpha-particle, we must assume that it lies above the 12 m.e.v. level, in order to account for the fact that it is not found in processes where more than 4 but less than 12 m.e.v. are available. The alpha-particle would, then, in the case of lithium, come off excited to 16 m.e.v. and emit successively a 4 and a 12 m.e.v. quantum. In this case the alpha-particles would have less than 1 m.e.v. (3 mm range) each, and would be difficult to observe. If only the 12 m.e.v. level were excited, the alpha-particle would have about 1 cm range and might correspond to the 9 mm particles reported by Kirchner and Neuert.[7]

If our speculation as to the origin of the 12 m.e.v. gamma-ray is correct, there should be the possibility of finding the same gamma-ray in several other accessible processes in which alpha-particles are given off with high energy. This would be the case, for example, when boron and nitrogen are bombarded by deutons, the reactions being

$$_5B^{10} + {}_1H^2 \rightarrow 3\ {}_2He^4 \qquad (+20\ \text{m.e.v.}),$$
$$_7N^{14} + {}_1H^2 \rightarrow {}_6C^{12} + {}_2He^4 \quad (+15\ \text{m.e.v.}).$$

Having a sufficient amount of energy available, however, may not be the only condition which must be satisfied to make possible the excitation of the resulting alpha-particle to a particular level.

Experiments are now under way to determine, by means of a Wilson cloud chamber, the energy spectra of recoil

electrons due to boron and nitrogen disintegrated by deutons, both of which should yield more information concerning the possibility of an excitation level in the alpha-particle.

We wish to thank Professor J. R. Oppenheimer and Professor R. C. Tolman for many valuable suggestions given us in connection with this problem.

C. C. LAURITSEN
H. R. CRANE

Kellogg Radiation Laboratory,
California Institute of Technology,
September 2, 1934.

[1] Crane, Delsasso, Fowler and Lauritsen, Phys. Rev. **46**, 531 (1934).
[2] Bothe and Becker, Zeits. f. Physik **76**, 421 (1932).
[3] Lauritsen and Crane, Phys. Rev. **45**, 345 (1934).
[4] Webster, Proc. Roy. Soc. **A136**, 428 (1932).
[5] Crane and Lauritsen, Phys. Rev. **45**, 226 (1934).
[6] Oliphant, Kinsey and Rutherford, Proc. Roy. Soc. **A141**, 722 (1933).
[7] Kirchner and Neuert, Phys. Zeits. **35**, 292 (1934).

Thermal Expansions of Alloyed Bi Crystals in the Region of the Eutectic Melting Point

Single bismuth crystals grown from melts having 1 to 5 percent of lead show a discontinuity in the thermal expansion as the crystals pass through the region of 125°C, the temperature at which the eutectic alloy (49 percent Pb, 51 percent Bi) melts.[1] Fig. 1 shows the type of curve

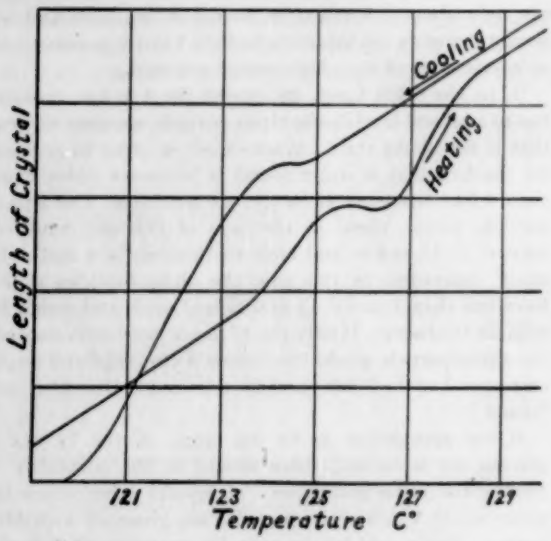

FIG. 1.

obtained. The curves shown were obtained on a crystal specimen which was grown from a melt containing 4.88 percent Pb. The crystal had been heated above 125°C several times. The curves first obtained contained discontinuities that were larger than those shown, the crystals showing more contraction on a part of the heating curve and more expansion on the cooling curve. After numerous heatings, the discontinuities became less marked than those shown in Fig. 1. The cooling curves differ from those obtained on heating but the characteristics of both curves are consistently obtained.

Crystals of various orientations give similar results. All usual tests show the specimens (2 cm long) to be single crystals. They were grown at the rate of 5 mm/min. by the method described by Goetz.[2] Work[3] done in this laboratory indicates that impurities are driven along the melt ahead of the region of crystallization so that it is very likely some of the specimens used had a smaller percentage of foreign atoms than in the melt. Crystals grown from melts containing 1 percent Pb show discontinuities somewhat less pronounced than those shown in Fig. 1.

Somewhat similar curves are obtained for Bi–Sn crystals containing a low percentage of Sn. The discontinuities are somewhat less pronounced. They occur in the region of 135°C, the temperature at which the eutectic alloy (56 percent Sn, 44 percent Bi) melts.

After heating the Bi–Pb crystals a number of times through the 125°C point, tiny drops of material are "sweated" out on the surface of the crystal. An approximate polarograph analysis gave 17 and 35 percent Pb in the droplets from crystals grown from melts containing 2.56 and 4.88 percent Pb, respectively.

This indicates that the foreign admixture is not uniformly distributed over the crystal lattice, although the concentrations in all cases are within the limits of solid solubility.[4]

These observations seem to be interesting due to the facts: that these specimens appear in the usual tests perfectly uniform and monocrystalline; that x-ray measurements do not show a discontinuity of the lattice parameter in this temperature interval, and that the diamagnetic qualities of such alloyed crystals are not changed by repeated transgressions of these temperatures, even not by "sweating." This indicates that the admixtures are partly precipitated within certain regions of the lattice in concentrations above the solubility limit, and furthermore that these precipitations are *uniformly* distributed over the volume of the crystal (since the melting of occasional local inclosures would not change the total length of the crystal), and that the geometric arrangement of this precipitation is such that it does not interfere with the single-crystalline habitus of the specimen. It may finally be added that such phenomena contribute necessarily to the discrepancy between the macroscopic and the lattice expansion of single crystals.

We are obliged to Dr. M. F. Hasler for the performance of the polarographic analyses.

A. GOETZ
J. W. BUCHTA*
T. L. HO

California Institute of Technology,
August 11, 1934.

[1] Reproductions of the complete phase diagrams of most of the binary systems of Bi are found in a recent publication (Phys. Rev. **45**, 170 (1934)). From them it is evident that the solubility limit of Pb in Bi lies above 5 percent at. and of Sn above 2 percent at.
[2] A. Goetz, Phys. Rev. **35**, 193 (1930).
[3] M. F. Hasler, *The Thermoelectric Analysis of Micro-Alloyed Single Crystals of Bismuth*, Cal. Inst. Tech. 1933. Thesis.
[4] On leave from the University of Minnesota.